Late Pleistocene glaciations and catastrophic glacial floods of Central Colorado

by

Cole C. Pazar

UNIVERSITY OF COLORADO, BOULDER

Defense date: April 4th, 2016

Honors thesis committee members:

Dr. Robert S. Anderson – *department of geological sciences*
Dr. Charles Stern – *department of geological sciences*
Dr. Suzanne P. Anderson – *department of geography*
Dr. Gifford Miller – *department of geological sciences*

Dedication

I dedicate my work to all scientists of the Earth, who as stewards of absolute truth, invest their passion and life energy in building and strengthening the foundations upon which our collective planetary knowledge manifests.

Acknowledgments

I give my utmost respect to my honors thesis advisor, Bob Anderson, to whom I thank for using his expertise, passion, and diverse knowledge to teach me how to treat the Earth's surface quantitatively, enabling me to read landscapes as a record of the geomorphic processes and events that created them. I especially would like to thank him for introducing me to the intersection between the fields of numerical modeling and planetary surface processes. This work could not have been possible without the funding through the exceptional UROP program at CU. I especially would like to thank my fieldwork and photography helpers, Rob Aranoff, Nabil Chaudhry and Michael Greene. This work was initially inspired through field conversations with Lon D. Abbott, Gage Hammel, Gordon Bowman, Sigrún Tómasdóttir, Einar Bessi Gestsson, Natalie Cristo, Unnur Þorsteinsdóttir, Haukur Arnarson, and Sigurdís Björg. Thanks to William Armstrong for help with QGIS data. I thank my honors thesis committee for being able to attend my defense and discuss my research, and everyone else who attended it. Special thanks to Emily Valencia, and the rest of my friends and family for the support they have given me both in the field, and in life. Lastly, I give a special thanks to my mom and dad, Kelly and Jerry, who raised me in the mountains, which ultimately has fed my passion for understanding the Earth's surface.

Late Pleistocene glaciations and catastrophic glacial floods of Central Colorado

by

Cole C. Pazar

Submitted to the Department of Geological Sciences at the University of Colorado, Boulder

on the 4th of April, 2016, in partial fulfillment of the

requirements for the degree of

Bachelor of Arts

Abstract

Late Pleistocene glaciations of the Sawatch and Elk Mountain Ranges of Central Colorado at ~130 and ~20 ka left behind glacial features in the topography, ideal for constraining the local climactic variability. In the northern end of the Sawatch Range, distinct lateral and terminal moraines reveal strong geologic evidence that multiple large glaciers drained eastward. Two of these appear to have dammed the Arkansas River. Very fine-grained lacustrine sediments, 'ice-rafted' boulders, and catastrophic glacial flood boulders down-valley, show at least two glacial-ice dammed lakes that catastrophically drained. We report flood discharge calculations consistent with previous estimates, on the order of ~50,000 m^3/s. For this study, we employ a 1-D finite difference staggered-grid mass conservation numerical model to reconstruct paleoglacier extent and equilibrium line elevations. I prescribe a mass balance based on a scaled approximation of the marine $\delta^{18}O$ record, with normally distributed random number generation. Modeled ELA's on the order of ~3400 m are consistent with temperature depressions nearly ~6 ^oC below the modern mean annual air temperature. Our model shows internal consistency with the dependence of catchment geometry and variable metrological forcing on glacier disequilibrium response time. In the West Elk Mountains lies Snowmass Creek Valley, where at ~20 ka the ice extent is required to have preserved the famous Ziegler Reservoir paleontological site. Employing our 1-D numerical model on this site, for the climate at ~20 ka, reveals that the required temperature depression is on the order of ~1^oC warmer than it was during the Bull Lake glaciation at ~130 ka.

Table of contents

Chapter 1 Introduction

1.1 Study areas and geologic setting

In the northernmost reach of Central Colorado's Rio Grande rift is the Upper Arkansas River Valley between the towns of Leadville to the north, and Buena Vista to the south, where the river flows south along the eastern flank of Central Colorado's Sawatch Range (see Figures 1 and 2). The Sawatch Range is pre-Cambrian basement rock at its core, dotted with Tertiary intrusive dikes, plutons, and batholiths (e.g., Tweto 1979). Snowmass Creek Valley (see Figures 1 and 3), ~50 kilometers to the west and slightly north of the Upper Arkansas River Valley, drains northward away from some of the highest peaks of the West Elk Mountains. Trending to the northwest, and stretching for more than ~80 km, these Elk Mountains are composed largely of Paleozoic and Cretaceous sandstones, siltstones, mudstones, and shale, as well as Oligocene intrusive rocks (e.g., Tweto 1979). They contain some of the highest peaks in the area, including Mount Daily, Capitol Peak, and Snowmass Mountain. In contrast, the North Maroon Peak consists of ~300 million year old Maroon formation (e.g., Tweto 1979). In total, there are 10 >14,000-foot (>4267 m) isolated peaks in the two study areas (Table 1, Figures 2 and 3). Driven by climate variability over the past 2 million years, many temperate valley glaciers have deeply scoured this elevated landscape into the high relief, mountainous landscape we see today.

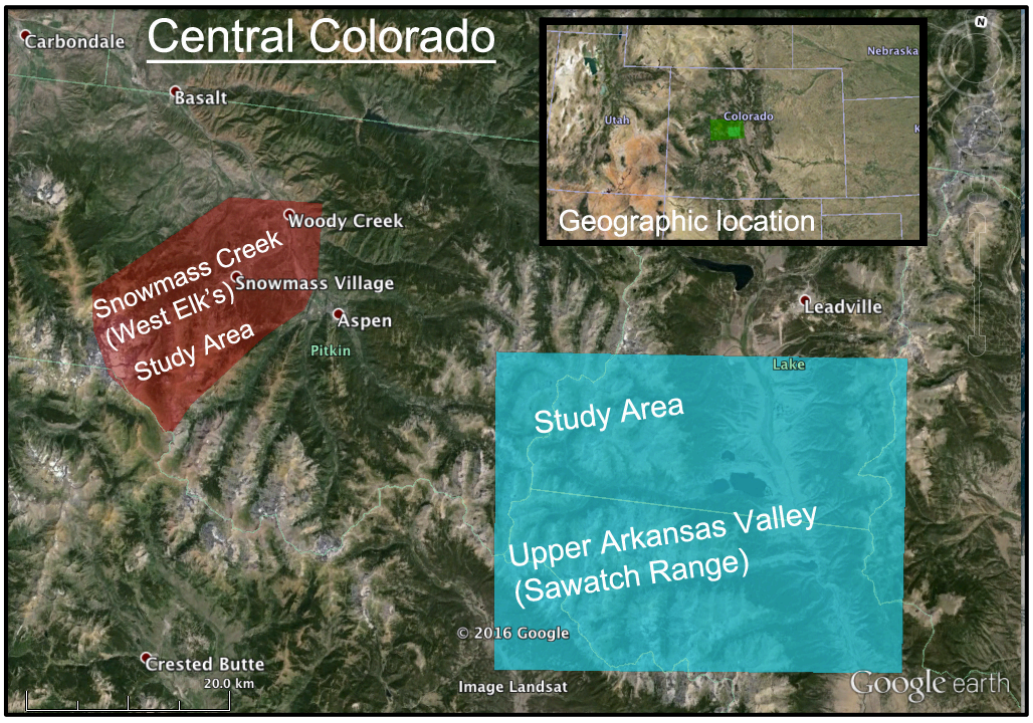

Figure 1

Geographic orientation for the study areas that I chose for this research (Google Earth).

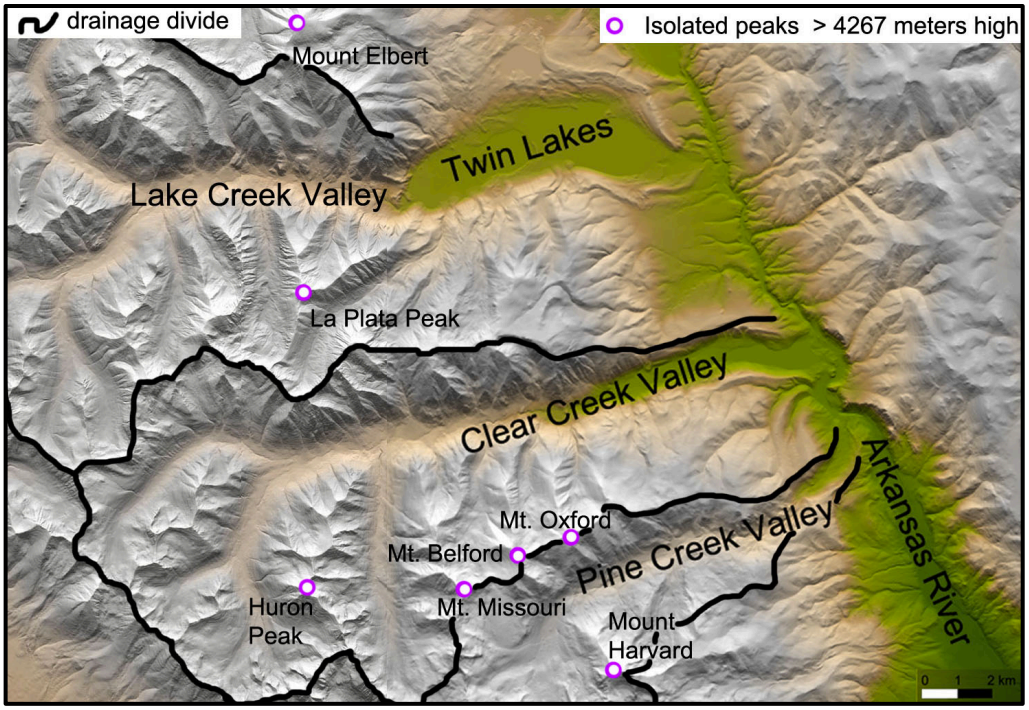

Figure 2

Geographic and geomorphic context for the Upper Arkansas River Valley (QGIS data).

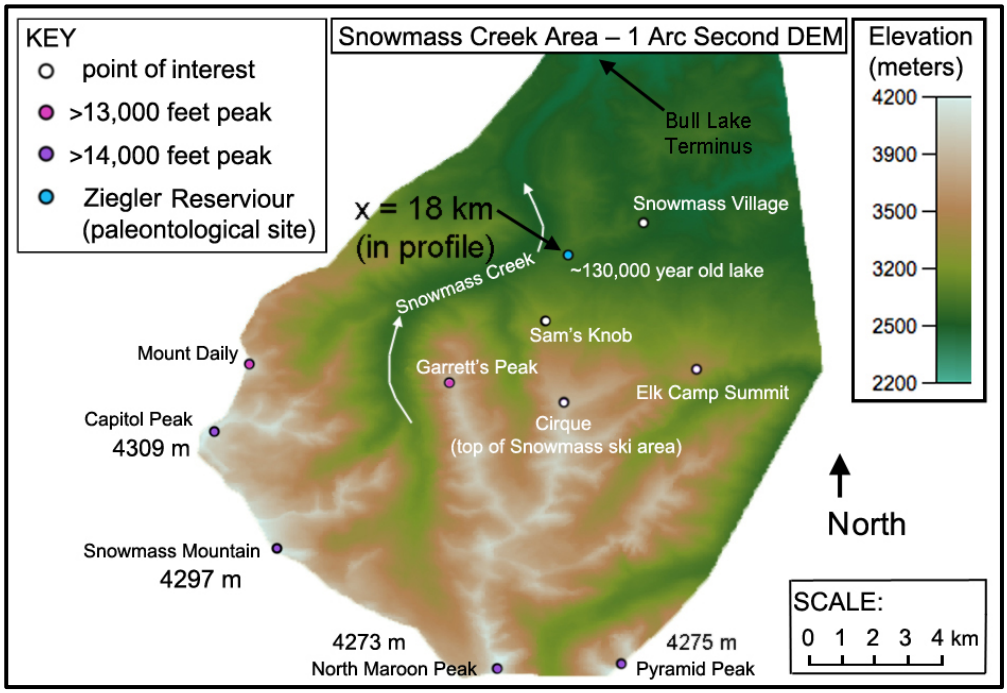

Figure 3

Geographic and geomorphic context for the Snowmass Creek drainage (QGIS data).

Table 1

Inventory of the 10 highest peaks that contribute to the drainage areas (QGIS data).

Mountain name	Elevation [m]	Range	Long. (º west)	Lat. (º north)
Capitol Peak	4309	West Elks	107.0829	39.1503
Snowmass Mountain	4297	West Elks	107.0665	39.1187
North Maroon Peak	4273	West Elks	106.9871	39.0760
La Plata Peak	4369	Sawatch	106.4729	39.0294
Huron Peak	4271	Sawatch	106.4380	38.9455
Mount Elbert	4401	Sawatch	106.4454	39.1178
Missouri Mountain	4290	Sawatch	106.3786	38.9477
Mount Belford	4329	Sawatch	106.3606	38.9606
Mount Oxford	4316	Sawatch	106.3388	38.9648
Mount Harvard	4396	Sawatch	106.3207	38.9244

1.2 Upper Arkansas River Valley overview

The Sawatch Range has several prominent, eastward-draining valleys that feed into the Arkansas River. The glacial valleys we analyze for this study (north to south) are Lake Creek Valley, Clear Creek Valley, and Pine Creek Valley (Figure 4). These tributaries were completely occupied by thick (200–500 m) glacial ice multiple times during the Pleistocene Epoch. Quantitatively extracting different aspects of the topographic geometries, e.g. the slope, width, and shape of these valleys, is accomplished using a topographic digital elevation model (DEM) and the open-source mapping program QGIS (see Figure 5). For these three drainage basins, I have calculated their total contributing areas (Table 2) relevant for our 1-D glacier model. See chapters 4 and 5 for the full detailed analysis on this valley and an assessment with numerical modeling.

Table 2

Approximated basin geometry data for all four glacial drainages (from QGIS).
See Appendix for the delineated drainage basin geometries and location.

	~Area [km^2]	~Perimeter [km]	~Drainage length [km]
Snowmass Creek Valley	110	60	27.0
Lake Creek Valley	300	90	34.0
Clear Creek Valley	200	70	28.5
Pine Creek Valley	60	40	19.0

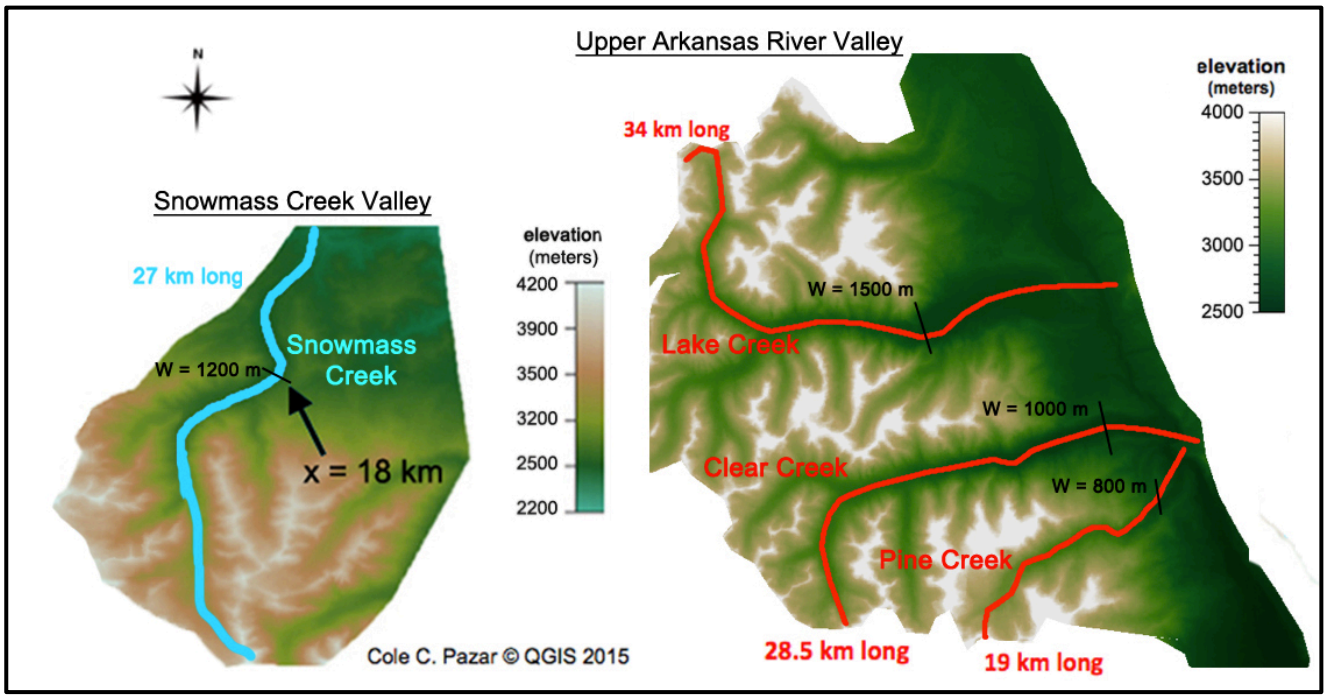

Figure 4

Topographic transects in the study areas for the 1-D glacial model (see Figure 5 for profiles). These maps are not plotted on the same coordinate system (i.e., the Snowmass Creek Valley is farther west-northwest in this figure).

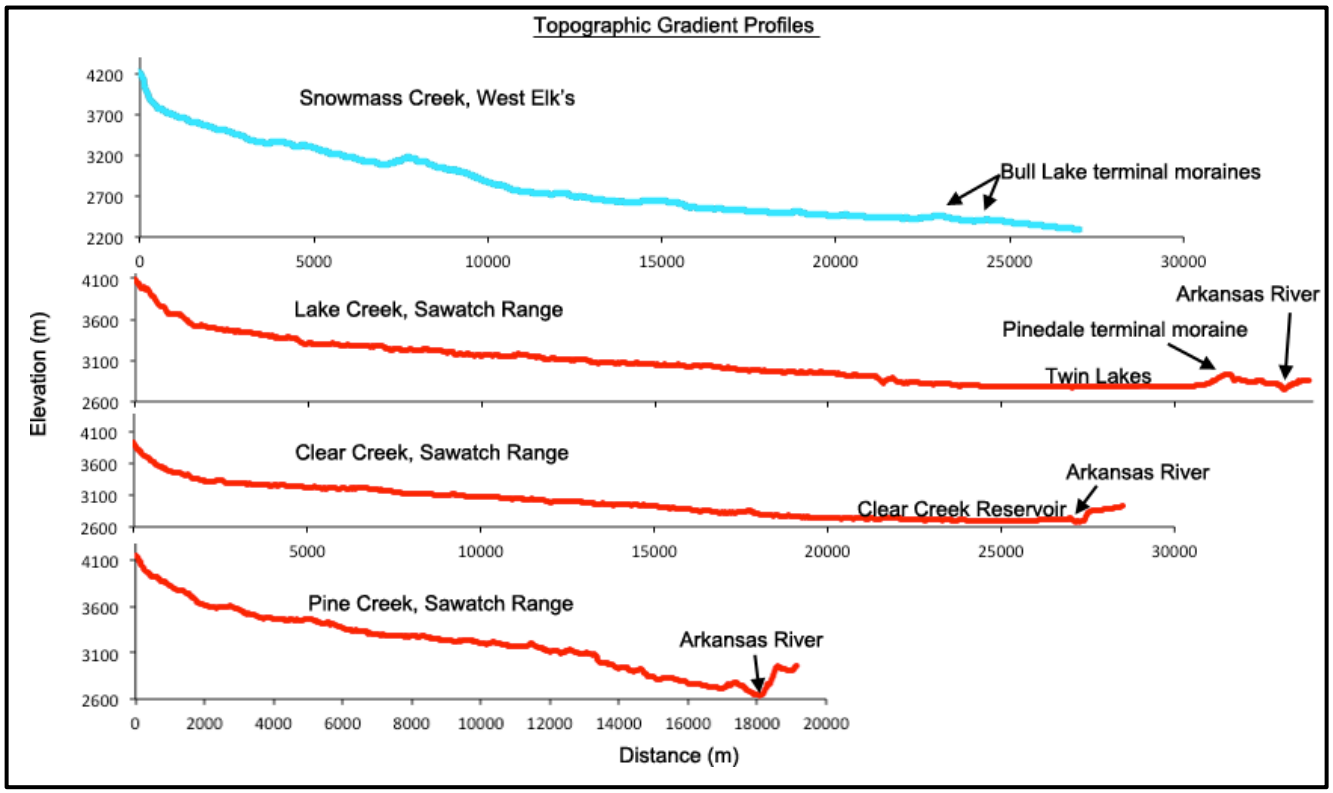

Figure 5

1-D topographic profiles, no smoothing function applied – note similarity between Clear Creek and Lake Creek.

Distinct glacial landforms (e.g., Figure 6) were deposited both beside and at the terminus of these ancient glaciers during the last glacial maximum (LGM). Since the LGM, the Arkansas River has been naturally removing and eroding away whatever terminal moraine deposits were left at the end of the Clear Creek and Pine Creek valleys (dashed lines, Figure 6). Further downstream from the dam site, we see large flood boulders as evidence of the catastrophic floods and 'ice-rafted' boulders expected within the lake extent (e.g., Lee 2010). At least two catastrophic glacial floods filled in the Arkansas River's paleochannel with these extremely poorly sorted deposits containing boulders several meters in diameter (Scott 1984; Nelson and Shroba, 1998; Lee 2010). These deposits were further incised and abandoned as nearly flat river terraces, on which the largest boulders remain, having not been transported since the catastrophic flooding during the Late Pleistocene (approximately 132 ka – 11.7 ka).

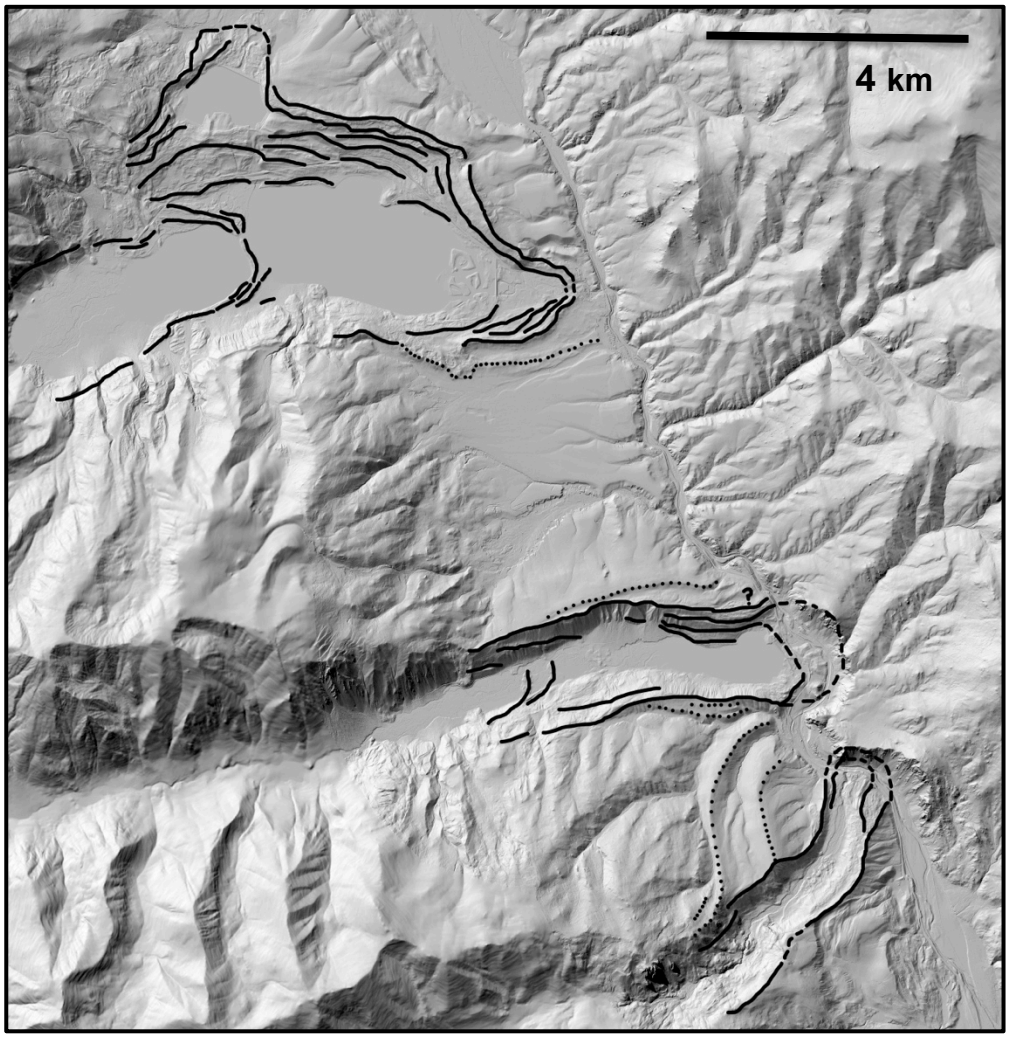

Figure 6

Mapped approximate moraine extent on a 10-meter resolution DEM (full LiDAR map in Appendix). The effect of inter-annual climate variability on the moraine record is obvious here as shorter recessional moraines behind the maximum extent terminal moraines. Solid black lines indicate approximate LGM (~20 ka) extent and the dotted lines indicate approx. Bull Lake extent (~130 ka), as suggested by Briner (2009). The dashed lines show the proposed glacial damming of the Arkansas River. Aided from field observations and previous work.

1.3 Snowmass Creek Valley overview

Just outside of the popular ski resort town of Snowmass Village, CO, is a drainage network stemming from some of the most prominent mountains of the Elk Mountain Range (Figure 3). Here, in the northern edge of the West Elk Range, three large tributaries, Snowmass Creek, Bear Creek, and East Snowmass Creek, drain northward from the high mountains, before combining near the base of Mount Daily and continuing further northward. Snowmass Creek Valley was occupied multiple times by large glaciers. Preservation of the Ziegler Reservoir Paleontological site (Pigati et al., 2014) shows us that the LGM glacial ice thickness at ~18 km down the valley, must have been less than the elevation of the highest left lateral moraines above the valley floor (~200 m). These LGM moraines are just below the reservoir to the west (Figure 7). See Chapter 6 for full analysis and modeling.

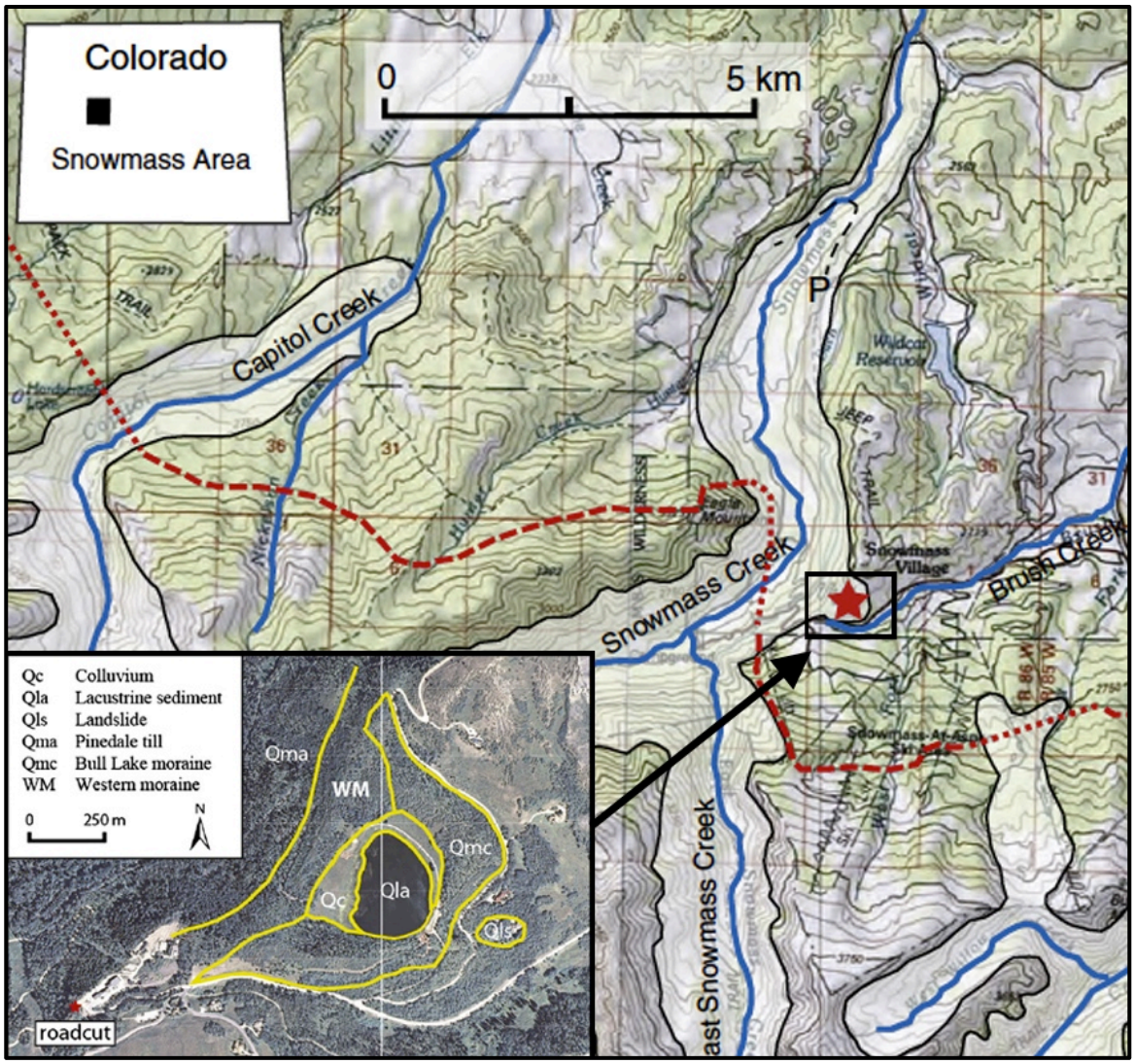

Figure 7

2-D glacier reconstruction in the Snowmass Creek Valley (adapted from Leonard et al., 2014) at ~130 ka. The black dotted line with a ' P ' indicates the Pinedale terminal moraines – the extent of the LGM glaciation of this valley. Figure inset: surficial geology map for the Ziegler Paleontological site, adapted from Pigati et al., (2014).

Chapter 2 Background

2.1 Quaternary climate

2.1.1 Orbital radiative forcing

Paleoclimate studies (e.g., Shakun et al., 2015) show that over the last ~800 thousand years there have been ~8 high amplitude glacial maxima, or ice ages, spaced ~100 thousand years apart (Figure 8), forced by variations in the solar energy reaching the top of the Earth's atmosphere as the Earth's orbit varies (e.g., Pierce 2003). Variations in the orbital parameters of the Earth (such as eccentricity and obliquity) over these timescales allow the Earth's radiative energy budget to oscillate. The position of the equilibrium-line altitude (ELA) relative to the top of the landscape is what dictates the presence or absence of glaciers in an alpine valley, the extent of glaciers in the valleys, the ice discharge through the valley, and the amount of basal sliding (Owen et al., 2009). The Late Pleistocene climate in Central Colorado was clearly affected by these energy variations (e.g., Pierce 2003; Briner 2009; Brugger 2010; Leonard et al., 2014), and manifested as atmospheric temperature depressions, generating snowfall as the dominant form of precipitation at high altitudes. The glacial geomorphic record is most abundant for the two most recent of these glacial maxima (i.e., Figure 6), because glacial erosion demolishes earlier deposits.

2.1.2 Terminology

For simplicity hereafter, we employ the following common terminology for the climate and regional glaciations. The last glacial maximum (LGM), known as the "Pinedale" glaciation, occurred at ~20 ka, and the penultimate glacial maximum, known as the "Bull Lake" glaciation, occurred ~130 ka. The names behind the glaciations trace back to Blackwelder (1915), who named the Bull Lake and Pinedale glaciations for the distinct moraines on the east and west flanks of the Wind River Range in Wyoming (i.e., Table 4). Following the terminology of previous work, such as Pierce (2003), the following regional terms will be used in accordance with their probable correlation with each marine oxygen-isotope stage (MIS) as follows: Pinedale (MIS-2), early Wisconsin (MIS-4), Bull Lake (MIS 6 and 5d), and pre-Bull Lake (pre-MIS 6). We focus this study around stage MIS-2.

2.1.3 Geomorphic evidence

The glaciation and de-glaciation history for Central Colorado in the Late Pleistocene has been largely constrained by geologic mapping of moraines (e.g., Bryant 1972; Shroba et al., 2014), and the gathering of direct geochronologic data (e.g., Briner 2009; McCalpin et al., 2010; Young et al., 2011). Pinedale moraines used to be commonly subdivided into early, middle, and late stages (Pierce 2003). Late stage moraines were 25-75% farther up valley from the terminal moraines to the valley heads (Pierce 2003). We see evidence of these late stage moraines in the Clear Creek and Lake Creek valleys. Recessional chronologies for the western United States from suggest rapid retreat of the glaciers post-12 ka (e.g., Pierce 2003), such that deglaciation occurred by 12–16 ka.

Figure 8

The diagram below shows in green a reconstruction of sea-surface temperature made from multiple marine sediment sequences, using the Mg/Ca ratios in the calcite ($CaCO_3$) of fossil planktic foraminifera, from Railsback's Fundamentals of Quaternary Science (published references within figure).

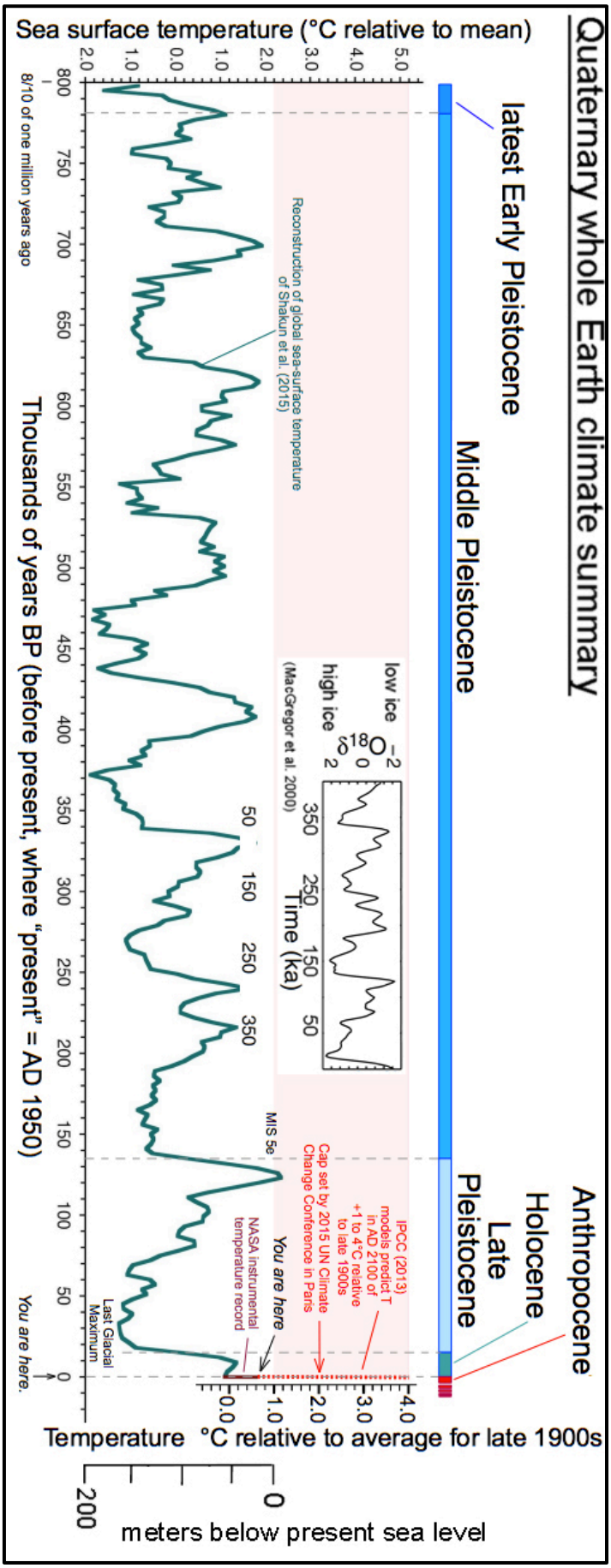

2.2 Glaciers and glaciations

2.2.1 Introduction

At high elevation temperate latitudes of the Earth, alpine valley glaciers scour the landscapes into networks (e.g., Figures 6 and 9) of broad, u-shaped valleys with over-deepened catchments, high relief, and are scattered with cut and abandoned hanging valley tributaries (e.g. MacGregor et al., 2000; Anderson et al., 2006). As we have seen thus far, glaciers leave behind a distinct record of their past extents, largely written in the position of their terminal moraines (e.g., Owen et al., 2009; Anderson et al., 2013). The terminus position of long glaciers that occupy shallowly sloped valleys, is more sensitive to climate variability than those of short glaciers, or glaciers in a very steep valley. As a result of their erosive efficacy, glaciers generate localized differential isostatic rock uplift of the sharp peaks, while still lowering their mean surface elevation (Molnar and England, 1990). The height of mountain ranges reflects the balance between tectonic rock uplift, deformation, and erosion. Tectonic deformation and denudation of the surface are interdependent, however, climate–dependent feedback mechanisms (e.g., Molnar and England, 1990; Egholm et al., 2009) are likely coupled to peak elevations. Egholm et al., (2009), has indicated that the maximum elevation of mountain ranges around the world is capped by an efficient erosive mechanism known as the glacial-buzzsaw (e.g., Brozovic et al. 1997; Foster et al., 2008). They showed that maximum mountain height correlates closely with climate-controlled gradients in approximate mean snowline altitude for many high mountain ranges across the world (e.g., Figure 9). Glacial erosion sets a maximum mountain height by driving elevations towards an altitude window just below the snowline, or near the ELA, supporting the claim (e.g., Egholm et al., 2009) that regional differences in the height of mountain ranges mainly reflect variations in local climate rather than tectonic forces.

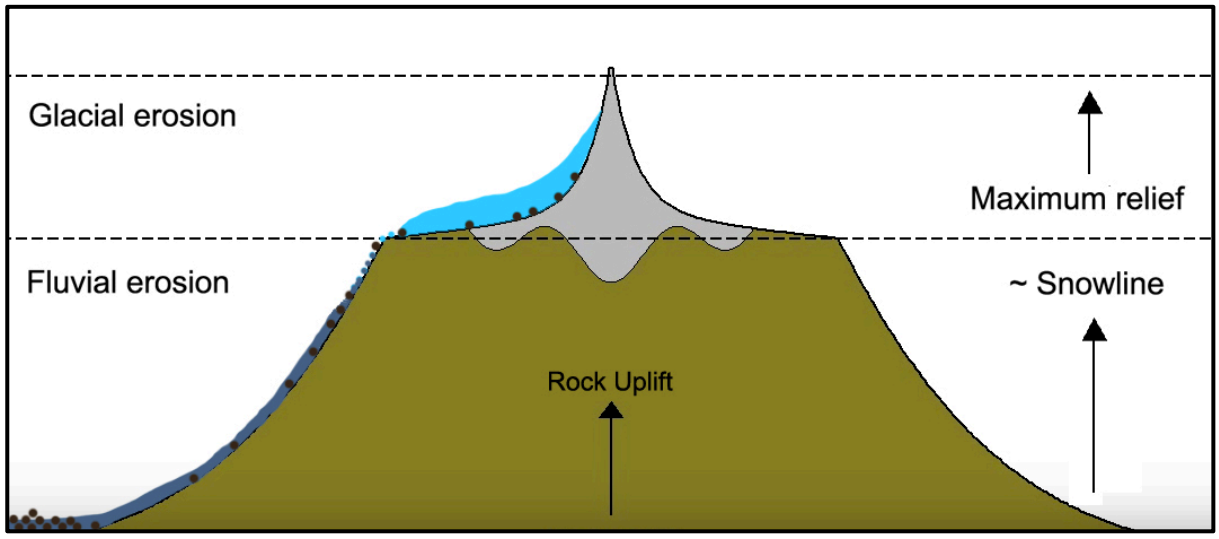

Figure 9

Generalized model of the "glacial buzzsaw" – adapted from Egholm et al., (2009)'s model and YouTube video. The two erosional domains are shown on the left, and the maximum mountain elevation depicted on the right.

Glacially carved valleys are easily identified in the topography, exemplified by their sharp horns and arête's, waterfalls, headwall cirques, and strings of small lake basins in the valley headwaters (e.g., Owen et al., 2009). Glacial valley profiles typically have a rapidly decreasing headwater gradient, with longitudinal profile characteristics resembling typical fluvial valleys (e.g., Figure 5). The occupation of alpine valleys with hundreds of meters of ice results in distinctly over-steepened catchment headwaters, flattening at lower elevations (e.g., Anderson et al., 2006) and topographic steps generated at tributary junctions (e.g., MacGregor et al., 2000). In the work of MacGregor et al., (2000), they produced a 1-D numerical simulation that succinctly modeled the processes involved in the topographic evolution of a simplified glacial, landscape – highlighting the strong correlation between ice discharge as a function of distance down-valley and the junction of tributaries in the location where valley steps and valley profile over-deepening's are formed.

2.2.2 Transport and erosion

Removal of rock from glacial catchments and the transport of glacial sediment down-valley is accomplished by internal deformation and basal sliding of the glacier, partitioning the relative efficacy of these mechanisms as a function of temperature (e.g., Paterson 1994; MacGregor et al., 2009). Ice deforms as a 3rd order (non-linear) viscous fluid whose effective viscosity is strongly temperature-dependent. Basal sliding is accomplished by a poorly understood complex processes that requires the presence of meltwater (e.g., Copland et al., 2003). Temperate glaciers, like those that occupied Central Colorado in the Late Pleistocene, are the most capable of significant sliding, and can erode at rates much higher than the fastest eroding rivers (e.g., Owen et al., 2009). Temperate glaciers are influenced by climate through surface melt, changing local hydrologic fluxes, and water transport.

2.2.3 Mass balance field

The essential role of glaciers in the Earth system is the transportation of ice from regions where excess ice mass accumulates (principally through snowfall – albeit in different forms) to regions where excess mass can melt, be discharged into the ocean, or evaporate (Owens et al., 2009). Heat resulting from energy balance at the glacier's surface is what physically ablates glaciers. This heat is composed of elements from sublimation, turbulent energy fluxes, atmospheric humidity, cloudiness, solar and terrestrial radiation, local slope aspect and shading, and percolation and refreezing of melt-water. Accumulation and ablation is affected by the patterns of snowfall, the efficiency of ice transport, and the patterns of ice loss. On a glacier, over annual timescales, there is typically a non-zero negative summer mass balance, and a non-zero positive winter balance. By measuring this field on various glaciers around the world (e.g., Figure 10), typical mass balance gradients, γ (in equations 3 and 4), have been shown to be ~0.01 m/yr/m. To understand the mass balance of a glacier, on the next page, we start with the mass conservation equation for glacial ice (e.g., Anderson et al., 2006):

$$\frac{\partial H}{\partial t} = b(z) - \frac{1}{W(z)}\left[\frac{\partial Q}{\partial x} + \frac{\partial Q}{\partial y}\right] \tag{1}$$

Which states that the time, t , rate of change of ice thickness, H , equals the mass balance, *b(z)*, (inputs) minus the discharge, Q , of ice (outputs), incorporating variable valley width, $W(z)$. To capture the essence of mass balance, we define the total mass balance of a glacier by vertically integrating the local mass balance and local width:

$$B = \int_0^{z_{\max}} b(z)W(z)\,dz \tag{2}$$

The typical equation used to describe the local mass balance of a glacier is simply a linear equation of the form:

$$b(z) = \gamma\left(z - E\right) \tag{3}$$

where the symbol E refers to where the elevation, z, is equal to the equilibrium line elevation, that is: $b(z) = 0$. Figure 10 shows us that the essence of mass balance profiles can be captured with a linear function that has a capped maximum value above a given maximum elevation. Gradients in mass balance have been shown to have a maximum value, b_z^{cap} , that commonly ranges from 2.0 m/yr in the Sierras (e.g., Kessler et al., 2006; Anderson et al., 2006) to as low as 1.25 m/yr elsewhere (e.g., Owen et al., 2009). Following what Anderson et al., (2006), has done, taking equation 3 while incorporating the mass balance cap commonly used in glacier modeling yields:

$$b(z) = \min\left\{ \gamma\left(z - E\right),\ b_{z\max}^{cap} \right\} \tag{4}$$

Such that particular values of mass balance above z_{max} in the topography are capped with a balance of b_z^{cap} .

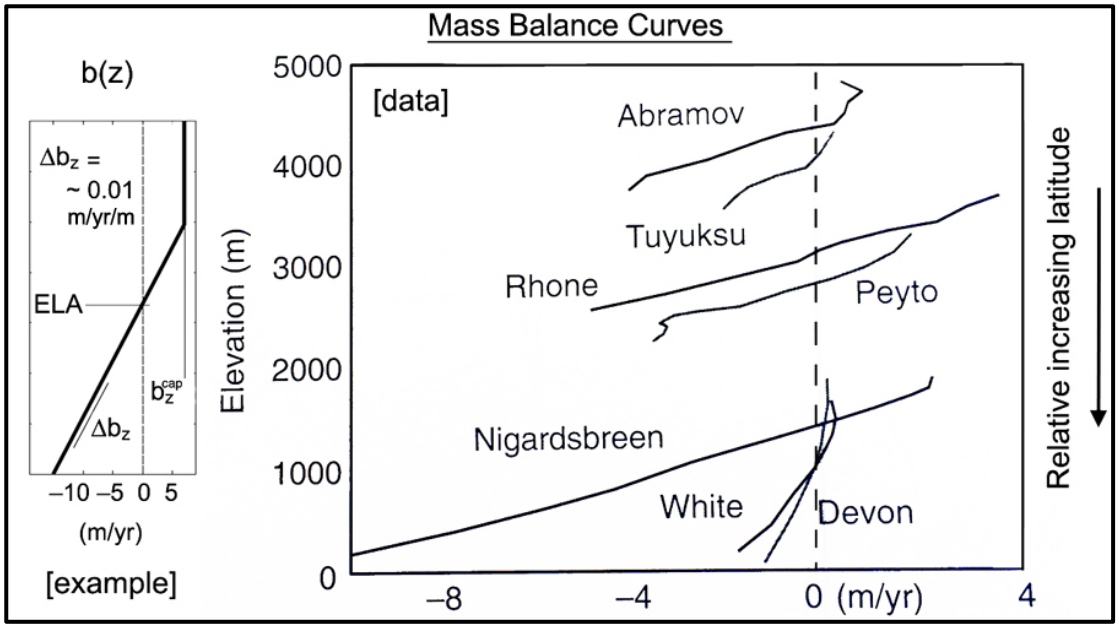

Figure 10

Various mass balance fields as a function of elevation. Capped mass balance profile commonly used in glacier modeling (left). Data for mass balance profiles of 7 glaciers around the world (right). The relative latitude of these glaciers increases downward in the plot. High latitude (near-polar) glaciers show much lower ELA's than (temperate) glaciers at lower latitudes. Graphics and data adapted directly from Anderson and Anderson, (2010).

The term commonly used to label the position on a glacier where the net average mass balance is zero over a 1-year period (Bakke and Nasje, 2011), is known as the equilibrium-line altitude, or ELA (i.e., left side Figure 10, or see equation 3). It can also be thought of as the average separating line between the accumulation zone and the ablation zone. If the annual mass balance of the glacier as a whole is negative, the ELA rises, and when the balance is positive, the ELA falls. In reality, this ELA varies across the entire width of the glacier due to local topographic and climatic variations in accumulation and ablation. Thus, the ELA is closely related to the local climate, particularly sensitive to maximum winter precipitation and maximum summer air temperature. Variations in the ELA therefore are dominated by changes in these two variables alone. A steady-state glacier requires a nearly steady ELA. Under long-term steady ELA conditions, a glacier will self-adjust its geometry and velocity such that mass transferred by flow processes in the glacier exactly balances mass sources and sinks, and the glacier geometry remains steady in time (e.g., Owens et al., 2009). From my modeling, we see that glacier disequilibrium response time for glaciers that are approximately 20–30 km in length is on the order of 1000–2000 years. Variations in the ELA and mass balance have been measured for many glaciers worldwide, showing how fluctuations in ELA provide information on a glacier's response to climate changes.

2.2.4 Importance of local climate

The following discusses why the relevant climate for alpine valley glaciers is that of a local climate. The glaciers that are the last to melt in an alpine landscape are those in spots favorable to the accumulation of snow, and where direct radiation is lowest. For many glaciers, wind-blown accumulation during large storms is also an important part of the mass budget. Orographic effects change the interaction between wind and precipitation fields with topographic geometry (e.g., Kessler 2002), which can lead to drastic asymmetry of glacial extent. Mountainous terrain can dramatically affect patterns of precipitation and ablation. For example, glaciers that drained west in the Sierras were ~7 times as long as the east-draining glaciers (Kessler et al., 2006). This highlights the effect of topography on mass balance, such that an E-W orographic effect can produce asymmetry in precipitation and temperature distributions (Figure 11). Topographic asymmetry, combined with orographic atmospheric effects, can therefore lead to a complex climactic asymmetry. Also, depending on aspect, slope, and topographic shielding, some valleys can accumulate more snow than others, given the same temperature and precipitation conditions. Regional variations in atmospheric circulation can also lead to non-uniform response of glaciers to global climate cycles (e.g., Owen et al., 2009). Glaciers are affected by strong positive and negative feedbacks as they alter the local surface elevation. When a glacier erodes faster than it can

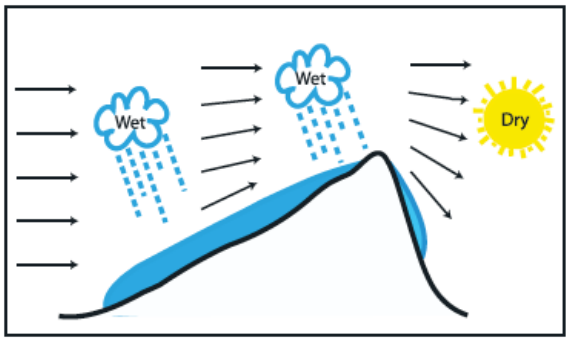

Figure 11

The basics of orographic precipitation due to topographic asymmetry (Kessler et al. 2006). The air looses moisture as it cools and is pushed up and over the mountain range.

grow vertically, a negative mass balance feedback kills the glacier (e.g., MacGregor et al., 2009). A strong positive mass balance feedback is due to the fact that the surface of a glacier is the lower boundary condition for the atmosphere, and as the glacier ice thickens, the elevation of that spot in the landscape rises and gets colder. This brings more of the landscape into the accumulation zone, further feeding the glacier's growth.

2.2.5 Ice physics and glacier dynamics

I now will define the rheological physics of ice and its deformation, then the pattern of ice discharge for glaciers. Following the notation of Anderson and Anderson, (2002), we first start with the definition of strain, ε , on an object as the fractional length change, Δl , divided by it's initial length, l_0 :

$$\varepsilon = \frac{\Delta l}{l_0} \tag{5}$$

The rate of this strain, $\dot{\varepsilon}$, for glaciers is equivalent to its velocity gradient, du/dz , which is therefore:

$$\dot{\varepsilon} = \frac{d\varepsilon}{dt} = \frac{du}{dz} \tag{6}$$

The velocity gradient within a glacier has been shown to be proportional to the shear stress on the object to the n = 3 power, multiplied by a Flow Law parameter, A , which dictates the response speed and behavior of glaciers:

$$\frac{du}{dz} = A\tau^n = A\tau^3 \tag{7}$$

For temperate glaciers near 0 °C, the value typically used for the Glenn-Nye Flow Law parameter, A, is ~2.1x10^{-16} yr^{-1} pa^{-3} (e.g., Paterson 1994). The shear stress field, τ , within the glacier along the x- and z-dimensions is:

$$\tau_{xz} = \rho_i g S\left(H - z\right) \tag{8}$$

where ρ_i is the density of ice, g is the gravitational acceleration, S is the local slope of the surface, H is the thickness of the glacier, and z is its height above the surface. Plugging this shear stress into equation 7 yields:

$$\frac{\partial u}{\partial z} = A\left(\rho_i g S\left(H - z\right)\right)^3 \tag{9}$$

When glacial ice accumulates over a non-uniform surface, the presence of topographic slope sets up a differential a gravitational pressure gradient, allowing internal deformation (e.g., Anderson and Anderson, 2010). The deformation velocity at a particular point of a glacier can be found by integrating the velocity gradient profile within the ice from 0 to H , yielding the following deformation velocity as a function of height above the surface:

$$u(z) = A\left(\rho_i g S\right)^3 \left(H^3 z - \frac{3z^2 H^2}{2} + z^3 H - \frac{z^4}{4} \right) + c_1 \tag{10}$$

Evaluating the constant of integration, we see that at the bed of the glacier, there is no deformation velocity, and in a temperate sliding glacier, the constant of integration becomes the sliding velocity. The sliding velocity can be related to the deformation velocity simply with a factor, f , that is typically about half of the deformation velocity:

$$u(z=0) = c_1 = u_{sl} = f \cdot u_{def} \tag{11}$$

$$u(z) = u_{def} + u_{sl} \tag{12}$$

$$u(z) = A\left(\rho_i g S\right)^3 \left(H^3 z - \frac{3z^2 H^2}{2} + z^3 H - \frac{z^4}{4} \right) + u_{sl} \tag{13}$$

The non-linear rheology of ice makes the dependence of deformation velocity on the thickness a 4th power-law. Evaluating the above equation where $z = H$, allows us to calculate the expected surface velocity of the glacier:

$$u(z=H) = u_{surface} = A\left(\rho_i g S\right)^3 \left(\frac{H^4}{4} \right) + u_{sl} \tag{14}$$

Given a velocity profile, and after characterization of the geometry of a glacial valley, we can address the specific discharge of glacial ice as a function of its local thickness by integrating the vertical velocity profile from 0 to *H*:

$$Q \equiv \int_0^H u(z)\ dz = \left(A\left(\rho_i g S\right)^3 \left(\frac{H^5}{5} \right) \right) + Q_{sl} \tag{15}$$

In the above equation, we can see the strong dependence of ice discharge as a function of its thickness to the 5th power, proving the sensitivity of discharge on ice thickness. The specific discharge is the cumulative discharge that is the sum of the sliding discharge and the deformation discharge. In equation 15, the discharge encapsulates our earlier relations between sliding and deformation (equation 12). Using this knowledge of ice dynamics, in conjunction with the mass balance equations from section 2.3.3, we can produce a dynamical numerical model to test the maximum extent and ELA of different paleoglaciers.

2.3 Catastrophic flooding

Catastrophic glacial outburst floods (also known as Jökulhlaups) are natural geologic hazards that result from the abrupt draining of a large body of water due to processes involving the interaction between glaciers and the land surface. The outburst of water caused by Jökulhlaups in an open channel is turbulent, i.e., Reynolds Numbers above ~1000. The dimensionless Reynolds Number for turbulent flows in fluid mechanics satisfies the condition:

$$\mathrm{Re} \equiv \left(\frac{\rho_w}{\mu} \right) \bar{U} H = \frac{\bar{U} H}{\upsilon} > 1000 \tag{16}$$

where $\bar{U}$ is the vertically averaged mean velocity of the flow, H is the thickness of the flow, and υ is the kinematic viscosity of the fluid, defined as the density of the floodwater, ρ_w, divided by its dynamic viscosity, μ.

2.3.1 Glacially dammed rivers

In the case of the Upper Arkansas River Valley, the maximum extent of the Late Pleistocene glaciers had reached the southward draining Arkansas River, leaving the terminus of the Clear Creek and Pine Creek glaciers to dam the river (e.g., Lee 2010; Shroba et al., 2014). The ice and debris at the toe of these glaciers likely had the ability

to completely fill the river channel, damming it with ice and rock, creating at least two widespread lakes that filled the Upper Arkansas River valley. These natural glacially formed dams can be composed of a mixture of ice, glacial till, moraine debris, sub-glacial sediments, and even finer-grained deposits. Whence formed, ice and/or moraine dams tend to be stable enough, unless the forces and pressures exerted on the dam is sufficient to break the structural integrity. These can drain within hours if a notch at the top of the dam is significantly breached by the water level of the glacially dammed lake, or when the stresses and pressures exerted on the dam's perimeter exceed their critical thresholds. If the terminus of the glacier retreats due to slight thermal fluctuations in climate, and/or if the dam is mostly made of ice, there should be a higher probability of Jökulhlaups.

2.3.2 Dam formation and timescales

Qualitative estimates of the rates of ice dam formation vs. glacial-till dam formation allow us to interpret the time interval expected between the two floods. If the dam is made of ice both times, we would expect a short time interval between floods, reflected in the CRN dates of the flood boulders (Figures 28 and 29). On the contrary, if the dam was made of glacial till and rock then the time interval expected between the floods would be much greater, making it harder to completely drain the lakes. Through numerical modeling, I attempt to show that there is a high probability that the damming of the Arkansas was dominated by glacial ice, allowing the dam to breach and drain catastrophically. The evidence lies in the strong correlation of the timescales between these floods and the disequilibrium response of the glaciers to small-scale thermal variations in the climate. We report estimates of the minimum amount of time required for the lake to fully drain (e.g., schematic Figure 12) assuming a catastrophic breach, by taking the total lake volume, V_{total} , and dividing by Q_{peak} , the peak discharge:

$$t_{drain} \approx \frac{V_{total}}{Q_{peak}} \tag{21}$$

From preliminary estimates, and previous work, we expect this calculation to yield timescales within a day for the majority of the lake(s) to fully drain.

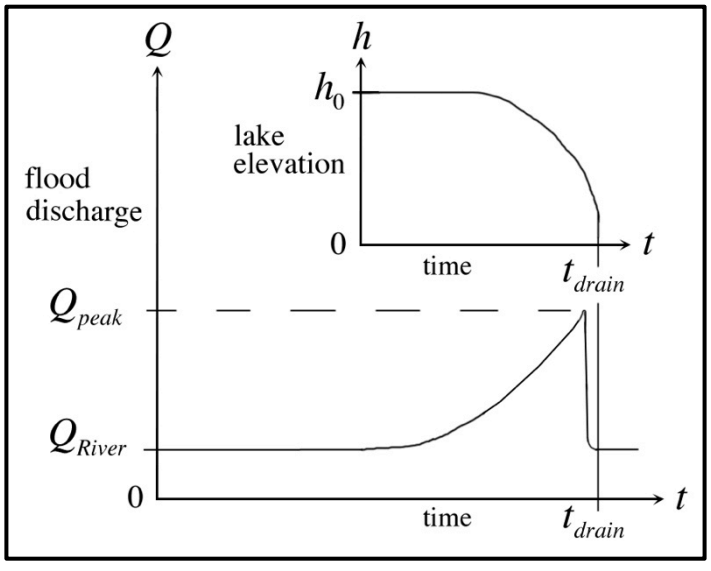

Figure 12

This figure at right depicts the discharge and height of the lake as a function of time, showing the timing and discharge expected for the catastrophic draining of a glacial lake. Growth of the breach at the top of the dam follows an exponential decay relationship. Based on the Summit Lake Jökulhlaups and the work from Walder et al., (1997; 1998).

2.3.2 Flood discharge

In order to understand the discharge of the lake, we take the 'law of the wall' for the vertically averaged velocity from the definition derived in Anderson and Anderson (2010):

$$\bar{u} = \frac{\sqrt{gHS}}{k}\left(\ln\left(\frac{10 \cdot H}{D_{84}}\right) - 1\right) \tag{17}$$

where k is the Von Karman constant, ~0.4, and D_{84} is the 84th median diameter of the grain sizes on the bed. This equation incorporates the shear stresses involved and the roughness of the channel. In paleodischarge analyses, depending on the type of problem, the roughness of the bed is the least known value. Therefore, discharge estimates are commonly given as a range of values within the maximum and minimum bed roughness. To estimate the roughness, we use field data collected for 120 measurements of the grain sizes on the modern terraces. The law of the wall assumes that the flow is essentially steady and that there are edge boundary conditions at the 'walls' of the flow. In the case of these jökulhlaups, the following water balance allows us to derive an expression for the discharge of the lake. The time rate of change of the total volume of the lake is:

$$Q \equiv \frac{\partial V}{\partial t} = Q_{in} - Q_{out} \tag{18}$$

where in the above equation, Q_{in} incorporates the sum of all the inputs of water, and Q_{out} is the sum of all the outputs of the water. For simplicity, and since the timescale for drainage is small compared to the magnitude of water leaving the lake, we assume that Q_{in} = 0, making the time rate of change of lake volume just the discharge out. We use a simplified form of the discharge equation for open channel flow derived from the Navier-Stokes equations to compare our calculations to previous estimates of the catastrophic discharge from the lake(s). The mean discharge is the product of the vertically averaged mean velocity and cross sectional area of the channel:

$$Q = \bar{u}WH \tag{19}$$

where W is the approximated mean width the channel (extrapolated from QGIS). The height of the breach above the channel bottom gets deeper and deeper exponentially as the dam breaks and is incised. Combining equations 17 and 19, we arrive at the following expression for the discharge, or the time rate of change of the lake volume:

$$Q = \frac{\partial V}{\partial t} = \frac{W \cdot H^{3/2}\sqrt{gS}}{k}\left(\ln\left(\frac{10 \cdot H}{D_{84}}\right) - 1\right) \tag{20}$$

This equation for the discharge of the lake allows us to make estimates of the magnitude and the timing of the two different catastrophic glacial outburst floods that produced the flood boulders on two different terraces. The discharge from such catastrophic floods can transport large boulders downstream, leaving them behind on elevated terraces. The depth, or height, of the flow, H , can only be found through calculating the mean diameter of these boulders that it transported, by using a torque balance and shear stress analysis (Chapters 4 and 5).

Chapter 3 Methods

3.1 Fieldwork and remote sensing

The fieldwork that I conducted for this project was largely composed of three main elements: 1) glacial-lake sediment analysis, 2) flood boulder and grain size analyses, and 3) geomorphic landform mapping with LiDAR. Field observations were combined with the principles of superposition to understand which moraines, glacial lakes, and floods happened first and in what subsequent order. Such relative age relationships are crucial to understanding the timing of events in the landscape. If we have precise dates, then we need to ask ourselves if this age fits with the relative age relationships observed in the field. This fieldwork, combined with geologic maps and the published CRN age data, provides a baseline reference, both statistically and geologically, for this study.

3.1.1 Lake sediment organics

For the proposed carbon–14 dating I obtained ~5 grams of organic matter from previously undiscovered lake sediments approximately ~5 km up Clear Creek Valley a few meters below the left shoulder of the dirt road (see Figures 19 and 20). I carefully dug into the sediments with a shovel and then resolved the horizontal laminae of the lacustrine sediments to show the in situ nature of the plant material I discovered. I quickly photographed the site and removed the organic matter carefully with gloves, placing it in individual plastic bags. I repeated this process twice, once in the summer of 2015, and once in the fall of 2015. Currently, our samples are being prepared for radiocarbon dating through Scott Lehman's geochemistry and geochronology lab at INSTAAR.

3.1.2 Flood boulders

The fieldwork relevant to the magnitude of the catastrophic floods is directed toward an accurate statistical representation of the size of flood boulders distributed between the two separate terraces. The sampling technique I used was to measure the b-axis (median approximate diameter) of as many of the largest flood boulders on the two flat terraces as I could without generating sampling bias. This was accomplished with field partners by randomly choosing the direction to walk in a picking the nearest boulder along that line, and repeating that procedure after each b-axis was measured. I measured 71 of the largest flood boulders left behind on two terraces caused by the catastrophic glacial outburst floods. The data that I collected can be found in Table 3 and Figure 25.

Table 3

Flood boulder data	Terrace 1	Terrace 2
Number of measurements	N = 47	N = 24
Mean size of flood boulders	375 cm	680 cm
Standard deviation of data	161 cm	164 cm
Standard deviation of the mean	24 cm	33 cm
Sizes used for discharge calculations	**375 ± 25 cm**	**680 ± 40 cm**

3.1.3 Moraine and lake extent

Glacial landforms were mapped in using a combination of fieldwork, global positioning satellites (GPS), maps from the USGS, satellite imagery, and LiDAR. Collecting these different aspects of the data, this formed the basis for my detailed work on all of the lake sediment locations, flood boulder lithologies, flood boulder size distributions, ice-rafted boulder locations, and mapping of the moraine morphology and extent. I have additionally utilized the available USGS maps, Google Earth®, and local LiDAR data to approximate the volume of the lakes by using shoreline evidence, lake sediment locations, and the approximate height of the dams.

3.2 Geochronology

Age-determination techniques used in paleoglacial studies (e.g., Pierce 2003) and reconstruction of alpine valley deglaciation histories (e.g., Briner 2009) commonly include both relative age dating (constraints via. stratigraphic and geomorphic methods), and numerical ages. The two most common absolute geochronologic methods (Pierce 2003) used in paleoglacial studies include radiocarbon dating and cosmogenic radionuclide dating (CRN's). Lesser used, possibly providing useful insight in future studies, is the technique OSL dating (Mahan et al., 2014).

3.2.1 Radiocarbon dating

As an attempt to further build the record of the deglaciation and paleolake geochronology of Clear Creek Valley, I have proposed to use the organic plant material aforementioned in section 3.1.1, and shown in Figure 19, as a means of reconstructing the age of the lake. My tool of choice for this, based on expense and time was radiocarbon dating. This technique is based on measuring the activity of ^{14}C in a sample of organic matter. In order to calculate radiocarbon dates for deposited organic plant matter, we initially need a sample size around 5.0 g of total carbon. By measuring the activity of ^{14}C in the sample and assuming the initial activity is constant over the past ~70 ka, we can derive the expression for the death date of the organic material. The production of carbon–14 in the atmosphere is due to cosmic ray spallation. This nuclide spontaneously decays with a half-life of ~5730 years. From Faure and Mensing, (2005), we see that the decay reaction of ^{14}C into ^{14}N can be represented by: ${}^{14}_{6}\mathrm{C} \rightarrow {}^{14}_{7}\mathrm{N} + \beta^{-} + \bar{\nu} + 0.16\ \mathrm{MeV}$. After sending prepared carbon samples for analysis, solving for time in the radioactive decay equation, allows for the computation of a numerical depositional date.

3.2.2 Cosmogenic radionuclide dating

Cosmogenic radionuclide (CRN) exposure age dating is based on the production of the radioactive isotope beryllium–10 (^{10}Be) in quartz (SiO_2) crystals by cosmic ray spallation of oxygen. First, cosmic rays from outer space intercept the Earth in our orbit around the sun, and they interact with the uppermost atmosphere. After the first cosmic ray collision with a particle in the atmosphere occurs, a chain reaction sends the cosmic ray energy

into a spallation of nuclear reactions until the energy reaches the surface. Integrating this cosmic ray flux over geologic timescales at a particular location on the surface, allows us to interpret the time at which a rock, or a surface itself, was last exposed to the cosmic at the surface of the Earth. The CRN ages for the upper Arkansas River Valley, specifically Clear Creek Valley, have been collected and analyzed by Briner (2009), McCalpin et al., (2010), and Young et al., (2011) (section 4.4, Figures 28 and 29). The sampling strategy, adapted from previous work, for the analysis employed by Young et al., (2011), was designed to reduce the chance of nuclide inheritance, and exclude the possibility of nuclide loss through erosion, by sampling the top of the largest and tallest boulders where possible. Cosmogenic radionuclide data and analysis hinges on assumptions including snow cover, topographic shielding, and local erosion. In accordance with previous research, we simply assume the analytical assessment of CRN data accurately reflects the actual exposure ages of the samples. All exposure ages referred to in this study have been published, and we assume are accurate within their reported uncertainties. Pinedale and Bull Lake type locality CRN ages, from the work of Pierce (2003), are listed below.

Table 4

Cosmogenic radionuclide ages for the Pinedale and Bull Lake type locality moraines (Pierce 2003).

	Bull Lake	Terminal Pinedale	Recessional Group	Difference (last two columns)
^{10}Be age	120–130 ka	20.1 ± 1.0 ka	17.6 ± 0.8 ka	2.5 ka

On the other hand, the only cosmogenic radionuclide work done for the Snowmass Creek Valley has been on the 'Qmc' deposit, which can be found in the Figure 7 inset, that yields a correlation to the Bull Lake glaciation (e.g. Mahan et al., 2014; Pigati et al., 2014). This age, along with very robust OSL dates of the basal lake sediments (e.g., Mahan et al., 2014), constrains the maximum thickness, ~200 m, of the paleoglacier during the Pinedale glaciation because the Ziegler paleontological site has been preserved since the Bull Lake glacier formed the moraine that the modern reservoir sits within.

3.3 Numerical modeling

Numerical models allow the visualization of complex outcomes, nonlinear couplings, and distant feedbacks. Dynamical models of Earth processes permit computational experimentation by compressing geologic time. Good mathematical models tend to be simple models – that is they have minimum 'knobs' to 'turn', and no hidden feedbacks or poorly interpreted boundary conditions. Numerical instabilities must always be addressed, especially when dealing with power-law relationships, for example: in the case of glacial ice rheology. The complicated nature of glaciers discussed thus far, reveals the merit behind the development of a dynamical model in order to both compress geologic time, and to mathematically encompass the interconnected processes involved in the evolution and dynamics glaciers over thousands of years. Numerical calculations carried out through computers allow for the visualization of how ancient glaciers occupied and shaped the landscape.

The development of a mathematical model begins first with a question aimed toward the understanding of a geological processes or system, which is then translated into a physical-mathematical description of changes in the important geological variables (e.g., Slingerland and Kump, 2011). After defining the problem in an organized and mathematical description, we transform the differential equations into finite difference approximations, allowing us to generate numerical models (Pelletier 2008; Slingerland and Kump, 2011). The logic behind a mathematical model goes as follows: if the premises are true, and the math is true, then the solution must be true (Slingerland and Kump, 2011). Model verification as defined by Slingerland and Kump, (2011), is the process of determining that a model implementation accurately represents your conceptual description of the model and the solution to the model. Model validation, on the other hand, determines the degree to which a model is an accurate representation of the real world from the perspective of its intended uses.

When referring to the dimensionality of a model, we use the following syntax, suggested by Pelletier (2008): 1-D numerical models have two spatial variables and one temporal, (i.e., landscape evolution of a topographic profile, or see Figure 13), for example, $f(x,z,t)$, and 2-D numerical models have three spatial variables and one temporal, (i.e. flow of a glacier over a real land surface) for example, $f(x,y,z,t)$. 2-D models tend to be computationally expensive, and are sometimes overly complicated. For these reasons we focus on 1-D numerical models to assess paleoglacial extent and Late Pleistocene climate conditions. Finite difference approximation algorithms are typically used, where most are either 1-D or 2-D staggered-grid, forward in time centered in space (FTCS) numerical models. Given that the mass balance of a glacier is driven by a combination of temperature (T) and precipitation (P) conditions in time and space, the most rigorous of models encompass all T, P, x, y, z, and t. Climate reconstruction models of this kind have been based on growing a model glacier to steady state with the right climactic parameters to match the terminus positions with the terminal moraine record. For example, Kessler et al., (2006), produced one of the first of these 2-D glacier models over a 50 km x 50 km map of King's Canyon National Park, CA, revealing the model's internal consistency with the mapped LGM moraine extent. Their model uses a mass balance cap of 2.0 m/yr and a mass balance gradient of 0.01 m/yr/m. Along these same lines Leonard et al., (2014), produced a 2-D glacial ice flow model over the Snowmass Creek Valley and the surrounding drainages to show the glacial ice extent at ~130 ka (e.g., Figures 7 and 39).

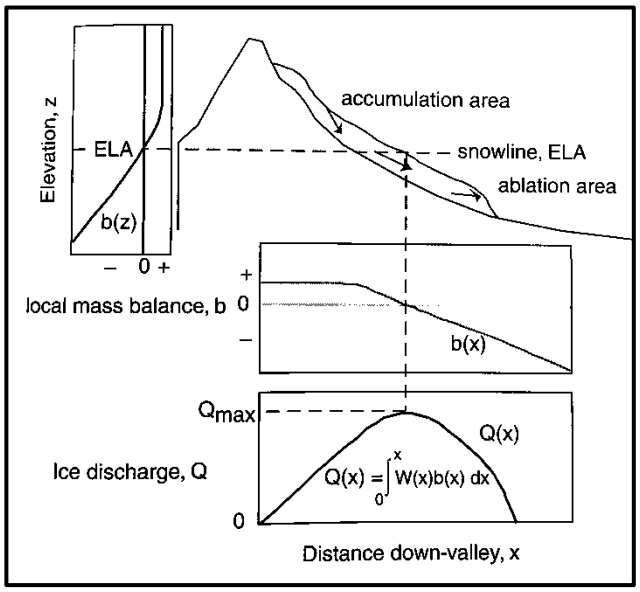

Figure 13

Simple 1-D schematic glacier model showing the relationship between discharge and mass balance from Anderson and Anderson, (2010).

Chapter 4 Upper Arkansas River Valley

4.1 Local geology and geomorphology

The study areas in this research are dominantly covered with two USGS quadrangles: the Granite quadrangle (Shroba et al., 2014) and the Harvard Lakes quadrangle (Kellogg et al., 2013). Figure 14 is a cropped version of the Harvard Lakes quad, which shows the Pine Creek valley on the left and the flood terraces on the right, while the Granite quad (next page) shows the surficial geology in the Clear Creek and Lake Creek glacial valleys.

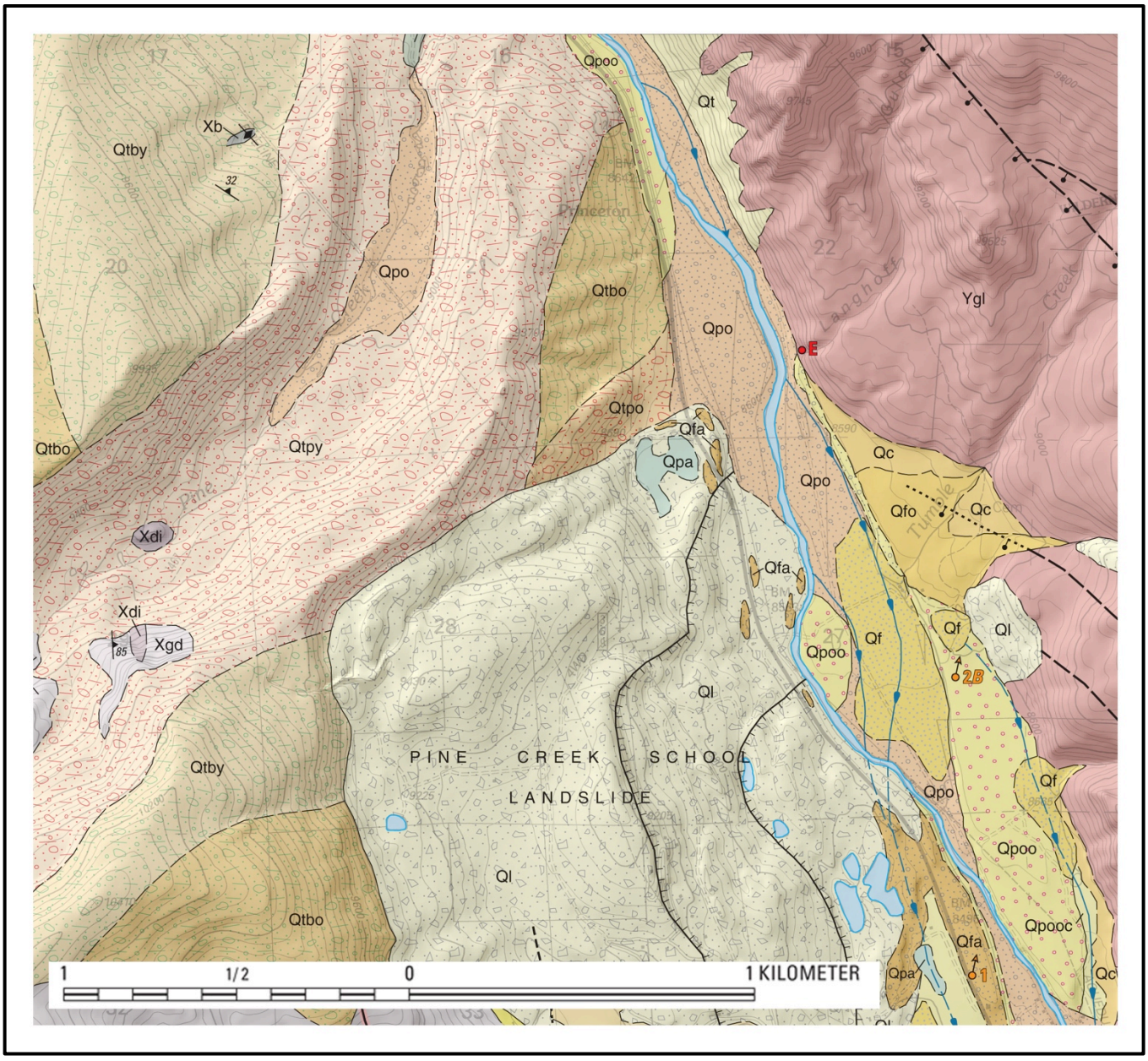

Figure 14

Condensed USGS geological map of the Harvard Lakes quadrangle. The flood terraces are denoted by Qpoo and Qpo. The Pinedale-aged Pine Creek glacial till is denoted by Qtpy, while the bill lake is Qtby. The ages of these two terraces are ~19 and ~17 ka, respectively (Young et al., 2011). Adapted from Kellogg et al., (2013).

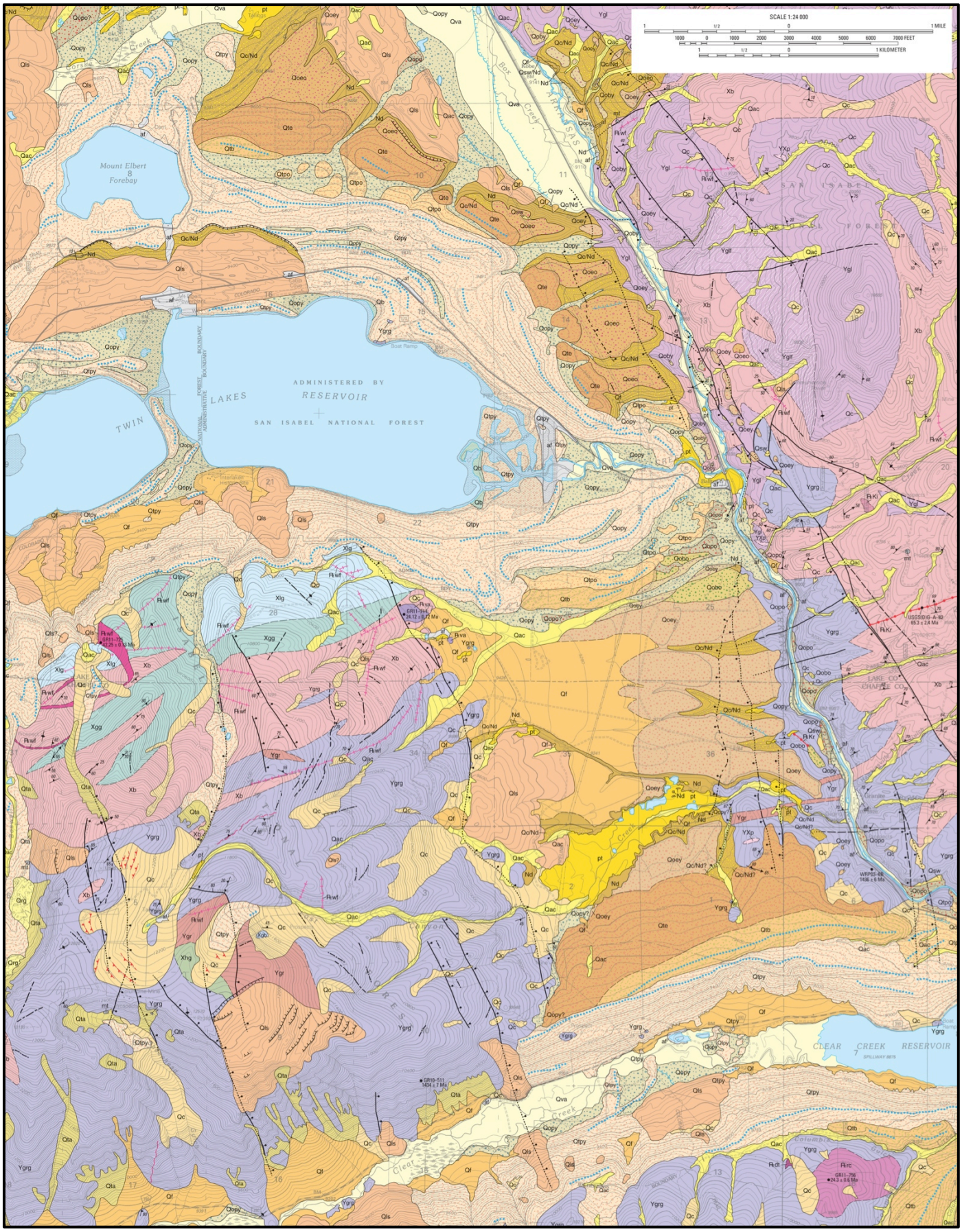

Figure 15: USGS geologic map of the Granite quadrangle (Shroba et al., 2014), map key found in the Appendix.

4.1.1 Bedrock and igneous geology

The complex geologic history of the upper Arkansas valley and along the lower flanks of the Sawatch Range and Mosquito Range near the town of Granite ranges from ancient Precambrian bedrock to recent surficial deposits The oldest rocks, exposed in the southern and eastern parts of the quadrangle, include gneiss and plutonic rocks of Paleoproterozoic age, which are intruded by younger plutonic rocks of Mesoproterozoic age (Tweto 1978). These range from felsic hypabyssal dikes, plugs, and plutons, ranging in age from Late Cretaceous or Paleocene to late Oligocene, locally intrude the Proterozoic rocks (Tweto 1978). There are even small andesite lava flows of upper Oligocene age that overly Paleoproterozoic rocks, just south of the Twin Lakes Reservoir (Tweto 1978). Gravelly fluvial and fan deposits of the Miocene and lower Pliocene Dry Union Formation are preserved in the post-30 Ma upper Arkansas valley graben, a northern extension of the Rio Grande rift (Shroba et al., 2014). Mostly north-northwest-trending faults displace deposits of the Dry Union Formation and older rock units, and LiDAR data suggests that two short faults, near the Arkansas River, may displace surficial deposits as young as middle Pleistocene (Kellogg et al., 2013; Shroba et al., 2014).

4.1.2 Glacial sedimentology and stratigraphy

Widespread and visually abundant, both in the landscape and via LiDAR imagery, glacial deposits range from Late Pleistocene (~11 ka at the youngest) in age to Pre-Bull Lake (~600 ka at the oldest) in age (Kellogg et al., 2013; Shroba et al., 2014). The youngest deposits are those from Holocene and very latest Pleistocene rock glaciers, Qrg on the map (Kellogg et al., 2013; Shroba et al., 2014). Then comes the till of Pinedale age (late Pleistocene), which is composed of mostly non-sorted and non-stratified, subangular and subrounded boulders to granules in a matrix composed of very slightly clayey, slightly silty sand (Kellogg et al., 2013; Shroba et al., 2014). Typical characteristics of these glacial diamicton deposits can be found in Figure 17. The stratigraphic correlation of these map units is also found in Figure 17. The Pinedale glaciers were as nearly ~400 m thick in the valley of Lake Creek and flowed ~31 km down-valley from an altitude of ~3,900 m to an altitude of ~2,780 m (Shroba et al., 2014). In the valley of Clear Creek, the glaciers were also as thick as ~400 m and flowed ~28 km down valley from an altitude of ~3,800 m to an altitude of about 2,680 m (Shroba et al., 2014). These glaciers generated abundant till deposits (Qt: Qtpy, Qtpo, Qtb, and Qte) and outwash gravel deposits (Qo: Qopy, Qopo, Qoby, Qobo, Qoey, and Qoeo) forming both large moraines and extensive outwash terraces, discussed above, within and near the upper Arkansas River valley (Nelson and Shroba, 1998; Shroba et al., 2014). Areas where glaciers have eroded pro-glacial lacustrine sediments, outwash, or sediments of the Dry Union Formation are richest in silt (Kellogg et al., 2013; Shroba et al., 2014). Deposits form boulder rich, prominent, sharp-crested lateral moraines along Clear Creek, as well as lateral and end moraines with similar surface morphology along Lake Creek and along Pine Creek (Kellogg et al., 2013; Shroba et al., 2014). Some of the boulders situated on the moraines are of granitic composition and get as large as 4–7 metes in diameter (Kellogg et al., 2013; Shroba et al., 2014). Units

Qtpy and Qtpo locally include small bodies of silt, sand, and gravel deposited by meltwater, overlain by till-derived landslide deposits, Qls (e.g., Figure 15). Moraine boulders typically are more abundant on moraines of the Pinedale glaciation than on those of older glaciations. This difference in relative abundance is probably due in part to weathering of surface boulders and possibly due to fewer and smaller boulders in till of Bull Lake and pre-Bull Lake age. Moraine boulders are less abundant and are more weathered on moraines of the Bull Lake and pre-Bull Lake glaciations than on those of the Pinedale glaciation, which we confirmed qualitatively in the field with a rock compressibility hammer. The deposits of the older Bull Lake unit, Qtb, form less prominent lateral moraines with rounded crests along and near the Twin Lakes Reservoir, Clear Creek Reservoir, and Dry Gulch near Pine Creek (Kellogg et al., 2013; Shroba et al., 2014). Glacial ice during the Bull Lake and pre-Bull Lake glaciations also must have flowed ~31 km down the Lake Creek valley to an altitude of ~2,800 m, and ~21 km or more down the valley of Clear Creek to an altitude of ~2,780 m (Shroba et al., 2014). Almost certainly, the pre-Bull Lake glaciations ultimately established the location of the modern glacial valleys. The very oldest till, Qte, on the north side of Clear Creek, ~80 meters above the river, was likely deposited at ~650 ka (Lisiecki and Raymo, 2005).

The extent of the glaciers that occupied the Clear Creek and Pine Creek valleys, thus far, is nicely constrained by the aforementioned geologic and geomorphic information,. The terminal moraines record the response of the Twin Lakes glacier to LGM inter-annual to decadal-scale climate variability (e.g., Figure 6). I approximated the expected Late Pleistocene glacial extent (e.g., Figure 16) by tracing existing geomorphic moraines (Figure 6), and with the help of Briner, (2009), McCalpin et al., (2010), and Lee, (2010). The steep eastern flank of the river channel, previously dubbed the 'whamout', would have allowed the glacial ice and debris to completely slam into the wall and dam the Arkansas River.

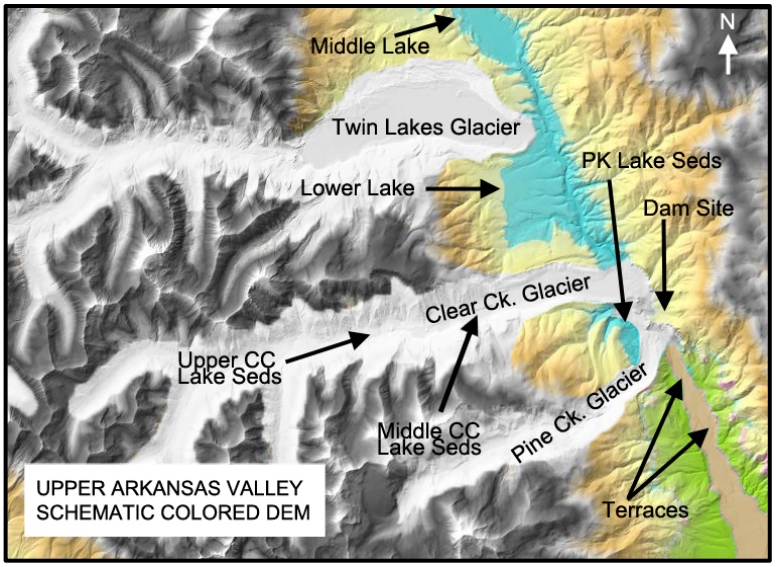

Figure 16

This annotated DEM schematically depicts the landscape, including the approximate glacial extent around ~20 ka. The flood terrace deposits (only present below the dam site) are brown, glacial ice and snow is white, glacially dammed lake is blue, the lowest elevations are green, the medium elevations are yellow, and high elevations are dark gray. The lake sediments and terraces that I found are shown with the black arrows.

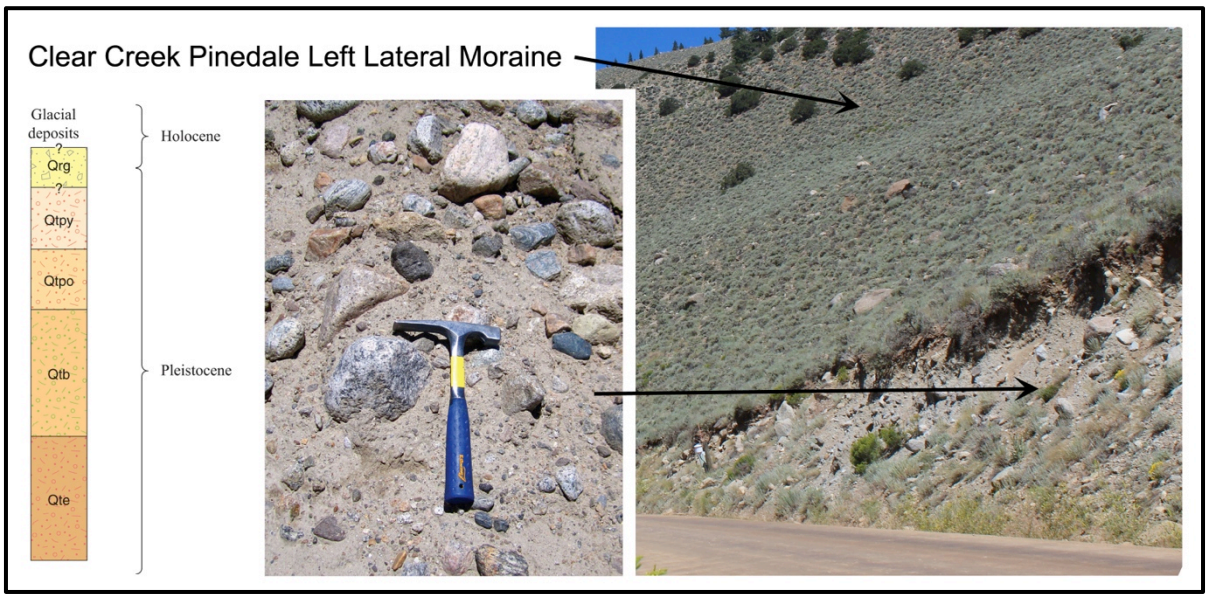

Figure 17

Typical diamicton-glacial deposits of study area look like this. The photo on the right is the Clear Creek road cut. Deposits are matrix supported, sub-rounded to sub-angular clasts, with grain sizes ranging from clay to boulders.

4.1.3 Lacustrine sedimentology and stratigraphy

Deposits of Late Pleistocene age are widespread in the Granite quadrangle (Shroba et al., 2014). Glacial outwash and post-glacial alluvium; mass-movement deposits transported by creep, debris flow, landsliding, and rock fall; till deposited during the Pinedale, Bull Lake, and pre-Bull Lake glaciations; rock-glacier deposits; and placer-tailings deposits from hydraulic mining all exist in the study area. Well-preserved glacial lake sediments are less abundant, and are generally too small to depict on the geologic map quadrangles. I discovered three small outcroppings (e.g., Figure 16 or 18) of fine-grained glacial lake sediments.

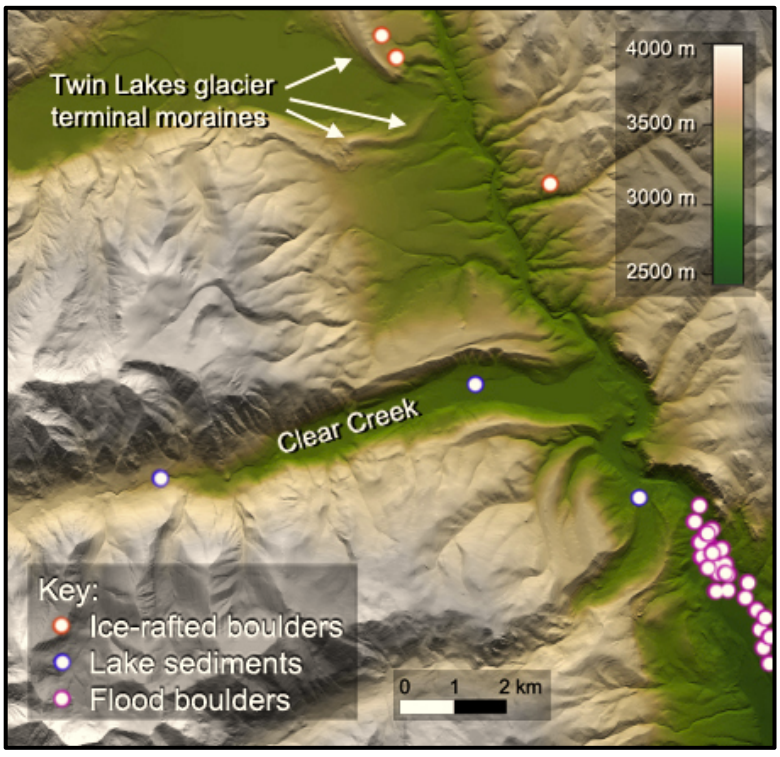

Figure 18

The figure to the right shows the three key pieces of evidence for this study. Three new locations of lake sediments are the blue dots, the red dots show the ice-rafted boulders, and the purple shows the flood boulders. The lower lake sediments (Figure 23) are the eastern most plotted in this figure.

Only one of these locations (see upper lake sediments, Figure 16) has horizontally laminated glacial lake sediments, ideal for in situ geochronologic methods. These sediments were found at an elevation of 2840 meters ~5 km up Clear Creek valley. This new evidence (e.g., Figures 18–21) shows that a lake up Clear Creek must have existed after the glacier that occupied the valley had already retreated, sometime post ~15 ka, based on one CRN age up-valley. After making this first discovery, I made a second trip in the fall and found preserved organic matter in the horizontal laminae, as well as more lake sediments elsewhere in the valley.

Figure 19

Organic plant matter samples from the highest lake sediment site: both in situ (left), and after extraction (right). The figure at right is a 60 times magnification of the organic matter. The organic layer here is ~190 cm long.

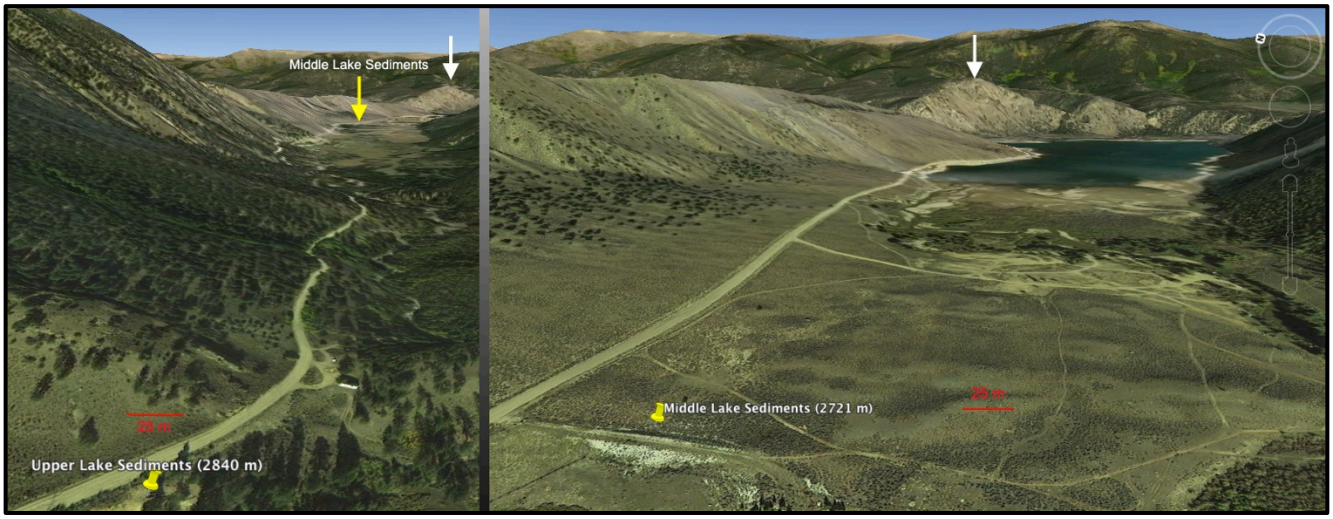

Figure 20

This figure shows the location and elevations of the upper and middle Clear Creek glacial-flour lake sediments. The white arrow in the figures is the top crest of the 'whamout' of the damsite. The middle lake sediments were not preserved fully, and were deformed without laminations, seemingly reworked since deglaciation (see Figure 22). Better preservation of the upper lake sediments is shown by their horizontal laminae (Figures 19 and 21).

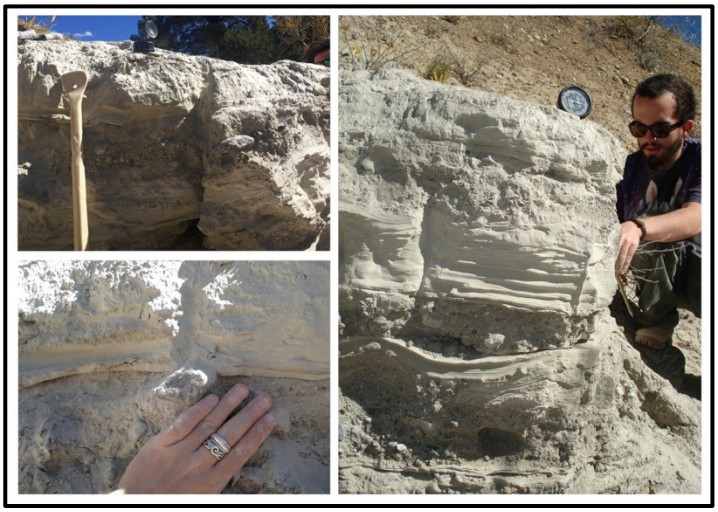

Figure 21

Field images of the upper lake sediments, capped by an aggradation transition into shoreline/fluvial deposits.

Figure 22

Field images of the middle lake sediments location, found beside the road, with no organic matter present.

Figure 23

Field images of the lower lake sediments near Pine Creek terminus possibly sub-glacial. Field notebook in the image at right for scale. Complete deformation suggests the sediments have been transported since deposition.

The difference in elevation between the upper and middle lake sediments suggests a total thickness of the glacial-flour stratigraphy that is nearly ~120 m thick (2840 m – 2720 m). This thickness suggests that this smaller glacial lake in Clear Creek valley was longer lived than the large lake impounded by the glaciers. The age of the middle sediments that I have found is likely older or the same age as the upper sediments, if OSL dating or other dating techniques were to be employed in future studies. One additional outcropping of gray silty glacio-lacustrine deposits has been reported by Shroba et al., (2014), that is too small to show at map scale, also exists on the north shore of the Twin Lakes Reservoir ~2 km northwest of the eastern edge of modern Twin Lakes. Additional evidence of the existence of these lakes lies in deposits of very fine sands ~20 m thick, penetrated by drill holes beneath deposits of till and outwash along the axis of the Twin Lakes dam (e.g., Tweto 1979) that probably records the proglacial or ice-marginal lake impounded by the during the Pinedale glaciation. Three landslides along the estimated shoreline of the 'Granite' glacial lake (i.e., Figure 26) provide the last pieces of indirect evidence of this lake, which has been suggested to be caused by reversed hydraulic gradients in the saturated sediments when the dam failed and the lake rapidly drained (e.g., Lee 2010; McCalpin et al., 2010).

4.1.4 Catastrophic flood and outwash deposits

The class V whitewater rapid, dubbed the 'Pine Creek' rapid, owes its existence to large boulders (>5 m) in the channel bed that were likely deposited during catastrophic floods caused by the breach of glacial dams. Just downstream of this rapid there are two abandoned terraces that have different flood boulder size distributions. Just above the Pine Creek rapid, the river gradient is mellower and there are no flood boulders. Based on the field evidence discussed so far, the dam site for the lake(s) that catastrophically drained to produce the flood boulder deposits is directly on top of the modern Pine Creek rapid location, at the terminus of the Pine Creek valley.

Outwash deposited by the Arkansas River is rich in clasts of granitic composition, porphyry, and pegmatite. As expected, both the lithological composition of the floods boulders and the clasts in the outwash deposits primarily reflects that of the main bedrock units in the glaciated headwaters of these streams. I measured boulders on the two terraces, which are the two most widespread flood deposits resulting from the Jökulhlaups. For simplicity hereafter, we refer to the older, higher elevation terrace (Qpoo) as terrace 2, and the lower, younger terrace as terrace 1 (Qpo). The flood boulder deposits of terrace 2 are higher than the terrace 1 deposits, and seem to reflect a flood of larger magnitude. Terrace 2 is older, as confirmed by the ^{10}Be surface-exposure ages of ~19.2 ± 0.1 ka, while terrace 1 has ^{10}Be surface-exposure ages of ~17.8 ± 0.6 ka (Young et al., 2011). This older flood may have undercut the right-lateral Pine Creek moraines, creating slope instability allowing for the slumping of the Pine Creek School landslide, composed almost entirely of till of the Bull lake glaciation. Although the Bull Lake moraines of the Clear Creek and Pine Creek valleys indicate the Bull Lake glaciers were at least as large as the Pinedale glaciers and similarly dammed the Arkansas River (Lee 2010), no clear evidence of a Bull Lake flood

exists in this part of the valley. Additionally, the oldest possible flood based on field evidence has been recognized as a flood that coursed down, at the time, a relatively broad and flat valley probably around MIS-16, at ~640 ka.

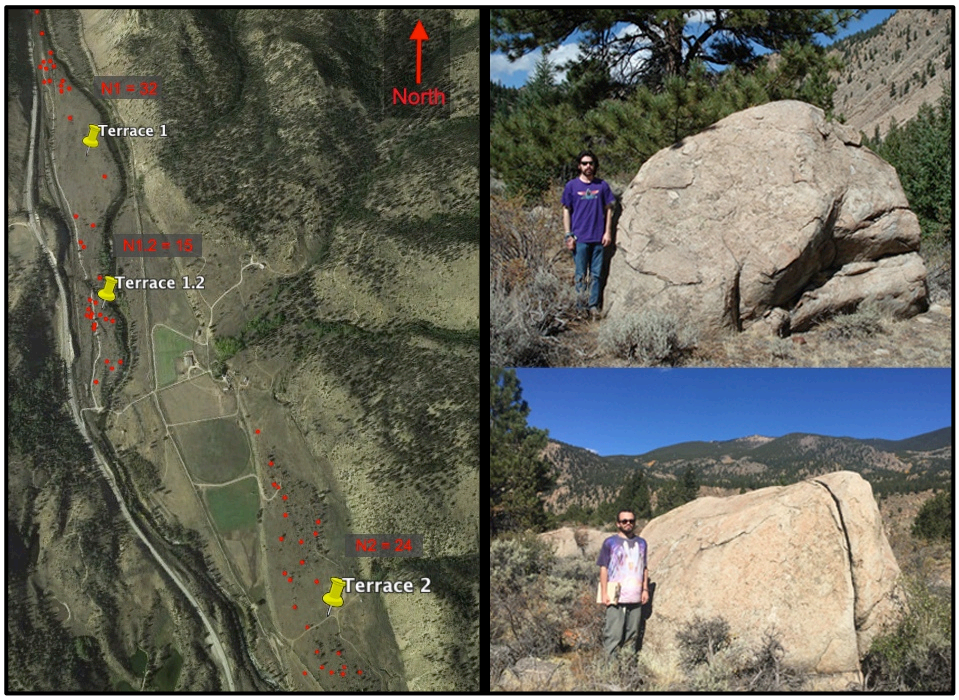

Figure 24

Field images of two of the largest catastrophic glacial flood boulders on the right, and in Google Earth mapped locations of the flood boulders (red dots) are given on the left. See appendix for raw field data of boulder sizes.

The Jökulhlaups seem to have eroded a new channel and outwash plain ~18 m below the Qpoo gravels; the youngest terrace gravels, Qpo, that composes the surface of terrace 1. It has been previously suggested (e.g., Lee 2010; Brugger et al., 2011) that the two different lakes that produced the two Jökulhlaups probably nearly the same dimensions as previous lakes because boulders of similar size were deposited. I however, present new evidence that the two floods were of different magnitudes, and occurred concurrently, 1000–2000 years apart. Contrary to the suggestion of Lee, (2010), that the upper terrace is Bull Lake in age, these two different floods are almost certainly Late Pleistocene in age, based on the ^{10}Be ages, and the results of my numerical modeling.

After the last breakout flood that produced the Qpo deposit, the ancestral Arkansas River changed course several times, eventually establishing a channel, Qpoc, against the west side of the valley south of Morrison Creek. The southeast part of the Pine Creek School landslide failed again, diverting the Arkansas River to the east into its present course. Subsequent alluviation by tributary streams built alluvial fans that buried many areas along the valley margin, which has since partially obscured some of the terrace and flood relationships.

4.2 Flood boulders: field data and statistics

Building on what I discussed in section 3.1.2, the boulders from the two terraces can be statically characterized with the histograms plotted below, revealing the two different modes of flood boulder sizes. Each time the ice dam failed, the glacial lake emptied almost instantly and catastrophically. The surging floodwaters tore out the end moraines, as well as large granitic blocks from the eastern valley wall, and carried these boulders downstream. We use a torque balance (see Chapter 5) to analyze the depth of the water, and hence the discharge required to transport the largest boulders found on the downstream terraces. The data in Figure 25 reflects both human error and natural randomness of catastrophic floods. We use the standard deviation to calculate the standard deviation of the mean as a method of propagating the uncertainties involved in flood discharge calculations. The roughness of the channel bed for the discharge calculations was determined by systematically measuring 120 of the b-axes (median diameter) of the cobbles and rocks distributed on terrace 1. The roughness of the bed is taken to be $1/10^{th}$ of the calculated 84^{th} percentile of the size distributions, D_{84}. The channel roughness is ~7.5 cm, because 84% of the 120 grains measured are smaller than ~75 cm in diameter (see Appendix for raw field data).

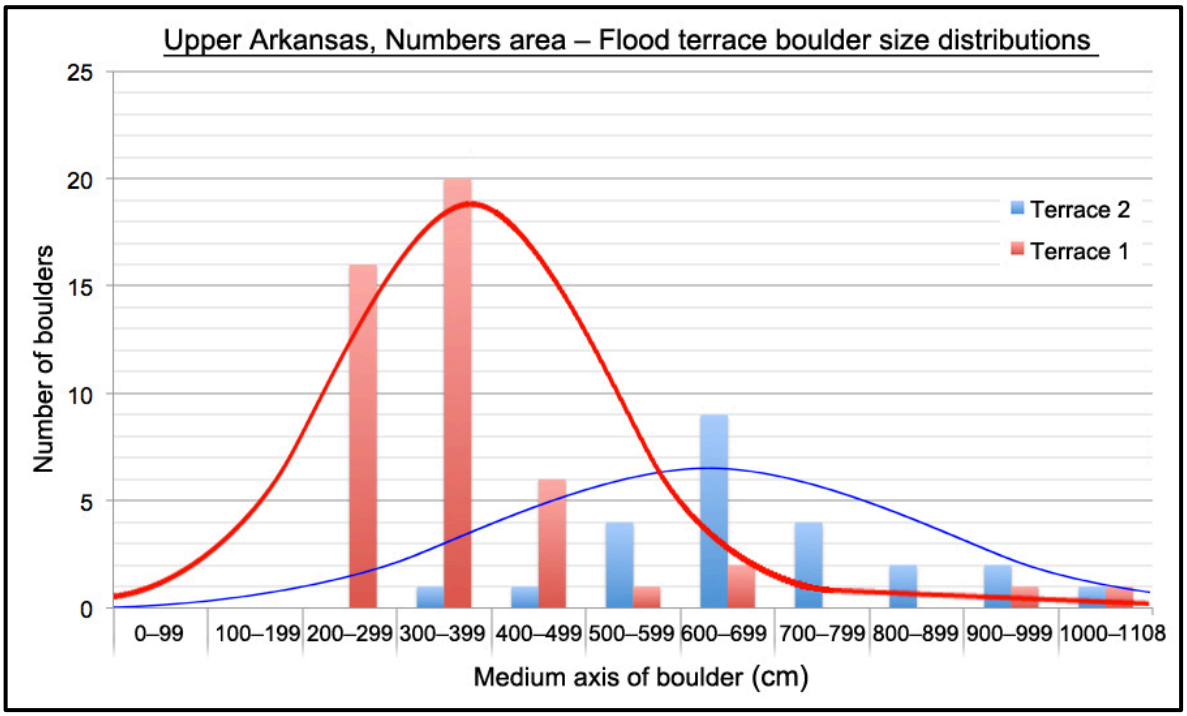

Figure 25

Graphical depiction of the glacial flood boulders size distributions. Statistics are also given in Table 3. This shows the bimodal distribution of boulder sizes between the two terraces. It is likely that this results from two different magnitude floods, where the mean boulder transported was ~3.8 m and ~6.8 m in diameter. The blue line (older, terrace 2) represents a flood of larger magnitude than the red line (younger, terrace 1). Flood discharge calculations are after the figures section in this fieldwork summary.

4.3 Glacial lakes: probable extents and volumes

The aforementioned strong evidence reveals that the glaciers in the Clear Creek and Pine Creek valleys impounded the Arkansas River and created at least two large lakes in the Arkansas valley upstream of the glacier twice during the Pinedale glaciation, probably at ~19 ka and ~17 ka. These lakes are required to have been short lived because widespread lacustrine deposits from the large lakes do not exist in the study area, and geomorphic features (such as shorelines) associated with these lakes are very difficult to observe within the Granite quadrangle. However, the field guide from McCalpin et al., (2010), shows hints of evidence that these shorelines did in fact exist. Further evidence lies in three ice-rafted boulders (e.g., Figure 19) near the toe of the Lake Creek glacier, which suggests the glacier was calving into the lower-middle portion of the lake, carrying large boulders from within the glacier on icebergs across the lake. The glacial lakes that formed above the ice dams were on the order of ~200 m deep and ~18 km long based on the estimated heights (also ~200 m, see Appendix) of the glacial dams from Lee (2010), which I confirm as a reasonable estimate based on my calculations in QGIS. This means that the lake level was ~2860 m, which has allowed me to calculate the total volume of the large lake, ~1.8 km^3.

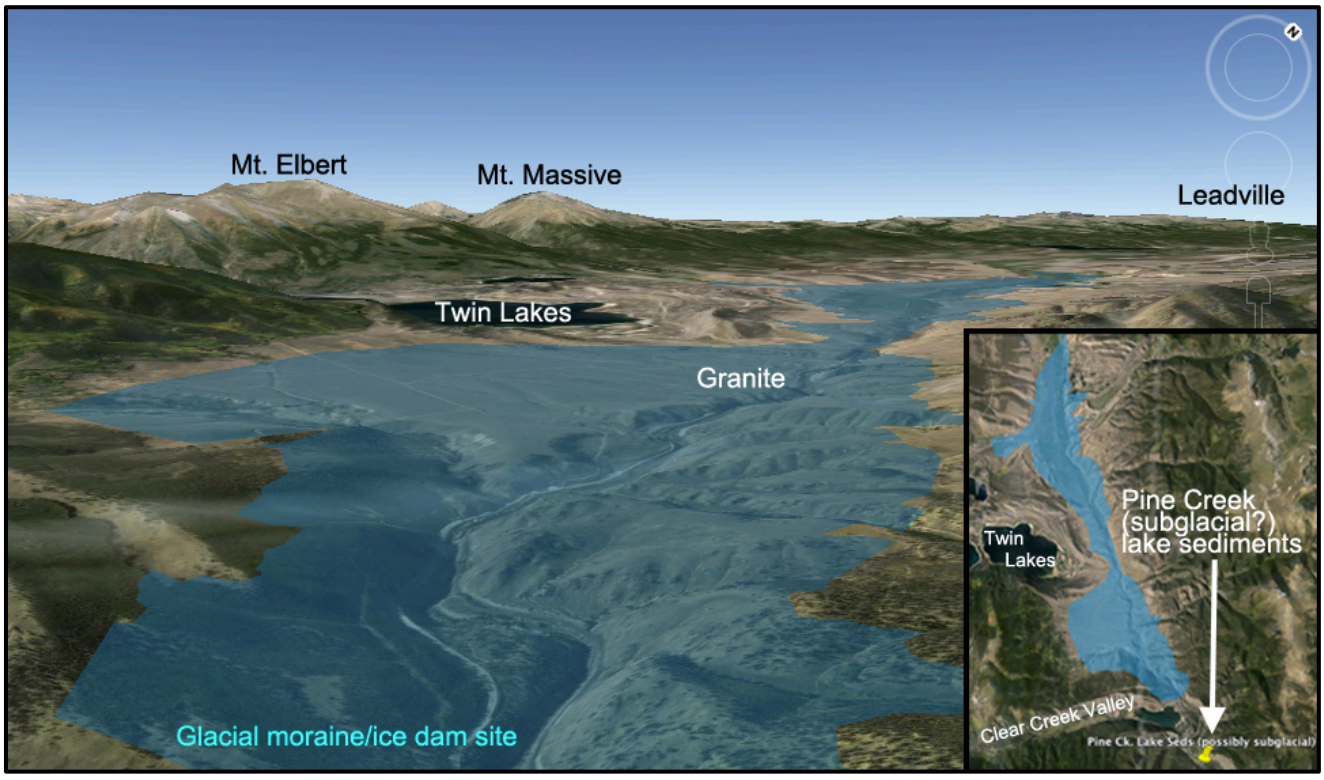

Figure 26

Extent of the upper, 'Granite', lake, by extending the water level across the topography at 2860 m. By taking the average depth of this volume in QGIS, and multiplying by the surface area, this yields a volume of ~1.8 km^3.

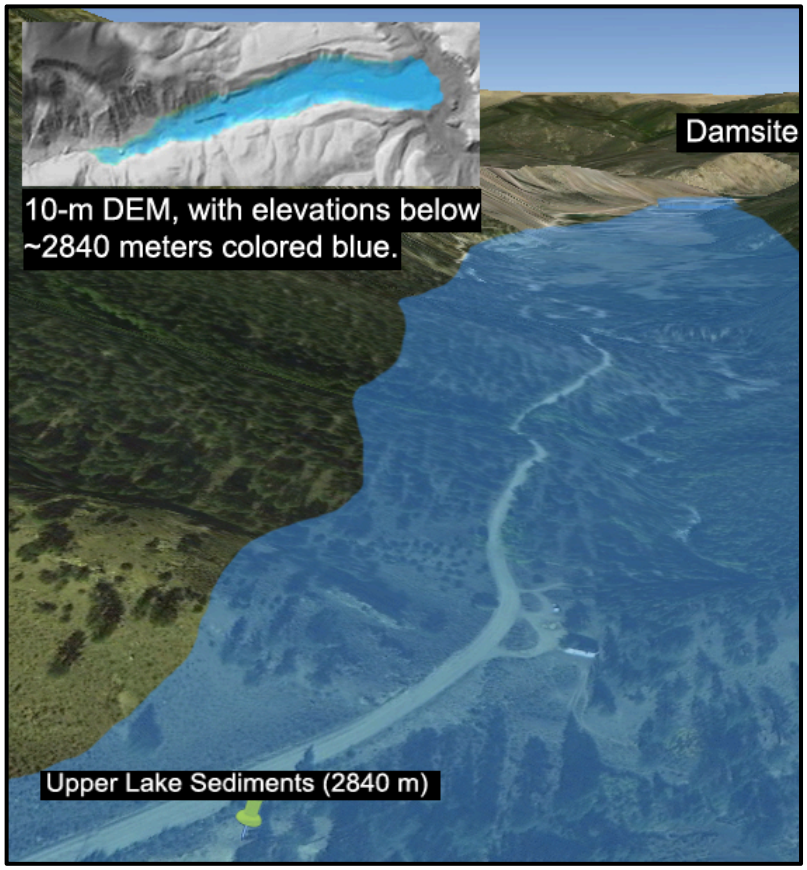

Figure 27

Estimated extent of the 'Clear Creek' lake, by extending the water across the topography at 2840 m. I have calculated the volume of this smaller lake in Google Earth to be on the order of ~0.2 km^3.

The approximate extent of these glacial paleolakes shows a larger 'Granite' lake, produced by damming the Arkansas River, and a smaller 'Clear Creek' lake, that was likely dammed by recessional moraines. These lakes are required to have existed at two different times. The 'Granite' lake would have existed at ~19 ka and catastrophically drained to produce the terrace flood boulders, with a maximum size of ~10 m. The 'Clear Creek' lake would have existed post deglaciation, or at least after the maximum glaciation, forming between 16–14 ka.

4.4 Geochronologic data

Six ^{10}Be surface-exposure ages of boulders on moraines within the map area indicate that till of unit Qtpy in the valleys of Lake Creek and Clear Creek dates from between 22–15 ka (e.g., Young et al., 2011). These ages are compatible with five ^{10}Be surface-exposure ages (21–16 ka) reported by Brugger, (2007), for boulders on deposits that form the outermost moraines of the last glacial maximum in the Taylor River drainage, ~20 km southwest of the map area. Three of these ^{10}Be surface-exposure ages are located in the valley of Lake Creek ~3, ~8, and ~17 km west of the map area, two ages are within a cirque ~12 km northwest of the map area, and one is in the valley of Clear Creek near the southern boundary of the map area (e.g., Young et al., 2011).

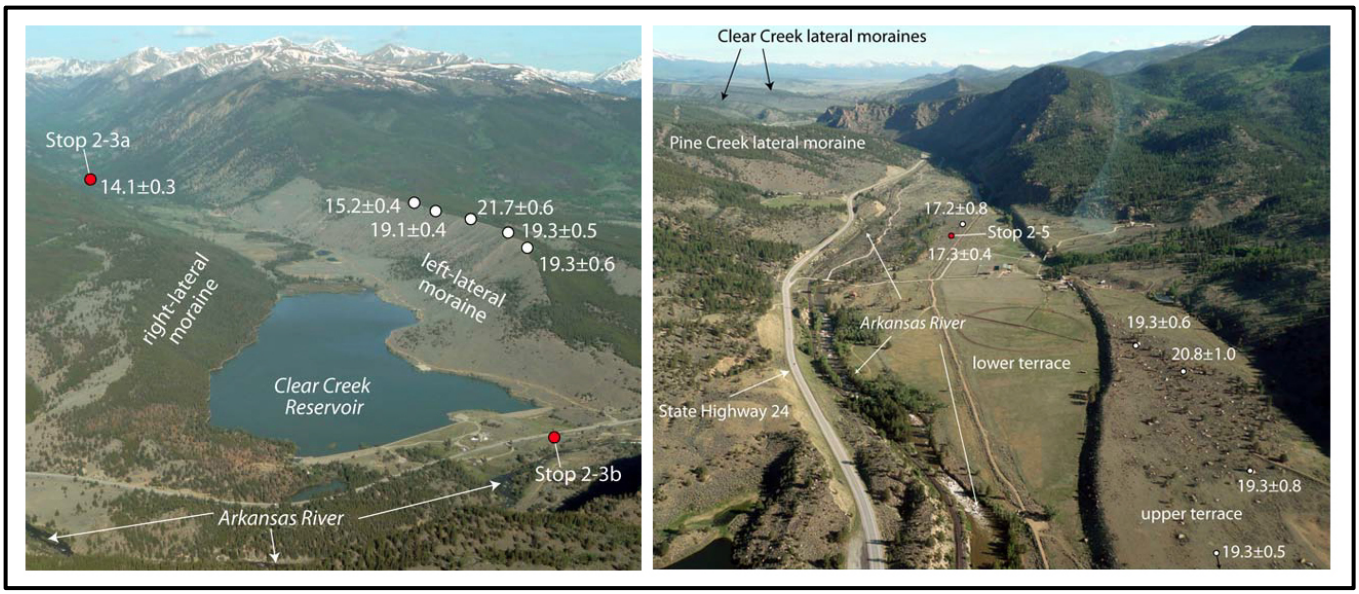

Figure 28

This figure shows the geographic location of the ^{10}Be ages collected and analyzed by Young et al., (2011). The upper terrace, at ~19 ka, is terrace 2 (Qpoo), while the lower terrace, at ~17 ka, is terrace 1 (Qpo).

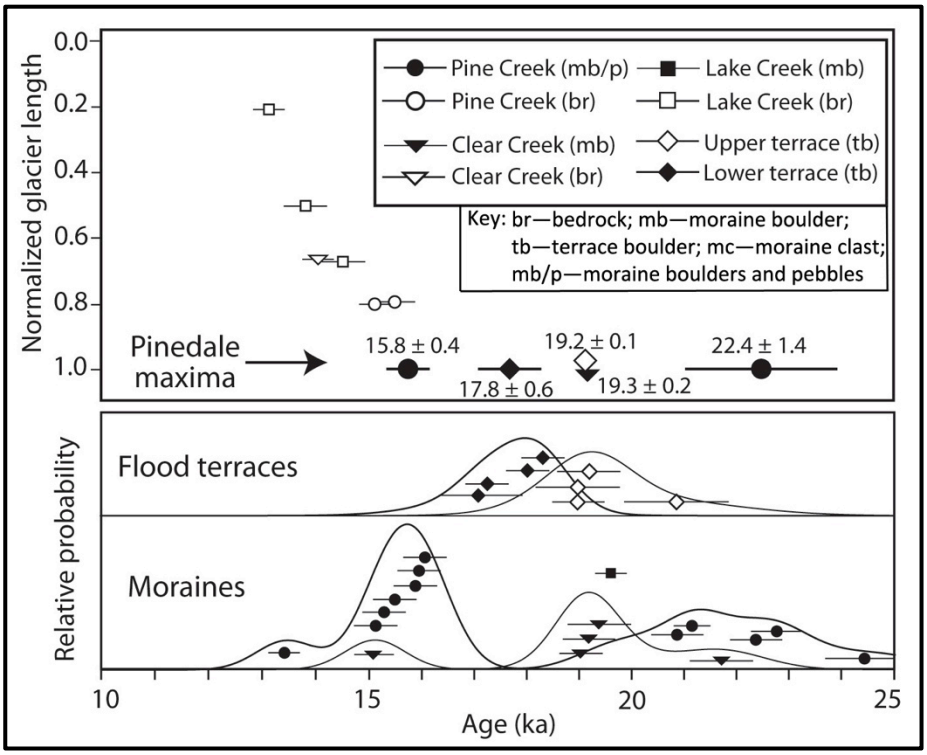

Figure 29

All ^{10}Be ages from upper Arkansas River study area (error bars are 1–sigma uncertainty); curves show summed probability distribution of all Pine Creek and Clear Creek moraine ages, and of all upper and lower flood terrace ages. Larger symbols at bottom of upper panel are average ages of each terrace and moraine mode, interpreted as four glacier maxima achieved by study glaciers. Positions of ^{10}Be ages from glacially sculpted bedrock from three valleys are normalized with respect to Pinedale max. length of each respective study glacier. (Young et al., 2011)

Chapter 5 Numerical modeling and calculations

5.1 Glacial model description

Our numerical models capture the essence of a simple glacial cross section. We use the geomorphic field observations, cosmogenic radionuclide ages, and the marine $\delta^{18}O$ record to constrain more than just the terminus position, but a dynamical evolution of the response of the glaciers to small thermal variations in the climate over time. We have used the computational program MATLAB to write a 1-D finite difference approximation, staggered-grid, forward-in-time and centered-in-space (FTCS), numerical model based on mass conservation in a column of ice. This follows the same principles employed by MacGregor et al., (2000), and Anderson et al., (2006), in which we force a temperate valley glacier over the valley axis topography, (e.g., Figure 5). We give a fixed mass balance gradient with an ELA approximated to the $\delta^{18}O$ record, and given random noise proportional to the uncertainty in the ELA, of ~200 m, suggested by Brugger (2010). One might expect a gaussian distribution of ELA's as shown in Anderson et al., (2006), as:

$$P(E) = \frac{2}{\sqrt{\pi}} \exp\left[-\left(\left(E - \bar{E}\right)/\sigma\right)^2\right] \tag{21}$$

which is also supported in the work of Anderson et al., (2014), and describes the probability density of the position of the ELA around its mean value at any given point within the desired time interval. In order to vary the ELA around its mean value, we generate random numbers at every calculation so that the ELA oscillates around its a mean value that we take as apparent ELA of the paleoglaciers. Our numerical model differs from previous models (e.g., MacGregor et al., 2000; Anderson et al., 2006), in which the glacier is eroding, because the bedrock profiles (i.e., Figure 5) in my numerical models are fixed in time and space. To check the validity of this assumption, there is a line of code that applies a smoothing function on the topography, which can be turned on or off, to view the effects of variable topographic noise on the response of the glaciers. The pattern of steady state glacial ice discharge can be found by integrating the total discharge down the valley, assuming that the time rate of change of ice thickness is zero:

$$Q(x) = \int_0^x W(x) \cdot b(x)\ dx \tag{22}$$

where $W(x)$ is the width of the glacier as a function of distance down-valley. Although our model is a 1-D cross-sectional replica of the glacial valleys, we incorporate the valley width as a function of distance down each valley. A simplification of glacial valley profiles (e.g., Anderson et al., 2006) can be expressed with following equation:

$$w(x) = w_{\min}\left(1 + \phi\left(\frac{x}{x_*}\right)^m \exp\left(-\frac{x}{x_*}\right)\right) \tag{23}$$

in which $w_{\min}$ corresponds to the width of the glacial valley at its distal end, ϕ determines the importance of the tributary widening, that is the number of tributaries in the top of the valley, m incorporates the shape of the

upstream expansion of width, and x_* is the length scale for the down-valley position of the maximum width and tapering scales the width. Figure 30 shows the final widths used in our numerical models:

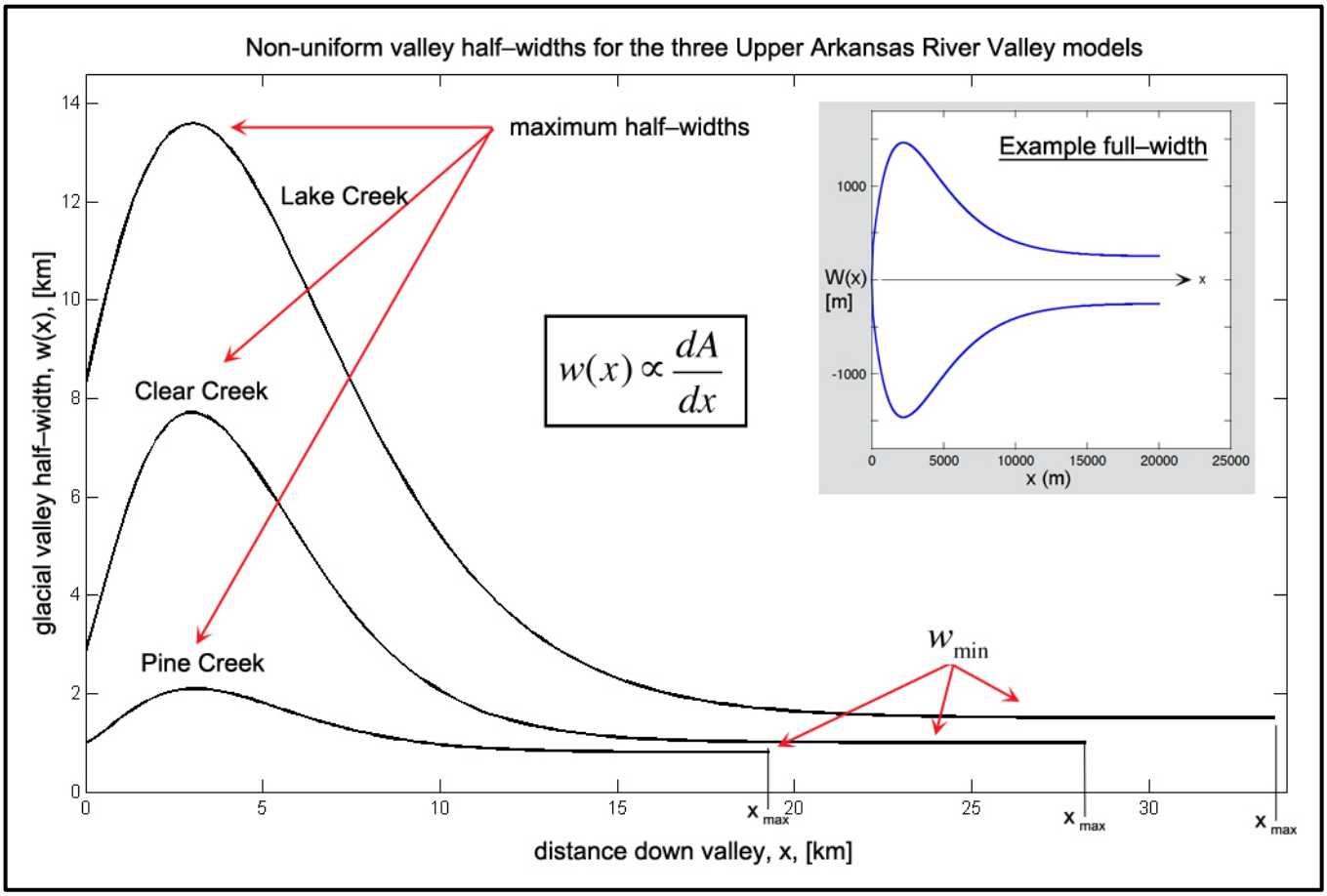

Figure 30

Graph showing the numerical assessment of non-uniform valley widths used in our models, based on equation 23.

5.2 Meteorological and climate constraints

ELA's and moraines generally decrease in altitude northward through the Rocky Mountains (Pierce 2003). Being that out study areas are near the same latitude, such variations are ignored. Modern ELA's in the Sawatch Range of Central Colorado have been suggested to be near the tops of the highest peaks, which in some areas is >4500 m. Keeping the models internally consistent, we prescribe an initial growth phase of the glacier (see Figure 31), with an ELA much lower than estimates of modern ELA's. This allows the glacier to reach nearly steady state initially and grow to a length that is suitable for expected extent in the valley for sometime between ~24 ka and ~22 ka. After this approximation, while the glacier is now occupying the land surface, growth of the glacier is accomplished by two small oscillations of cold temperatures. To keep our models consistent, and as simple as possible, following Figure 10 we use a mass balance gradient of 0.01 m/yr/m. We give a mass balance cap value of

~0.6 m/yr, because our preliminary 2-D modeling was never consistent with our 1-D models for any other value. For example, glacier ice thickness vastly exceeded 400 m in nearly all valleys for mass balance caps above 1.0 m/yr.

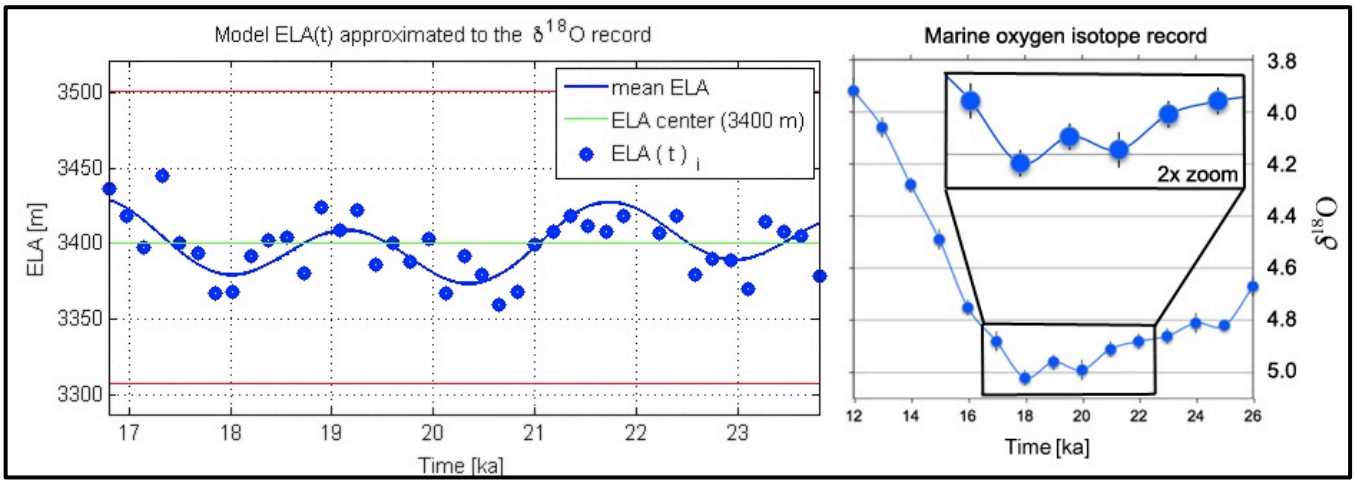

Figure 31

Prescribed climate chosen for our Upper Arkansas Models (left), based on the marine $\delta^{18}O$ record on the right. The curve that runs through the data in the $\delta^{18}O$ record was made through a simple cubic-spline interpolation. These small oscillations in the Earth's mean global temperature were likely felt by the glaciers here in Colorado. Note that the actual ELA that I gave the climate is my modeled Fourier-style fit to the $\delta^{18}O$ record and does not have actual data input to the model (i.e., it is simply a mathematical sine and cosine equation).

We checked the consistency of these assumptions with the preliminary 2-D runs with different code written by my advisor, Robert Anderson, incorporating the full topography of the glacial valley networks. The center of the prescribed climate runs with a mean ELA of ~3400 m, with a 2-sigma uncertainty denoted by ELA range of ~200 m, all based on Brugger's, (2010), statistics of the different ELA's in glaciers of the Sawatch and Elk Mountain ranges. This size of error in the ELA of ~200 m corresponds to ~1 °C of temperature variation, based on an adiabatic lapse rate of ~0.005 °C/m.

5.3 Upper Arkansas glacier model outputs

Our model runs over 7000 years of modeled time, between 23.8 ka and 16.8 ka, and has a very small time step that is required of glacial systems, of 0.0035 years (1.28 days), which therefore requires 2 million time steps:

$$n_{calcs} = \frac{t_{total}}{dt} = \frac{7000}{0.0035} = 2 \times 10^6 \qquad (24)$$

From this, the gaussian-style random number generation gives a maximum and minimum possible ELA that oscillates ~200 m above and below (red lines) the ELA 'center' (green lines) in my numerical models. We see that although the random noise has that high of an amplitude, the plotted $ELA(t)_i$ in the figures (~40 calculations plotted on each figure) still centers around the mean ELA curve prescribed. Each time the model runs a calculation, a different random number is generated that makes no two runs in the loop have the exact same numerical value. In order to optimize the model, I spent a lot of time doing guess-and-check manual optimization

to explore what parameters in my code best fit the expected constraints. Holding the climate fixed, the only parameters that I varied had to do with the 2-dimensional geometry, i.e., the width, of the glacial valleys (dominantly varying ϕ in equation 23). Various parameters combinations produce a given desired output, which is why parameter optimization is needed, and should be required for future studies. However, given the fixed meteorological conditions, and the characterization of basin geometry, my models produce reasonable estimates of the glacial extent and response to thermal forcings, which at least replicates one area of parameter space that reflects the CRN ages that have been published for the region.

We estimated the thickness expected for the glaciers using QGIS by taking topographic cross sections across the valleys, intersecting the end later moraines. An example of this kind of calculation is given in Figure 32, where we see the heights of the Clear Creek lateral moraines are ~250 m above the valley floor. Accounting for the bulge of ice that is typical of the distal ends of glaciers, modern sedimentation, and the presence of the Clear Creek reservoir, we see that the ice thickness should not exceed ~400 m at the end of the valley. Additionally, the height of the Pine Creek lateral moraines, 15 km down-valley, is ~200 m above the valley floor.

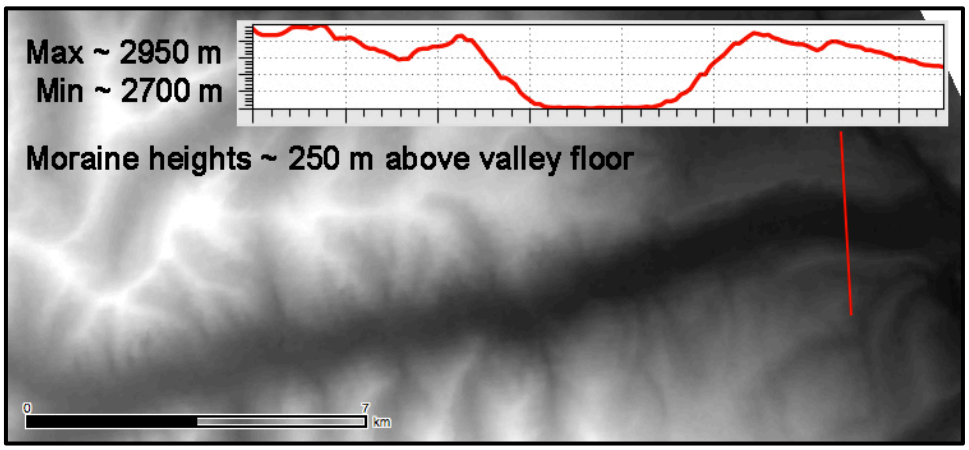

Figure 32

DEM calculation for the end lateral moraine heights in Clear Creek, used for approximating max ice thickness.

Moraine deposits that were left behind after the glaciers had begun to retreat have also allowed us to interpret fluctuations in ice extent, particularly in the case of the Lake Creek glacier (e.g., Figures 6 and 35). The response of the Lake Creek glacier to climate fluctuations is greater than that of the other valleys because it is the longest valley, with the widest catchment, and the lowest gradient in its distal portion. Our numerical model provides insight into the maximum extent of the Lake Creek glacier (Figure 35), timing constrained by the CRN age at the distal end of the terminal moraine (see Appendix for CRN data map) giving its approximate maximum extent.

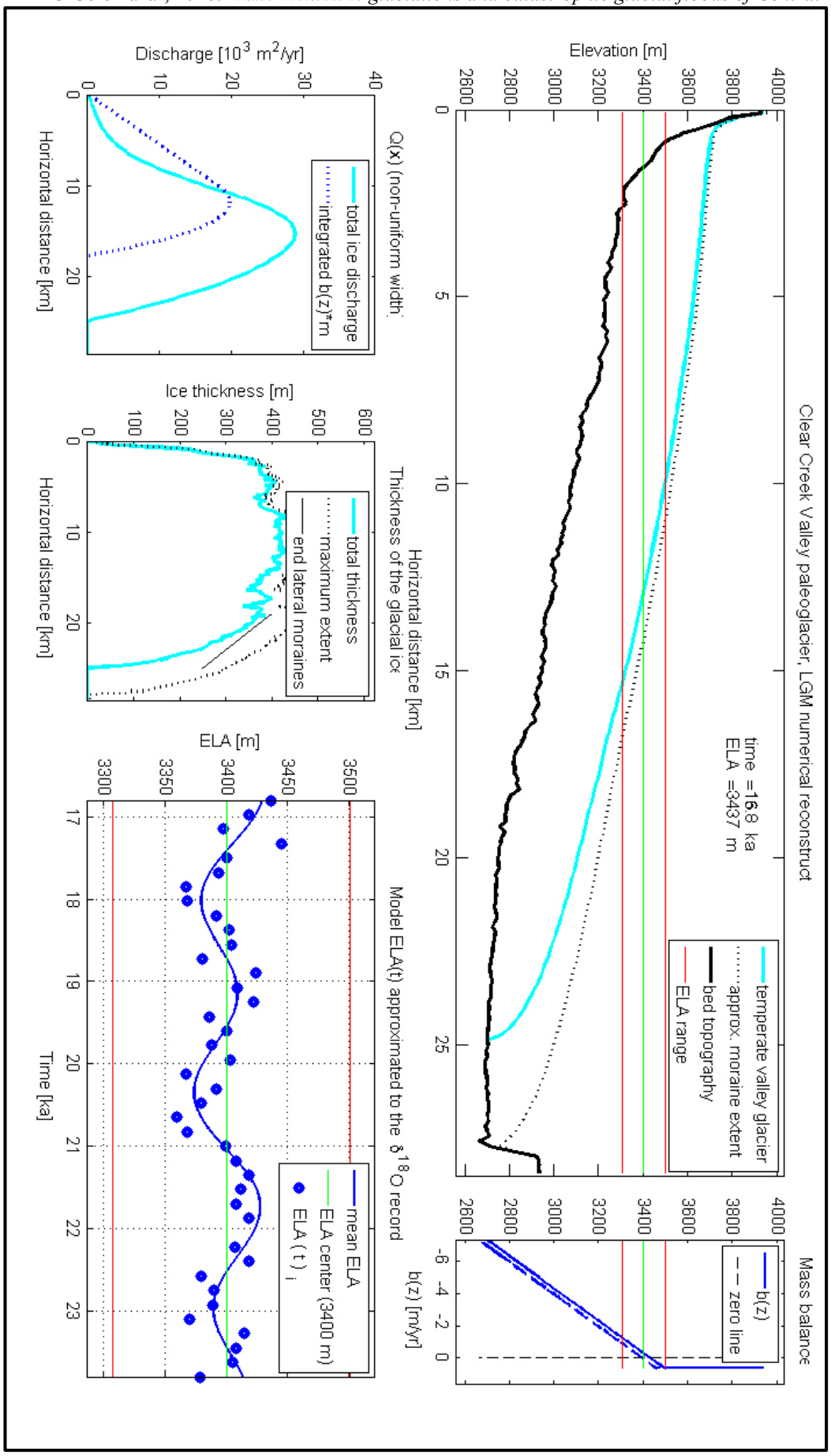

Figure 33

1-D mass conservation FTCS numerical model final output, 2 million calculations, after 40 frames for Clear Creek Valley

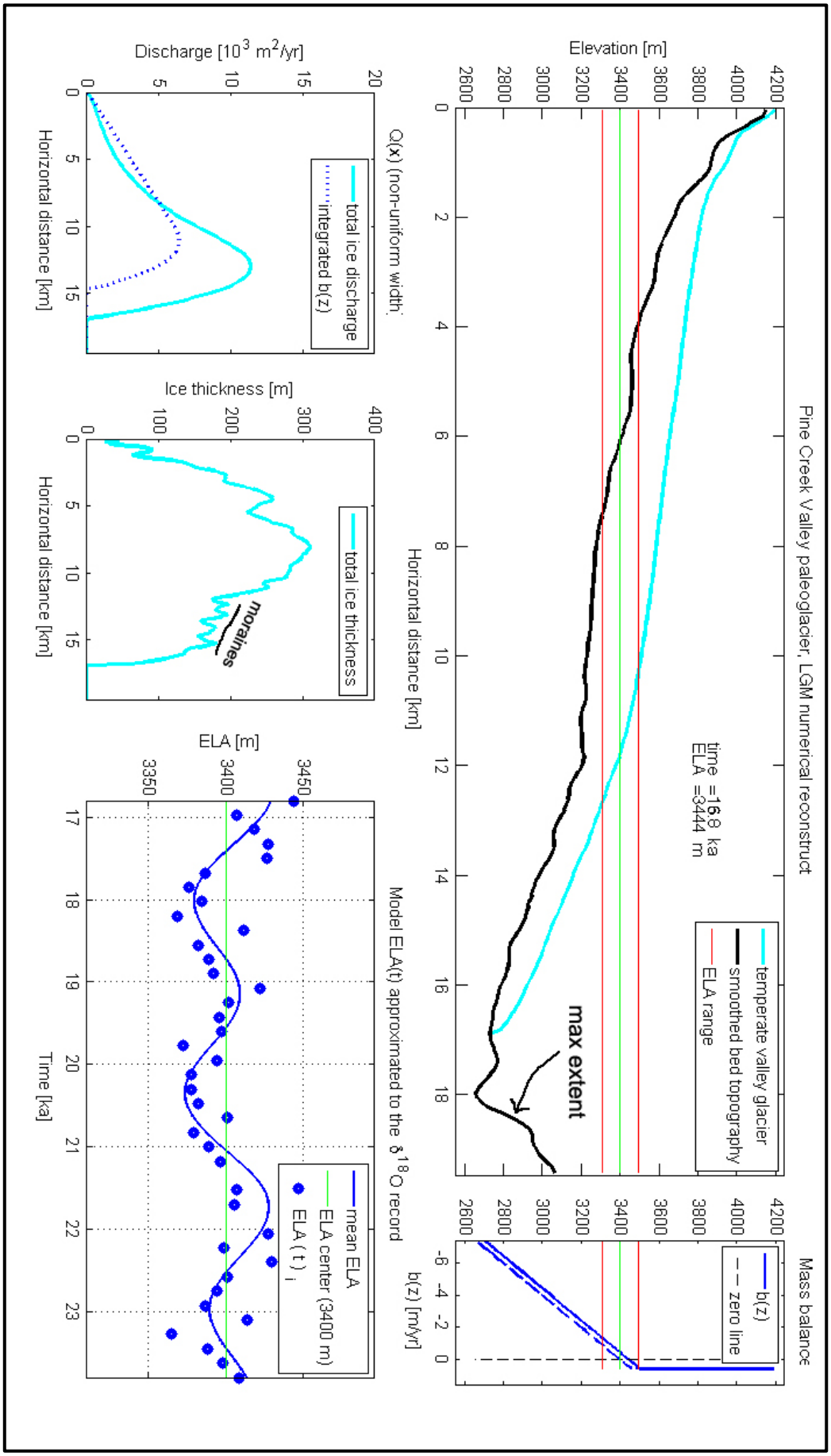

Figure 34
1-D mass conservation FTCS numerical model final output, 2 million calculations, after 40 frames for Pine Creek Valley

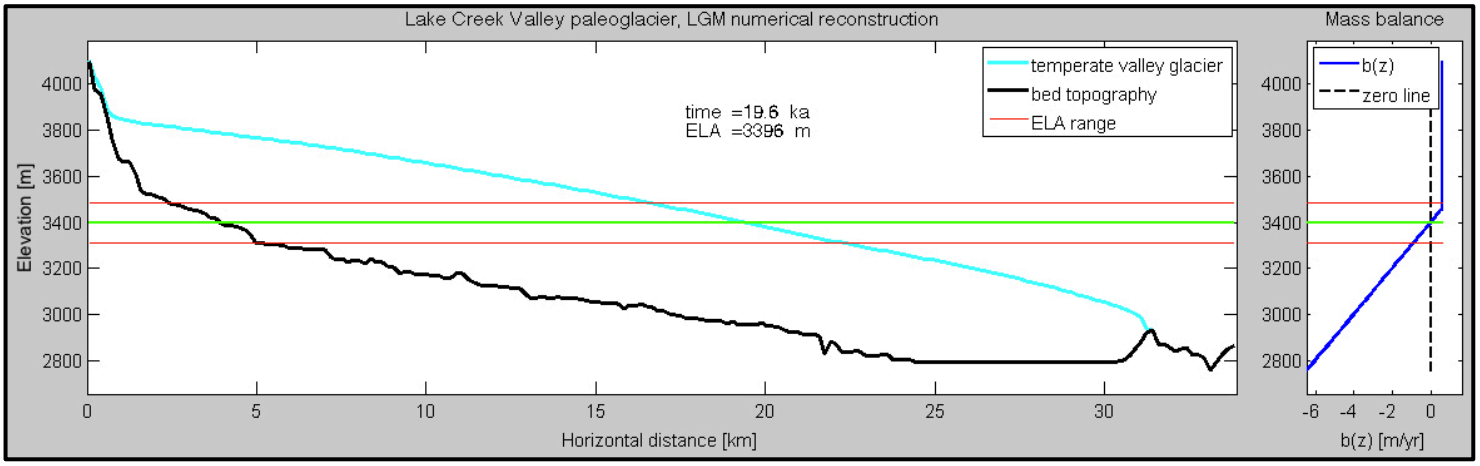

Figure 35

1-D mass conservation model final output, at ~19.6 ka, for the maximum extent of the Lake Creek Valley glacier.

5.4 Interpretations

The modeled ~3400 m ELA is consistent with the work of Brugger (2010), who suggests that temperatures in this region were on the order of –6 ºC to –7 ºC below the modern mean annual air temperature. Based on these small variations in the ELA, the damming of the Arkansas River was at ~20 ka and ~18 ka, and subsequently the jökulhlaups of the Granite glacial lakes occurred in between, at ~19 ka and ~17 ka. Although no numerical model can determine the exact nature of these glacial systems during the Late Pleistocene, these models we produced made provide further evidence that the time interval between floods was on the order of ~2000 years, an interval of time that is similar to the glacier disequilibrium response time due to thermal variations in the atmosphere over the same timescales. This model shows that the characteristic response time required to bring the glacier, that is out of equilibrium with the atmosphere, back to steady state, also depends on basin geometry.

The general topographic trend due to the elevation of the mountain ranges scattered around Central Colorado, and direction of the westerly winds at these latitudes, is that moisture in the atmosphere is depleted as you move eastward across Colorado. This is consistent with our choice for the mass balance cap of 0.6 m/yr compared to the higher value used later, of 2.0 m/yr, in the modeling of the Snowmass Creek glacier (i.e., Chapter 6). Additionally, we note that the distribution of other ice sheets and glaciers in the Western U.S. could have changed the spatial and temporal pattern of moisture delivery to these glaciers, affecting atmospheric flow from the west. We also must address the possibility that non-climactic forcings (e.g., Young et al., 2011) unique to each glacier may produce the variance in moraine ages, and apparent ELA's, rather than being driven by climactic fluctuations.

5.5 Flood discharge analysis

In order to account for the non-linearity of the critical shear stress and grain size, we have to employ a torque balance while defining the critical and basal shear stresses. Torque is a force that occurs in the cases of spherical or round geometries in nature, which is defined as the cross product between the force on a body and the lever arm to a pivoting point, i.e., R =/= R_0. The gravitational torque lever arm (Figure 6) is expressed as:

$$r = \left(\frac{R_0 \cdot R}{R + R_0} \right) \tag{25}$$

where the different length variables involved in this equation are defined in Figure 36. This lever arm dimension is needed in order to define the gravitational torque holding the grain in place, which is:

$$T_G = \left(\frac{R_0 \cdot R}{R + R_0} \right) \left(\frac{\pi D^3}{6} \right) (\rho_b - \rho_w) g \tag{26}$$

where ρ_b is the mean density of the flood boulders, 2650 kg/m^3, and D is their mean diameter. The drag torque, acting to move the boulder in the + x–direction, can be expressed as:

$$T_D = R \cos\theta \cdot \rho_w C_D \bar{u}^2 \left(\frac{\pi D^2}{8} \right) \tag{27}$$

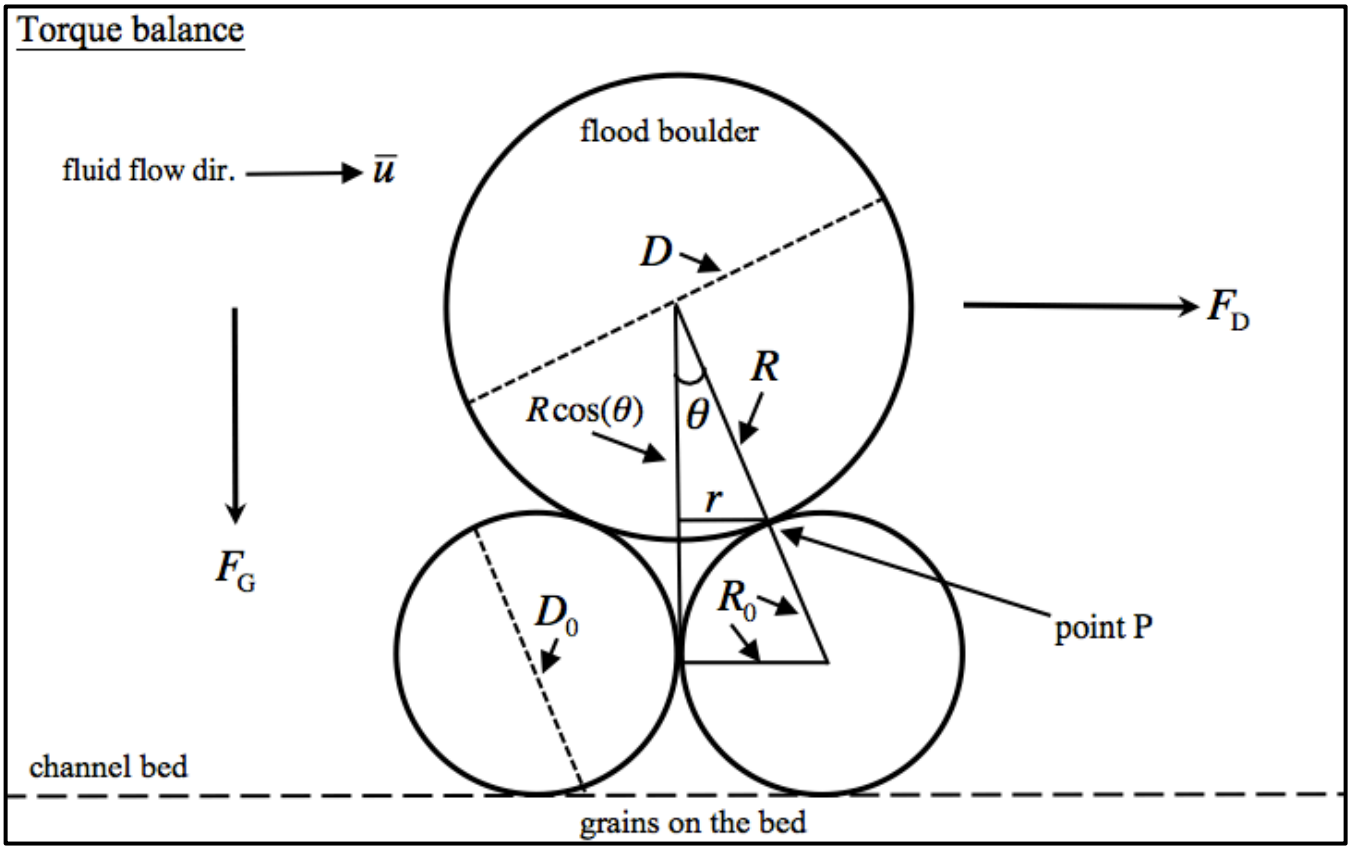

Figure 36

The set-up for the torque balance, made to figure out the geometry for the lever arms used in the torque equations.

where C_D is the drag coefficient, 0.4, for high-*Re*, of a nearly spherical boulder, and $\overline{u}$ is the 'law of the wall' velocity. Assuming that in order to for the boulder to be transported, the net torque on the object must exceed zero, we can equate the two torques:

$$\Sigma\, T_{NET} = 0 \quad \therefore \quad T_G = T_D \tag{28}$$

which means that in order for the boulder to move, the drag torque must overcome the gravitational torque. The critical threshold where the boulder starts to move and is entrained in the flow occurs therefore when:

$$\cos\theta \cdot C_D \overline{u}^2 = \left(\frac{R_0}{R+R_0}\right)\left(\frac{8}{6}\right)\left(\frac{\rho_b - \rho_w}{\rho_w}\right) gD \tag{29}$$

Now we define the critical shear stress and basal shear stress involved in order to simplify the above equation:

$$\tau_C = \rho_w g H S \quad ; \quad \tau_B = \rho_w u_*^2 \quad \rightarrow \quad \tau_C = \left(u_*^2\right)\left(\left(\rho_b - \rho_w\right) gD\right)\left(\frac{R_0 \cos(\theta)}{R+R_0}\right) \tag{36}$$

The effect of differing grain size on critical shear stress can be shown in Figure 37, in which we plot the threshold shear stress as a function of grain diameter on the bed. This can be illustrated through the simple torque situation calculation with equal grain diameters, the dotted red line, while the blue line shows the non-linear relationship, with different grain diameters ranging from $D_{84}/10$ to $10{*}D_{84}$. After performing this kind of analysis, we now can see how significant is the effect of the difference in grain size between the bed and the grain above it in the threshold shear stress.

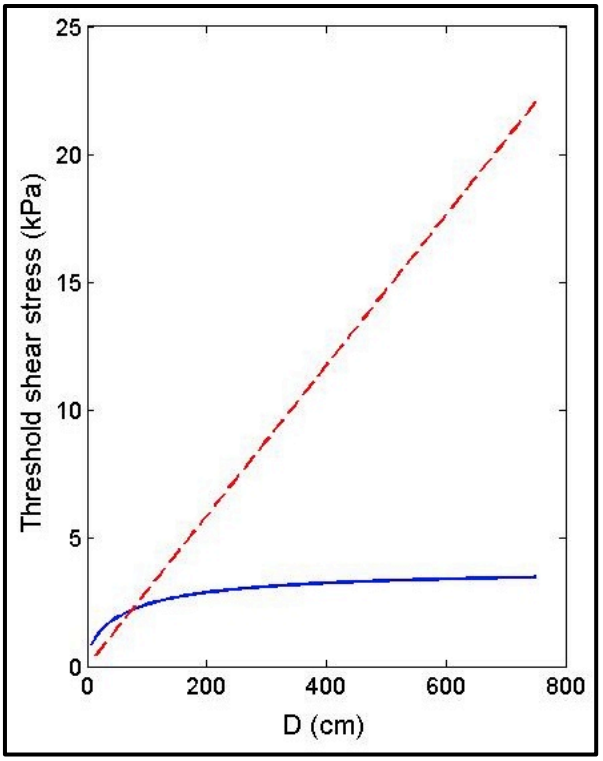

Figure 37

Threshold bed shear stress as a function of the diameter of the grains on the bed.

Plugging in the mean velocity (equation 17) into equation 29, and the shear stresses in equation line 30, allows for simplification by setting the two shear previous stresses equal to one another. Solving for the flow depth becomes:

$$H \approx \left(\frac{8}{6}\right)\left(\frac{k^2}{S}\right)\left(\frac{R}{R+R_0}\right)\left(\frac{D}{C_D \cdot \cos\theta}\right)\left(\frac{\rho_b - \rho_w}{\rho_w}\right)\left(\ln\left(\frac{10D}{D_{84}}\right)-1\right)^{-2} \quad (31)$$

This is the thickness of the fluid flow required to transport the boulders. This allows us to numerically estimate the flood discharge, to at least 1 significant figure. The fractions and ratios in this equation do not matter as much as the sizes of the boulders involved and the roughness of the bed. Using this equation, I have calculated the approximate depth of the catastrophic floods. Flood depths are approximately ~8 m and ~9 m deep for the deposits on terrace 1 and terrace 2, respectively. Therefore, we see that based on our assumptions and given the uncertainty, the thickness of the water that drove the boulders downstream can be said to be 28 m deep for the flood of lesser magnitude at ~17 ka, and 30 m for the flood of greater magnitude at ~19 ka.

Brugger et al., (2011), used a similar numerical approach, with midrange value for channel roughness, yielding discharges for these floods of ~46,000 m^3/s. Allowing for differences in channel roughness, and flood boulder diameters, using equation 20 for the discharge, incorporating these new calculated flood depths yields a range of peak discharge between 50,000 m^3/s and 70,000 m^3/s. This leads me to conclude that the average peak discharge from the lake of ~60,000 m^3/s. The timescale for this drainage, using equation 21 is on the order of 12–10 hours. This is consistent with previous estimates from McCalpin et al., (2010), that the entire lake emptied in less than a day. Using modern discharge average estimates of the discharge in the Arkansas River, the lake would have taken approximately 10 days to fill up. This magnitude flood would have posed an enormous natural geologic threat to any large mammals inhabiting the region. It is important to note that there is a possibility of damming the Arkansas in more than just the simple ways explained, but we feel this is the simplest explanation revealed by the rock record.

Chapter 6 Snowmass Creek Valley

6.1 Local geology and geomorphology

The geologic setting of the Ziegler Reservoir paleontological site is somewhat unusual because sediments containing the Pleistocene fossils were deposited in a lake on top of a ridge (e.g., Figure 7). The lake basin was formed near Snowmass Village in Central Colorado when the Bull Lake glacier flowed down Snowmass Creek Valley and became thick enough to overtop a low point in the eastern valley wall and entered the head of Brush Creek Valley (Pigati et al., 2014). The glacier retreated at about 155–130 ka, near the end of MIS-6, leaving a moraine that formed the small alpine lake (Pigati et al., 2014). A sequence of these events is given in Figure 38 (e.g., Pigati et al., 2014). The preservation of the Ziegler Reservoir paleontological site shows us that during the Pinedale glacial maxima the glacier did not overtop the valley to the east (e.g., Figures 7 and 38), like it did during the Bull Lake glaciation. The maximum thickness of the ice in this valley must not have exceeded much more than ~250 m at the time (e.g., Figure 40). This constraint allows us to model the extent of the Pinedale glaciation of Snowmass Creek Valley. Thus, this site presents a unique opportunity to contrast the high-altitude climate in Central Colorado between that of Snowmass Creek Valley, and the Upper Arkansas River Valley, ~50 km east.

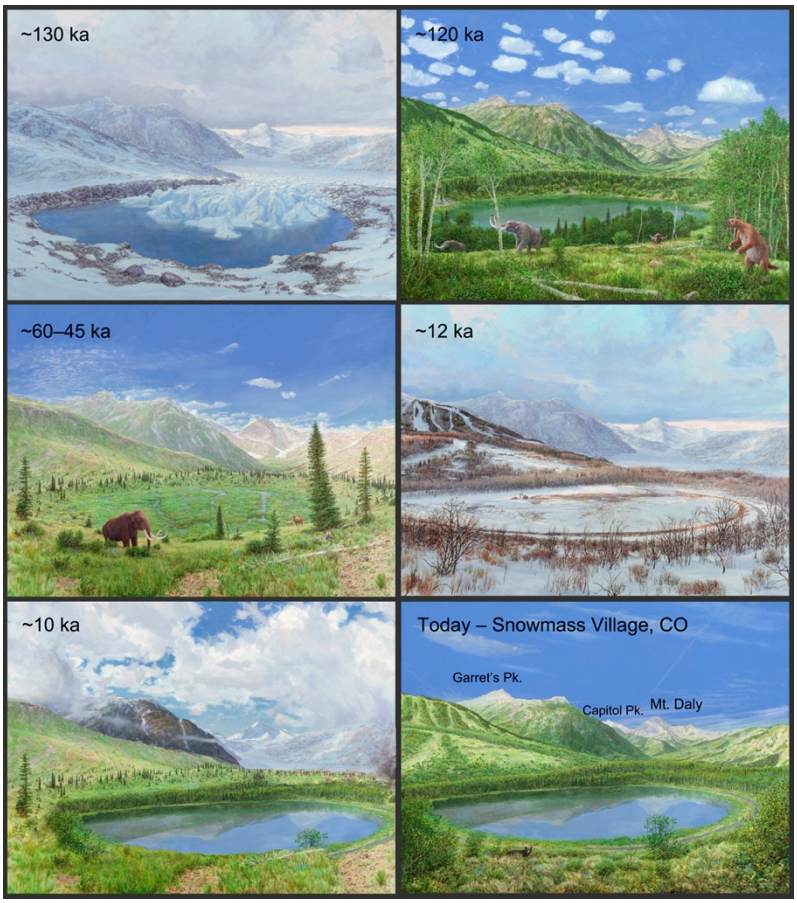

Figure 38

Artist's rendition of the sequence of events in the Snowmass Creek Valley at the Ziegler site (Pigati et al., 2014).

6.2 Numerical model and climate calculations

We used the same 1-D numerical model for reconstructing the glacier in the Snowmass Creek Valley as we did for the Upper Arkansas River Valley glaciers in order to estimate the difference in climate between the Bull Lake glacial maximum and the Pinedale glacial maximum in Snowmass. The 2-D glacier model (Figure 40) from Leonard et al. (2014), indicates temperature depressions on the order of approximately –6.7 ± 1.0 °C below the modern mean annual air temperature during Bull Lake glaciaiton.

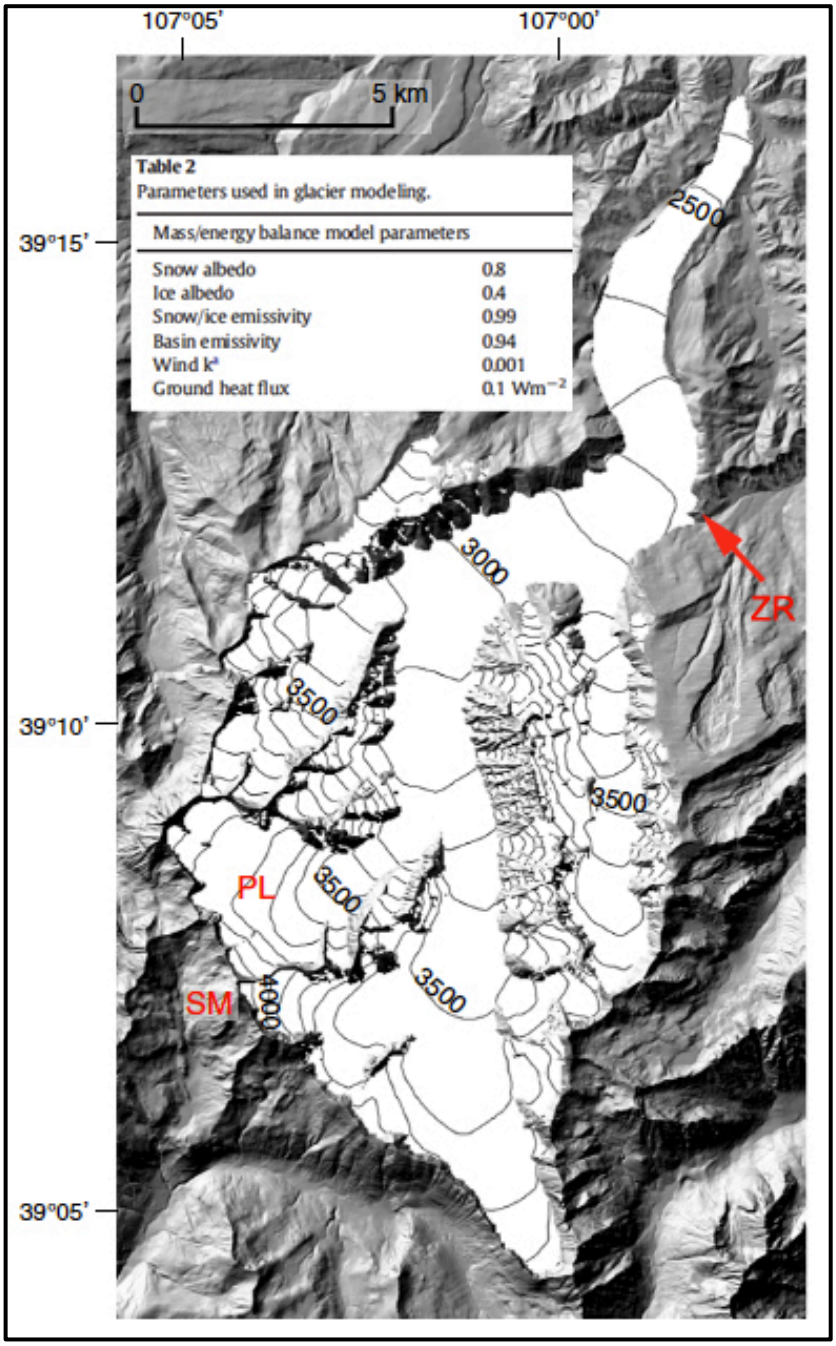

Figure 39

2-D glacier model output (Leonard et al., 2014) during Bull Lake (~130 ka) extent for the Snowmass Creek glacier, extending ~26 km down-valley, maximum thickness ~250 m, terminating at an elevation of ~2315 m.

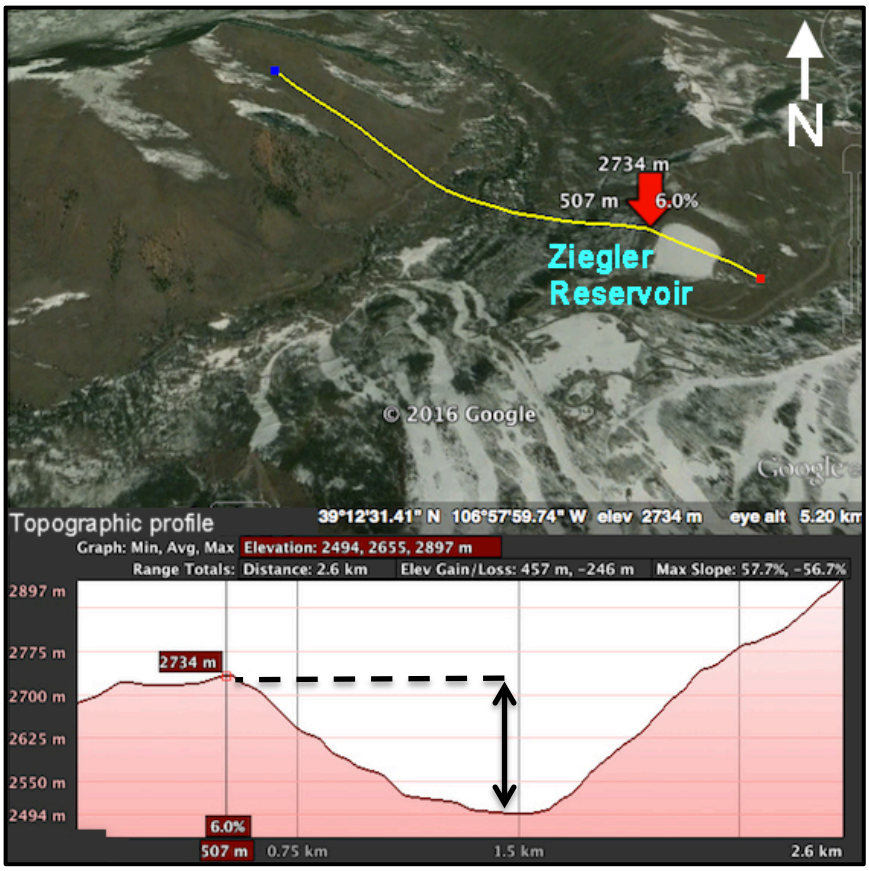

Figure 40

Google Earth image; profile used for determination of the maximum thickness of the glacier at Zeigler Reservoir.

My numerical model (e.g., Figure 41) indicates an apparent difference in the ELA of ~200 m between the glacial extent during Bull Lake glaciation (~3100 m) and during Pinedale glaciation (~3300 m). This would suggest that the glacier was approximately 4–5 km farther up-valley, reaching a maximum length of 20–22 km at its farthest extent near ~20 ka. This conclusion is also consistent with the location of mapped Pinedale moraines (e.g., the letter 'P' in Figure 7). This difference in ELA's corresponds to a temperature difference of ~1 °C warmer than the value reported the work of Leonard et al., (2014). Therefore, regardless of the actual scaled temperature values, we may estimate that the magnitude of temperature difference between the two glacial periods is a difference of ~1 °C, based on the adiabatic lapse rate we used of ~0.005 °C/m. It is important to note the possibility of the Snowmass Creek Valley ELA being ~100 m lower than the ~3400 m ELA's used in the Upper Arkansas River valley because of catchment shading, leading to colder localized temperatures due to the abundance of north-facing valley's. An east to west general decrease in ELA's has also been shown by the work of Brugger (2010). This would lead to significant discrepancies in our temperature depression interpretations for this region. We still suggest that the temperature difference between these two glaciations in the West Elk region was, $\Delta T = 1$ °C.

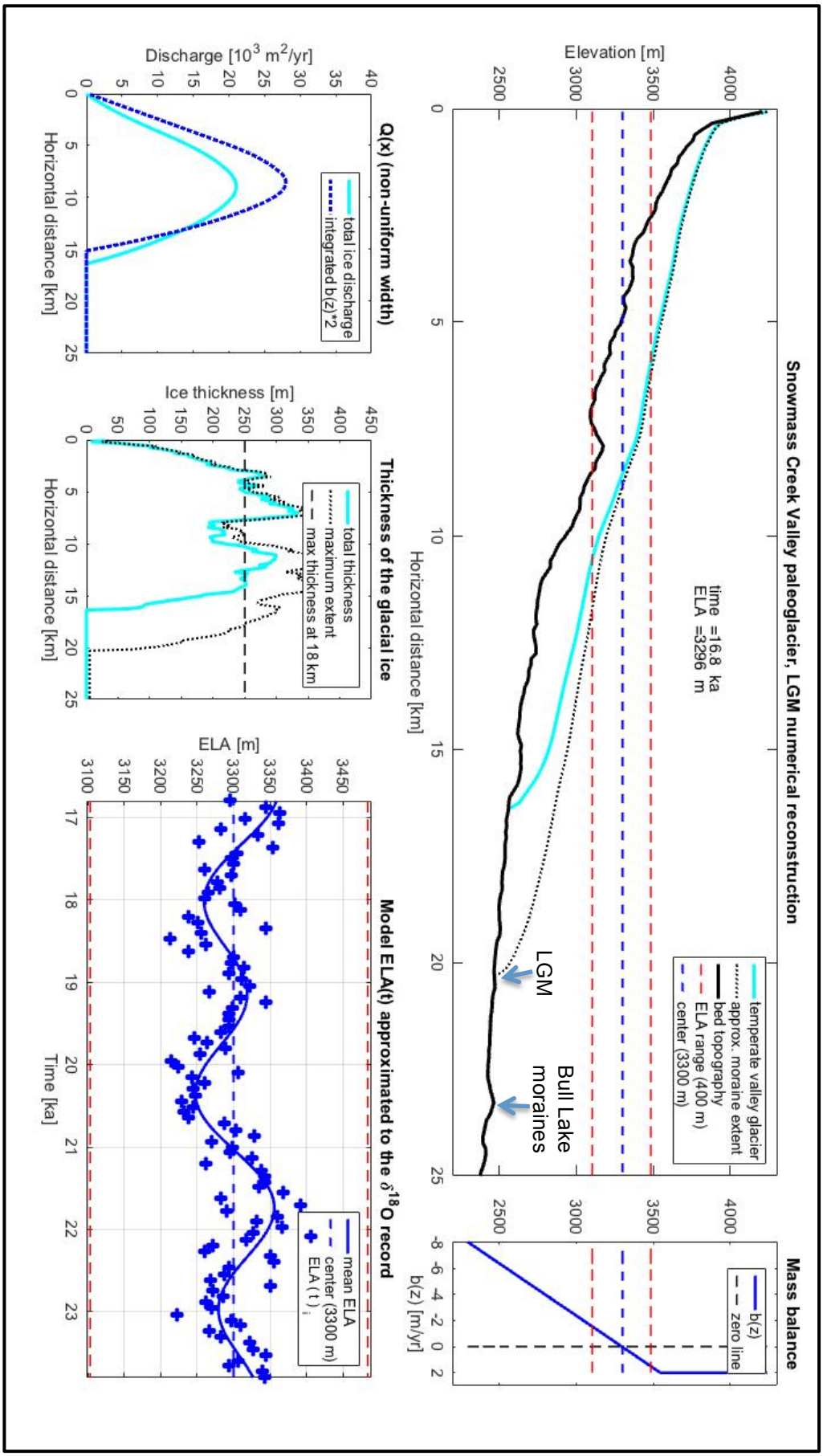

Figure 41

1-D mass conservation FTCS numerical model final output for the Snowmass Creek Valley glacier during the LGM.

Chapter 7 Discussion

I have calculated the probable climate of the Sawatch and Elk Mountain ranges of Central Colorado based on numerical glacier reconstructions. The uncertainty in my numerical glacier models is dominated by missing the complete 2-D catchment geometry, although we attempt to account for non-uniform glacial valley widths. Lesser, but still contributing to the uncertainty, is the lack of detail in the representation of the physical processes that occur underneath the glacier, i.e., glacial sliding, sub-glacial rivers and eskers, and the role of complicated and unknown bed geomorphology. An additional aspect of uncertainty is in my use of the non-eroding modern surface topography, because we are unable to know exactly what the bed topography that the glacier occupied thousands of years ago, and its pattern of bedrock erosion. In order to reduce the uncertainty, further 2-D modeling and specific parameter optimization would be required. There are many huge challenges facing future glacier and cryosphere modelers in reducing uncertainty, which I expect will require an interdisciplinary effort between glaciologists, geochronologists, climatologists, and computer scientists. Even with the best numerical model, if the data input used to constrain the model it is not reputable, then the predictions will not be reliable.

Approximate minimum ELA's for the two mountain ranges are on the order of ~3400 m for the Sawatch Range and ~3300 m for the West Elk's respectively, during the LGM. This corresponds to a range of temperature depressions of –6 °C and –7 °C. A detailed analysis of the catastrophic glacial outburst floods caused by the failures of these glacial-ice dams in the Upper Arkansas River Valley show large boulders, ranging from approximately 3–10 m in mean diameter, were transported by two different floods on the order of 40,000–60,000 m^3/s. The lake that existed over the modern town of Granite, Colorado would have drained in a day, with minimum timing estimates on the order of ~10 hours. New evidence has been presented of a previously undiscovered lake up Clear Creek Valley, that must have existed post-deglaciation, sometime after ~15 ka. Future work on the inter-annual climate variability on the moraine record left by the Lake Creek glacier may provide high-resolution insight into the past climate.

Glaciers are interconnected with human survival through natural geologic hazards, including: glacial outburst floods, groundwater storage fluctuations, and catastrophic rise in sea level. At least ~3.1 mm/year of the present rate of sea level rise, can be attributed to the loss of continental ice (Owen et al., 2009), while the other half of course is simply due to the net thermal expansion of the oceans. There is no longer any real debate on the fact that the Earth's natural climate variability, forced by changes in solar insolation over geologic time, has produced these natural glacial cycles that we can read in the landscape. However, the current rate of mean global temperature increase has skyrocketed, undeniably due to anthropogenic radiative forcing of greenhouse gasses. By creating models that reflect past climate conditions, this research builds on the knowledge of the magnitude of natural glacial hazards, glacier ablation rates, and potential groundwater storage over hundreds to thousands of years. In the near future the loss of glaciers will significantly impact human lives – through both natural geologic hazards occurring and in long-term groundwater depletion, on which thousands of people currently depend.

References

Anderson, R. S., Molnar, P., Kessler, M. A., 2006, Features of glacial valley profiles simply explained. Journal of Geophysical Research, v. 111, 1–14. doi:10.1029/2005FJ000344.

Anderson, R. S., and Anderson S. P., 2010, Geomorphology: the mechanics and chemistry of landscapes. Cambridge University Press, ISBN: 978-0-521-51978-6. Print – various chapters/pages cited.

Baker, V. R., 1978, Paleohydraulics and hydrodynamics of scabland floods, in Baker, V. R., and Nummedal, D., eds., The Channeled Scabland: A guide to the geomorphology of the Columbia Basin, Washington. Comparative planetary field conference, June 5-8, 1978. Planetary Geology Program, Office of Space Science, National Aeronautics and Space Administration, 59-79.

Bakke, J. and Nasje, A., 2011. Equilibrium-line altitude (ELA) definition, online dictionary, Springer 2016.

Blackwelder, E. (1915). Post-Cretaceous history of the mountains of central western Wyoming. Journal of Geology, 23, 97–117, 193–217, 307–340.

Briner, J. P., 2009, Moraine pebbles and boulders yield indistinguishable ^{10}Be ages: A case study from Colorado, USA. Quaternary Geochronology, v. 4, 299–305.

Brozovic, N., Burbank, D. & Meigs, A., 1997. Climatic limits on landscape development in the northwestern Himalaya. Science v. 276, 571–574.

Brugger, K. A., 2007, Cosmogenic ^{10}Be and ^{36}Cl ages from late Pleistocene terminal moraine complexes in the Taylor River drainage basin, central Colorado, USA. Quaternary Science Reviews, v. 26, 494–499.

Brugger, K. A., 2010, Climate in the Southern Sawatch Range and Elk Mountains, Colorado, U.S.A., during the Last Glacial Maximum: Inferences Using a Simple Degree-Day Model. Arctic, Antarctic, and Alpine Research, v. 42, no. 2, 164–178.

Brugger, K.A., Leonard, E. M., Lee, Keenan, and Bush, M. A., 2011, Discharge estimates for a glacial outburst paleoflood on the upper Arkansas River, Colorado, from an ice-dam failure model. Geological Society of America Abstracts with Programs, v. 43, no. 4, 10. [abstract]

Bryant, B., 1972, Geologic map of the Highland Peak quadrangle, Pitkin County, Colorado. U.S. Geological Survey Geologic Quadrangle Map GQ-932, scale 1:24,000.

Chaudhry, N. K., and Aranoff, R. P., 2015, Fieldwork in the Upper Arkansas River, CO. Locations: Clear Creek Valley and the Numbers whitewater rapid put–in, Central Colorado. Fieldwork pics in thesis document.

Copland, L., Sharp, M. J., Dowdeswell, J. A., 2003. The distribution and flow characteristics of surge-type glaciers in the Canadian High Arctic. Annals of Glaciology, v. 36, International Glaciological Society.

Faure, G., and Mensing, T. M., 2005, Isotopes: principles and applications. John Wiley & Sons, 3rd ed. ,613–638.

Foster, D., Brocklehurst, S. H., Gawthorpe, R. L., 2008. Small valley glaciers and the effectiveness of the glacial buzzsaw in the northern Basin and Range, USA. Geomorphology v. 102, 624–639.

Freeman, V.L., 1972, Geologic map of the Woody Creek quadrangle, Pitkin and Eagle Counties, Colorado. USGS Geologic Quadrangle Map GQ-967 scale 1:24,000.

Intergovernmental Panel on Climate Change (IPCC), 2013. Summary for Policymakers. In: Stocker, T.F., Qin, D., Plattner, G.-K., Tignor, M., Allen, S.K., Boschung, J., Nauels, A., Xia, Y., Bex, V., Midgley, P.M. (Eds.), Climate Change 2013: The Physical Science Basis. Contribution of Working Group I to the Fifth Assessment Report of the Intergovernmental Panel on Climate Change. Cambridge University Press, Cambridge, United Kingdom and New York, NY, USA.

Intergovernmental Panel on Climate Change (IPCC), 2014, Summary for Policymakers. In: Climate Change 2014: Impacts, Adaptation, and Vulnerability. Part A: Global and Sectoral Aspects. Contribution of Working Group II to the Fifth Assessment Report of the Intergovernmental Panel on Climate Change. Cambridge University Press, Cambridge, United Kingdom and New York, NY, USA.

Kellogg, K.S., Lee, Keenan, Premo, W.R., and Cosca, M.A., 2013, Geologic map of the Harvard Lakes 7.5' quadrangle, Park and Chaffee Counties, Colorado: U.S. Geological Survey Scientific Investigations Map 3267, v. 22, scale 1;24,000, http://dx.doi.org/10.3133/sim3267.

Lee, K., 2010, Catastrophic glacial outburst floods on the Arkansas River, Colorado. The Mountain Geologist, v. 47, no. 2, 35–57.

Leonard, E. M., Plummer, M. A., Carrara, P. E., 2014. Numerical modeling of the Snowmass Creek paleoglacier, Colorado, and climate in the Rocky Mountains during the Bull Lake glaciation (MIS 6). Quaternary Research, special v. 82, 533-541

Lisiecki, L.E., Raymo, M.E., 2009, Diachronous benthic $\delta^{18}O$ responses during late Pleistocene terminations: Paleoceanography, v. 24, 1–14.

Mahan, S. A., Gray, H. J., Pigati, J. S., Wilson, J., Liftond, N. A., Paces, J. B., Blaauw, M, 2014. A geochronologic framework for the Ziegler Reservoir fossil site, Snowmass Village, Colorado. Quaternary Research, special volume 82, 490-503.

MacGregor, K. R., Anderson, R. S., Anderson, S. P., Waddington E. D., 2000. Numerical simulations of glacial-valley longitudinal profile evolution. Geology, v. 28, no. 11, 1031–1034.

McCalpin, J.P., and Shannon, J.R., 2005, Geologic map of the Buena Vista West quadrangle, Chaffee County, Colorado: Colorado Geological Survey Open-File Report 05–8, scale 1:24,000.

McCalpin, J. P., Briner, J., Young, N., Leonard, E., Ruleman, C., 2010, Annual Meeting Quaternary Geology and Geochronology of the Uppermost Arkansas Valley. GSA, Field Trip 405, October 29-30.

McCalpin, J.P., Funk, J., and Mendel, D., 2010, Leadville south quadrangle geologic map, Lake County, CO, Colorado Geological Survey, 1:24,000 scale.

Menking, K. M., Anderson, R. Y., Shafike, N. G., Syed, K. H., and Allen, B. D., 2004, Wetter or colder during the Last Glacial Maximum? Revisiting the pluvial lake question in southwestern North America. Quaternary Research, v. 62, 280-288.

Molnar, P., England, P., 1990. Late Cenozoic uplift of mountain ranges and global climate change: chicken or egg? Nature v. 346, 29–34.

Mutschler F.E., 1970, Geologic map of the Snowmass Mountain quadrangle, Pitkin and Gunnison counties, Colorado. USGS Geologic Quadrangle Map GQ–853, scale 1:24,000.

Nelson, A. R., Shroba, R.R, and Scott, G. R, Quaternary Deposits of the Upper Arkansas River Valley, Colorado. Boulder, Colorado: American Quaternary Association, 8th Biennial Meeting, August 16-17, 1984, unpublished guide for Field Trip No.7, 51-57.

Nelson, A.R., and Shroba, R.R., 1998, Soil relative dating of moraine and outwash terrace sequences in the northern part of the Upper Arkansas River valley, central Colorado, U.S.A.: Arctic and Alpine Research, v. 30, p. 349-361.

O'Connor, J. E., 1993, Hydrology, hydraulics, and geomorphology of the Bonneville flood. Geological Society of America Special Paper 274, 83.

Pelletier J. D., 2008. Quantitative Modeling of Earth Surface Processes. Cambridge University Press, Cambridge, UK, 1st edition, p. xi–xiii. Print.

Paterson, W.S.B. 1994. The physics of glaciers. 3rd edition. Oxford, New York, Tokyo, Pergamon, ix, 480. ISBN 0-08037945 1.

Pierce, K. L., 2003, Pleistocene glaciations of the Rocky Mountains. Developments in Quaternary Science, v. 1, 63–76.

Pigati, J. S., Miller, I. M., Johnson, K. R., b, Honke, J. S., Carrara, P. E., Muhs, D. R., Skipp, G., Bryant, B, 2014. Geologic setting and stratigraphy of the Ziegler Reservoir fossil site, Snowmass Village, Colorado. Quaternary Research, special volume 82, 477–489.

Scott, G.R., 1975, Reconnaissance geologic map of the Buena Vista Quadrangle, Chaffee and Park Counties, CO. U.S. Geological Survey Miscellaneous Field Studies Map MF-657, scale 1:62,500.

Scott, G.R., Nelson, A.R., and Shroba, R.R., 1984, Pleistocene floods along the Arkansas River, Chaffee county, CO. Quaternary stratigraphy of the Upper Arkansas Valley - A field trip guidebook for the 8th Biennial Meeting of the American Quaternary Association, Boulder, Colorado. 51–57.

Shakun, J. D., Lea, D.W., Lisiecki, L.E., and Raymo, M.E., 2015, An 800-kyr record of global surface ocean delta18O and implications for ice volume-temperature coupling. Earth and Planetary Science Letters 426, 58-68.

Shroba, R.R., Kellogg, K.S., and Brandt, T.R., 2014, Geologic map of the Granite 7.5' quadrangle, Lake and Chaffee Counties, Colorado: U.S. Geological Survey Scientific Investigations Map 3294, 31, 1 sheet, scale 1:24,000, http://dx.doi.org/10.3133/sim3294.

Slingerland, R. L., and Kump, L., 2011. Mathmatical modeling of Earth's Dynamical Systems. Princeton University Press, Princeton, N.J., USA, 1st edition, 1–11. Print.

Summit Lake Jökulhlaup, schematic Figure 12: www.ec.gc.ca/eau-water/default.asp?lang=En&n=E7EF8E56-1.

Tweto, O., 1979, Geologic map of Colorado. USGS, 1:500,000 scale.

Tweto, O., 1979, The Rio Grande rift system in Colorado. USGS, in Riecker, R.E., ed., Rio Grande rift—Tectonics and magmatism: Washington, D.C., American Geophysical Union, 33–56.

Waitt, R. B., 1985, Case for periodic, colossal jokulhlaups from Pleistocene glacial Lake Missoula Geological Society of America Bulletin, v. 96, no. 10, 1271–1286.

Walder, J. S. and Costa, J. E., 1996, Outburst floods from glacier-dammed lakes: the effect of mode of lake drainage on flood magnitude. Earth Surface Processes and Landforms, v. 21, no. 8, 701–723.

Walder, J. S. and O'Connor, J. E., 1997, Methods for predicting peak discharge of floods caused by failure of natural and constructed earthen dams. Water Resources Research, v. 33, no. 10, 2337–2348.

U.S. National Aeronautics and Space Administration (NASA) GISS Surface Temperature Analysis Data at data.giss.nasa.gov/gistemp/graphs_v3/ accessed 20 December 2015.

Young, N. E., Briner, J. P., Leonard, E. M., Licciardi, J. M., Lee, K., 2011, Assessing climatic and nonclimatic forcing of Pinedale glaciation and deglaciation in the western United States. Geology, v. 39, no. 2, 171–174. doi: 10.1130/G31527.1.

Appendix

A.1 Additional figures

Upper Arkansas River Valley – LiDAR-based 10-m DEM

Delineated drainage areas

Delineated drainage basin areas and geometries from Google Earth plotting of my QGIS data. These basin outlines were used for the data in Table 2, and are useful for interpreting the relationship between glacier size and basin area, e.g., Figure 30, as well as how the valley width in general varies as a function of distance.

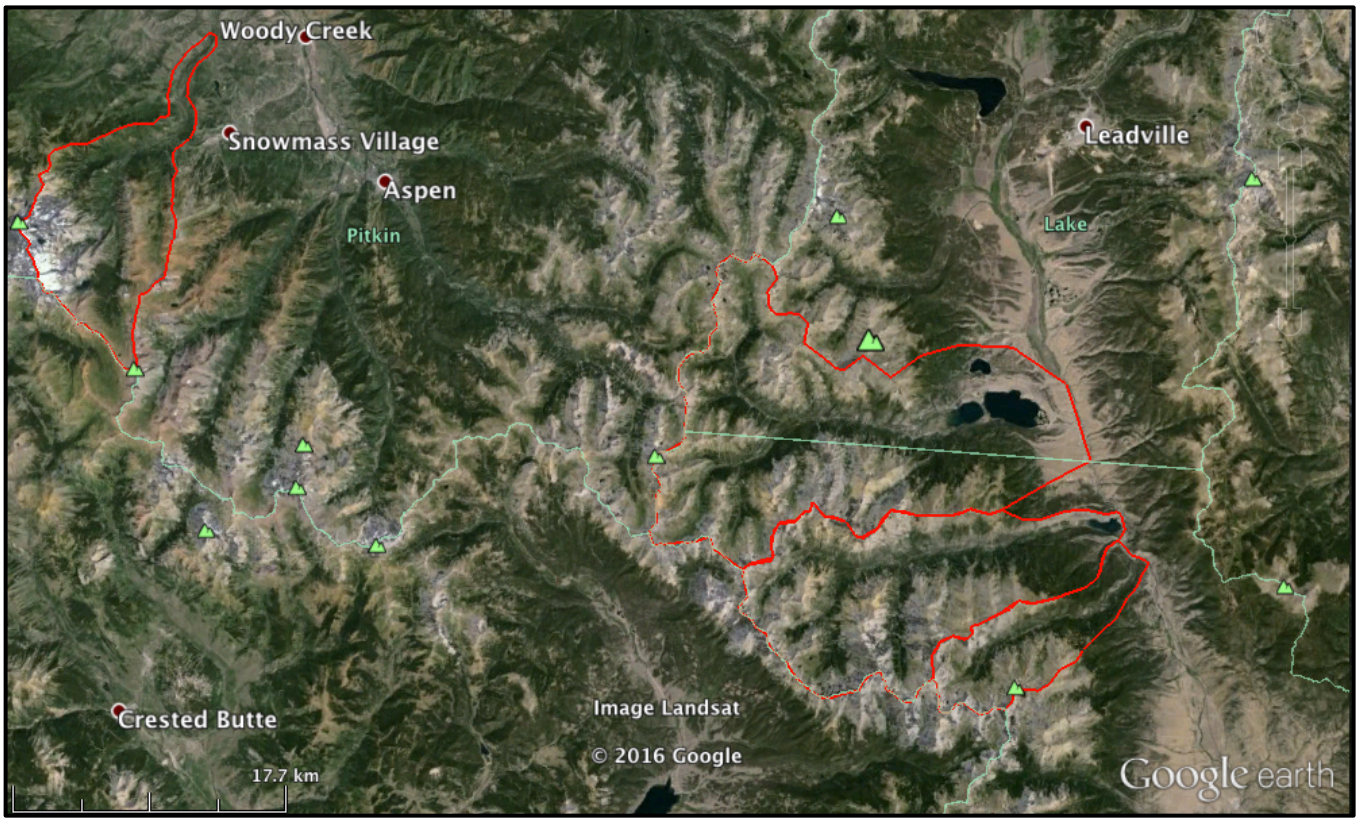

QGIS approximate extended elevation at ~2850 m for the Granite paleolake

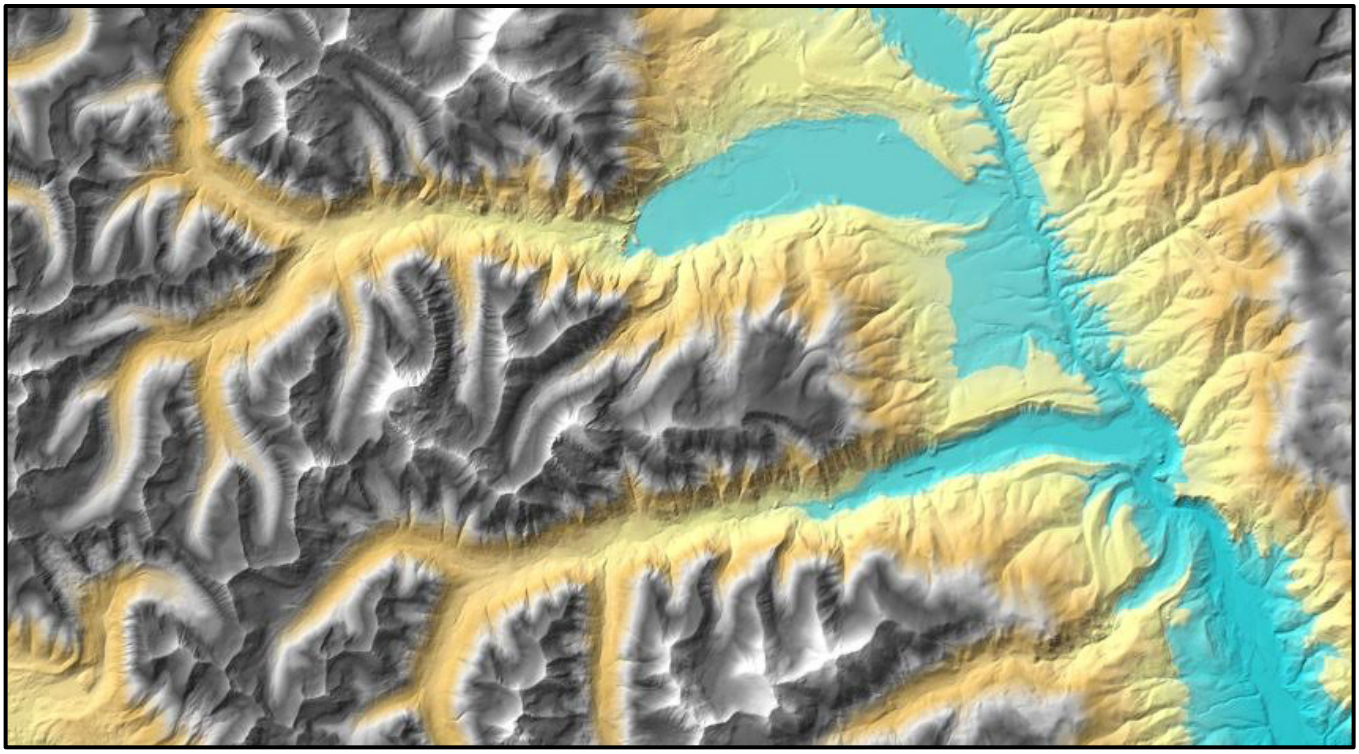

Upper Arkansas River Valley USGS geologic maps Key

LIST OF MAP UNITS

SURFICIAL DEPOSITS

Manmade deposits

- af — **Artificial-fill deposits (latest Holocene)**
- pt — **Placer-tailings deposits (latest Holocene)**
- mt — **Mine-tailings deposits (latest Holocene)**

Lacustrine deposits

- Qb — **Beach deposits (latest Holocene)**

Alluvial deposits

- Qva — **Valley-floor alluvium (Holocene and latest Pleistocene?)**
- Qsw — **Sheetwash alluvium (Holocene and late Pleistocene)**
- Qsw/Nd — **Sheetwash alluvium over Dry Union Formation**

Outwash of Pinedale age (late Pleistocene)

- Qopy — **Younger unit**
- Qopo — **Older unit**

Outwash of Bull Lake age (late and middle Pleistocene)

- Qoby — **Younger unit (late and middle Pleistocene)**
- Qobo — **Older unit (middle Pleistocene)**

Outwash of pre-Bull Lake age (middle Pleistocene)

- Qoey — **Younger unit**
- Qoeo — **Older unit**

Alluvial and mass-movement deposits

- Qac — **Alluvium and colluvium, undivided (Holocene to middle? Pleistocene)**
- Qf — **Fan deposits (Holocene to middle? Pleistocene)**

Mass-movement deposits

- Qta — **Talus deposits (Holocene to middle? Pleistocene)**
- Qc — **Colluvium (Holocene to middle? Pleistocene)**
- Qc/Nd — **Colluvium over Dry Union Formation**
- Qls — **Landslide deposits (Holocene to middle? Pleistocene)**

Glacial deposits

- Qrg — **Rock-glacier deposits (early Holocene? and latest Pleistocene?)**

Till of Pinedale age (late Pleistocene)

- Qtpy — **Younger unit**
- Qtpo — **Older unit**
- Qtb — **Till of Bull Lake age (late and middle Pleistocene)**
- Qte — **Till of pre-Bull Lake age (middle Pleistocene)**

BEDROCK UNITS

Post-volcanic sediments

- Nd — **Dry Union Formation (lower Pliocene? and Miocene)**

Volcanic rocks

- Pvva — **Vesicular andesite flow (upper Oligocene)**

Hypabyssal rocks

- Prc — **Hypabyssal rhyolite of Clear Creek (late Oligocene)**
- Pdt — **Microtonalite (late Oligocene?)**
- Pwf — **Felsic plutons and dikes of Winfield Peak and Middle Mountain of Fridrich and others (1998) (middle Eocene)**
- PKr — **Rhyolite dikes (Paleocene or Late Cretaceous)**
- PKi — **Felsic porphyry intrusive (Paleocene or Late Cretaceous)**

Proterozoic igneous and metamorphic rocks

- YXp — **Pegmatite (Mesoproterozoic and (or) Paleoproterozoic)**
- Ygr — **Monzogranite and quartz monzonite (Mesoproterozoic)**
- Ygl — **Monzogranite of Langhoff Gulch (Mesoproterozoic)**
- Yglf — **Strongly foliated phase**
- Ygrg — **Granite of Granite (Mesoproterozoic)**
- Xgg — **Granitic gneiss (Paleoproterozoic)**
- Xlg — **Leucogranite gneiss (Paleoproterozoic)**
- Xb — **Biotite gneiss (Paleoproterozoic)**
- Xhg — **Hornblende gneiss and amphibolite (Paleoproterozoic)**
- Xgb — **Gabbro (Paleoproterozoic)**

EXPLANATION

- **Contact**—Dashed where approximately located
- **Fault, type unspecified**—Dashed where approximately located; dotted where concealed beneath surficial deposits
- **Normal fault**—Dashed where approximately located; short-dashed where inferred; dotted where concealed beneath surficial deposits; bar-and-ball symbol on apparent downthrown side; traces of inferred faults were identified from lidar imagery
- **Shoreline**—Observed on lidar imagery
- **Fluvial scarp**—Observed on lidar imagery; hachures are on riser between lower and higher surfaces and point downslope
- **Landslide scarp**—Observed on lidar imagery and NAIP imagery; lower limit of hachures are on or near base of scarp. Prominent upslope facing scarps (sackungen) locally formed on the large landslide deposits derived from Proterozoic bedrock on the north side of Clear Creek near the southwest corner of the map area
- **Toe of inactive solifluction deposits**—Observed on NAIP imagery; sawteeth pattern is on the upslope side. Solifluction deposits were formed by downslope flowage of surficial material in the large alpine area near the head of Lost Canyon north of Clear Creek. Approximately located
- **Shear zone**—Marked by ductile deformation fabric in Proterozoic rocks
- **Crest line of moraine**—Observed on lidar imagery and NAIP imagery
- **Lineament**—Observed on lidar imagery and NAIP imagery. Linear features locally may coincide with zones of fracturing in Proterozoic bedrock, tabular intrusive bodies, or linear mass-movement deposits
- 10 — **Inclined bedding**—Showing strike and dip
- 80 — **Fault attitude**—Showing fault dip
- 80 — **Inclined foliation**—Showing strike and dip. Measurements of inclined foliation in areas of Quaternary surficial deposits (units Qc, Qac, and Qopy?) were made on Proterozoic bedrock outcrops that are too small to show at map scale
- **Vertical foliation**—Showing strike
- 65 — **Mineral lineation**—Showing bearing and plunge, depicted by an arrowhead
- GR11–725, 42.25 ± 0.13 Ma — **Sample**—Location and isotopic ages of bedrock (see table 3 in pamphlet)

R.R. Shroba mapped Quaternary surficial deposits and Neogene sediments during 2008–2012, and did reconnaissance mapping and soils research in and near the Granite 7.5' quadrangle between 1972–1974 during graduate studies at the University of Colorado at Boulder. K.S. Kellogg mapped the Paleogene and older rocks in the quadrangle during 2010–2011. T.R. Brandt prepared the digital topographic base map, digital compilation, and GIS database of the geologic map. He also generated slope and shaded-relief scenes from lidar data, which were used to interpret geologic, geomorphic, and shoreline features.

Base from U.S. Geological Survey, Granite, Colo., 1:24,000, 1994
North American Datum of 1927 (NAD 27)
Projection and 10,000-foot ticks: Colorado coordinate system, central zone (Lambert conformal conic)
1000-meter Universal Transverse Mercator ticks, zone 13

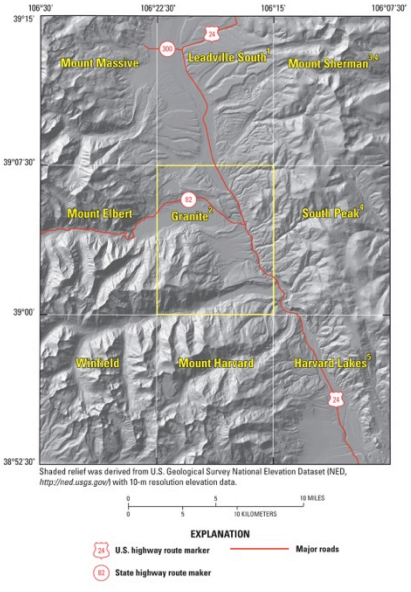

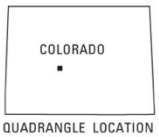

QUADRANGLE LOCATION

APPROXIMATE MEAN DECLINATION, 2013

Map of 10Be ages for the Upper Arkansas River Valley

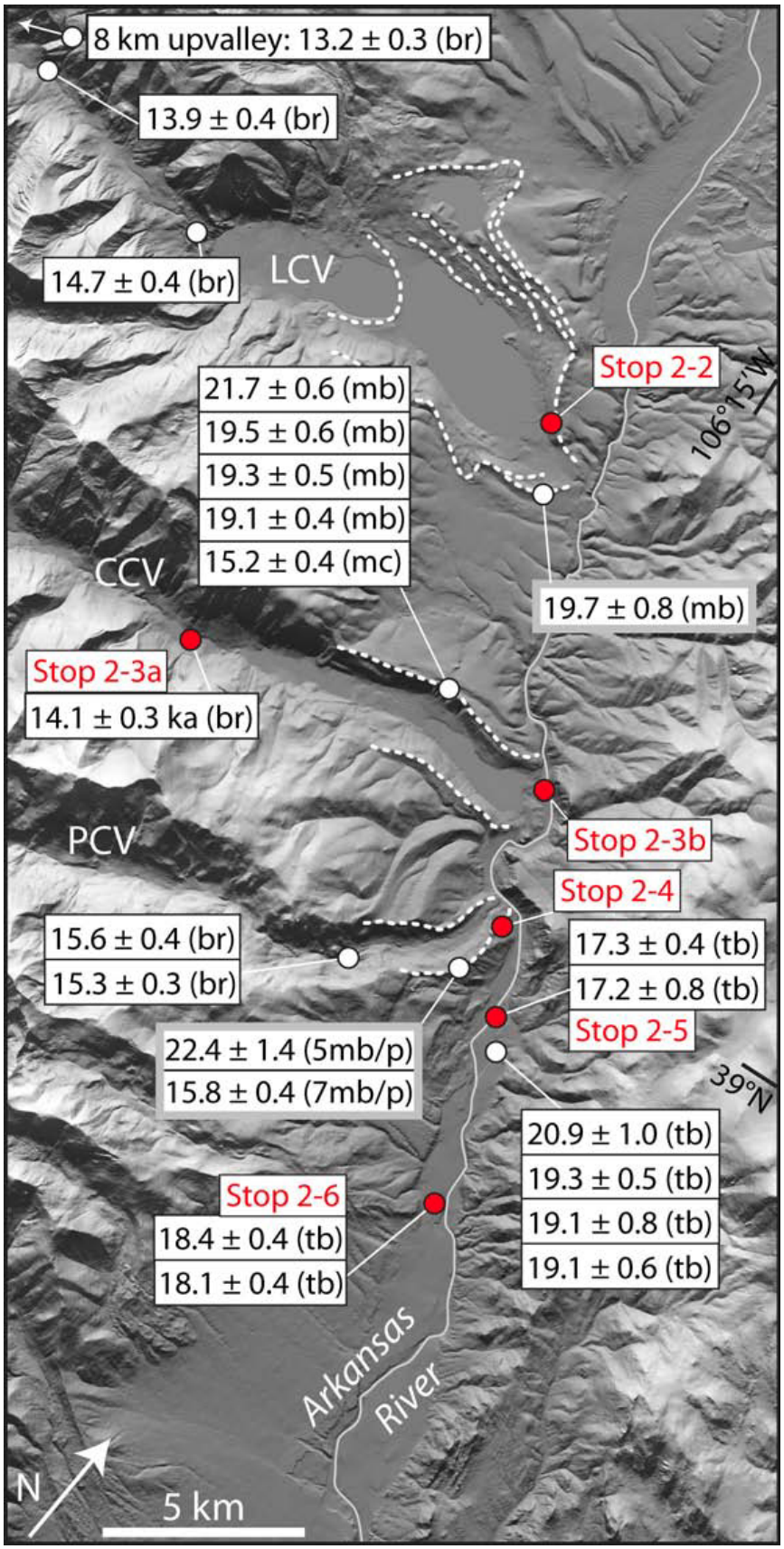

Moraine profiles from Lee (2010) and estimates of the height of the ice-dams

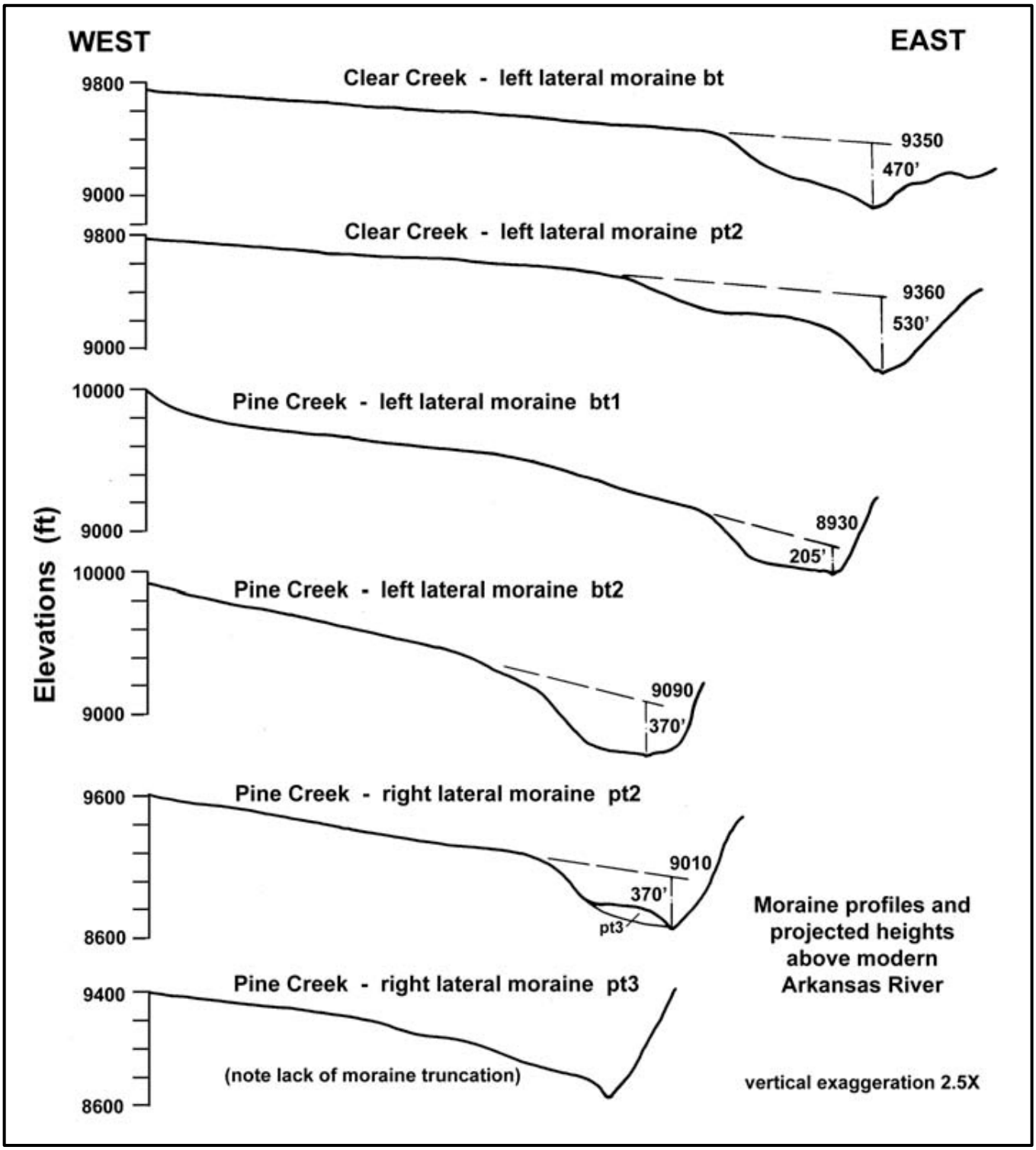

A.2 Raw field data

Channel bed grain size data

Terrace grain size data for 120 different cobbles and rocks on the bed, randomly chosen, for calculating D84 for roughness of the bed. Measurement numbers are italicized and the rounded grain sizes are in bold. Approximated 84th percentile is ~75 cm in size, which means that ~84% of the grains are less than ~75 cm in diameter.

grain size (cm)	measurement #, N	size	N	size	N	size	N	size	N
5	*1*	**20**	*25*	**30**	*49*	**46**	*73*	**71**	*97*
6	*2*	**20**	*26*	**30**	*50*	**46**	*74*	**74**	*98*
8	*3*	**20**	*27*	**33**	*51*	**46**	*75*	**74**	*99*
8	*4*	**20**	*28*	**33**	*52*	**46**	*76*	**76**	*100*
9	*5*	**20**	*29*	**33**	*53*	**48**	*77*	**76**	*101*
10	*6*	**22**	*30*	**33**	*54*	**51**	*78*	**76**	*102*
10	*7*	**23**	*31*	**33**	*55*	**51**	*79*	**76**	*103*
10	*8*	**23**	*32*	**33**	*56*	**51**	*80*	**76**	*104*
10	*9*	**23**	*33*	**33**	*57*	**51**	*81*	**81**	*105*
13	*10*	**23**	*34*	**36**	*58*	**51**	*82*	**84**	*106*
13	*11*	**25**	*35*	**36**	*59*	**51**	*83*	**84**	*107*
13	*12*	**25**	*36*	**36**	*60*	**51**	*84*	**84**	*108*
13	*13*	**25**	*37*	**36**	*61*	**56**	*85*	**86**	*109*
13	*14*	**28**	*38*	**38**	*62*	**58**	*86*	**89**	*110*
15	*15*	**28**	*39*	**38**	*63*	**61**	*87*	**102**	*111*
15	*16*	**28**	*40*	**41**	*64*	**61**	*88*	**102**	*112*
15	*17*	**30**	*41*	**41**	*65*	**61**	*89*	**107**	*113*
15	*18*	**30**	*42*	**41**	*66*	**64**	*90*	**114**	*114*
15	*19*	**30**	*43*	**41**	*67*	**66**	*91*	**117**	*115*
15	*20*	**30**	*44*	**43**	*68*	**66**	*92*	**127**	*116*
18	*21*	**30**	*45*	**43**	*69*	**69**	*93*	**140**	*117*
18	*22*	**30**	*46*	**43**	*70*	**69**	*94*	**142**	*118*
18	*23*	**30**	*47*	**43**	*71*	**69**	*95*	**145**	*119*
18	*24*	**30**	*48*	**43**	*72*	**71**	*96*	**180**	*120*

Flood boulder data

The following table also gives the raw field data for the terrace flood boulders sizes in centimeters. This data is succinctly summarized earlier in this work, found in Table 3.

Terrace 1	Field notes	Terrace 1.2	Terrace 2
360	numbers put in	321	600
323		364	925
225		277	573
250		285	825
355	First photo taken	375	622
213		687	1108
350	Second photo taken	490	935
327		365	572
260		536	717
638	~ 500 paces south	356	626
273		498	835
227		1015	510
284		912	346
238	~ 1000 paces south	492	684
232	headed back north now	391	432
323			630
252			612
365	above numbers put in		660
370			702
336			598
300			661
278			754
310			657
278	boulder that is nearest to dam		730
261	~ 10 m south of put in		
436	~ 100 m south (right side of road)		
400			
420			
365	~ 10 m south of last measurement		
350			
265			
380			
N =	**32**	**15**	**24**
mean =	**320**	**491**	**680**
1 sigma =	**84**	**221**	**164**
N =	**47**	*for terraces 1 and 1.2*	**24**
total =	**375**	*for terraces 1 and 1.2*	**680**
1 sigma =	**161**	*for terraces 1 and 1.2*	**164**